JAERI-M
92-202

REPORT OF THE JOINT SEMINAR ON SOLID STATE PHYSICS, ATOMIC AND MOLECULAR PHYSICS, AND MATERIALS SCIENCE IN THE ENERGY REGION OF TANDEM ACCELERATORS

January 22~23, 1991, JAERI, Tokai, Japan

January 1993

Department of Physics

日本原子力研究所
Japan Atomic Energy Research Institute

JAERI-Mレポートは，日本原子力研究所が不定期に公刊している研究報告書です。
入手の問合わせは，日本原子力研究所技術情報部情報資料課（〒319-11茨城県那珂郡東海村）あて，お申しこしください。なお，このほかに財団法人原子力弘済会資料センター（〒319-11 茨城県那珂郡東海村日本原子力研究所内）で複写による実費頒布をおこなっております。

JAERI-M reports are issued irregularly.
Inquiries about availability of the reports should be addressed to Information Division, Department of Technical Information, Japan Atomic Energy Research Institute, Tokai-mura, Naka-gun, Ibaraki-ken 319-11, Japan.

編集兼発行　日本原子力研究所
印　　刷　㈱原子力資料サービス

JAERI-M 92-202

Report of the Joint Seminar on Solid State Physics, Atomic and Molecular Physics, and Materials Science in the Energy Region of Tandem Accelerators

January 22 ~ 23, 1991, JAERI, Tokai, Japan

Department of Physics

Tokai Research Establishment
Japan Atomic Energy Research Institute
Tokai-mura, Naka-gun, Ibaraki-ken

(Received November 27, 1992)

The joint seminar on Solid Physics, Atomic and Molecular Physics and Materials Science in the Energy Region of Tandem Acceleration was held at Tokai Research Establishment of JAERI, for two days from January 22 to 23, 1991. about 60 physicists and material scientists participated and 18 papers were presented in this seminar.

The topics presented in this seminar included lattice defects in semiconductors, ion-solid collisions, atomic collisions by high energy particles, radiation effects on high Tc superconducting materials and FCC metals, radiation effects on materials of space and fusion reactors, uranium compounds and superlattice. All of these topics are most active and important fields in physics.

The organizing committee would like to thank all participants for their assistance and cooperation in making the seminar such a success.

Keywords: Tandem Accelerator, Solid State Physics, Atomic and Molecular Physics, Materials Science

---

Edited by Yukio KAZUMATA

JAERI-M 92-202

原研タンデム加速器研究会報告書
（固体物理，原子分子，材料）
1991年１月22～23日，東海研究所，東海村

日本原子力研究所東海研究所
物　理　部

（1992年11月27日受理）

タンデム加速器のエネルギー領域における固体物理，原子分子及び照射損傷を主とする材料科学３分野のジョイント・セミナーが国内の研究者約60名の参加を得て，1991年１月行われ18編の論文が発表された。

本報告書は上記セミナーでの報告をもとにしてまとめられた理論及び実験に関する総合報告及び研究論文を編集したものである。本報告の主なテーマは，半導体の欠陥，イオン・固体衝突，高エネルギー原子衝突，高温超電導及びＦＣＣ金属の照射効果，宇宙及び核融合材料の照射効果，そしてウラン化合物及び人工格子等の分野にまたがっている。いずれの分野も今日の物理学の最重要テーマの一つである。

東海研究所：〒319-11　茨城県那珂郡東海村白方字白根２－４
編集者：数又　幸生

Contents

1. Present Status of the JAERI Tandem Accelerator and Tandem Booster 1
C. Kobayashi
2. X-ray Observation of Silicon Single Crystals Irradiated with Energetic Heavy Ions 4
H. Tomimitsu
3. The Perfection of Silicon Crystals Required ULSI Device Processing 6
T. Abe
4. A Positron Lifetime Study of Defects in Neutron-irradiated Si ... 8
A. Li, S. Zheng, H. Huang, D. Li, H. Du,
S. Zhu and T. Iwata
5. Charged Beam Interaction with Solid Surfaces 9
T. Iitaka and Y. Ohtsuki
6. Acceleration of Convoy Electrons by Dynamic Surface Image Charge 15
A. Koyama
7. Ion Beam and Solid State Physics 20
M. Mannami
8. Physics of Ion Beam 24
Y. Mori
9. Theory of High-energy Ion-atom Collisions 25
N. Toshima
10. Charge State Distribution Measurements of 25.3 and 77 MeV/U Argon Ions Which Have Passed Through A Carbon Foil 27
Y. Kanai, T. Kambara, Y. Awaya, A. Hitachi
T. Niizeki, Y. Zou and K. Shima
11. A Brief Review of Radiation Effect of High Tc Superconducting Materials 29
Y. Kazumata
12. Effect of Electron-excitation on High Energy Ion Irradiation in Nickel and Copper 45
A. Iwase, T. Iwata, T. Nihira and S. Sasaki

13. The Approach to Heavy Ion Irradiation Effect (Single Event Phenomena) for the Semiconductor Devices for Space Use 53
T. Goka, S. Kuboyama and Y. Shimano

14. Irradiation Effects on Ceramic Breeders for Fusion Reactors 58
K. Noda, Y. Ishii, H. Matsui, T. Nakazawa and H. Watanabe

15. Physical Property of Uranium Compounds 63
H. Matsui

16. Quantum Size Effect on the Exciton Polariton In GaAs Thin Films 67
Y. Aoyagi, J. Kusano, Y. Segawa and S. Namba

17. Fourier Power Spectra of Aperiodic Conductance Fluctuations in Narrow Wires of GaAs/AlGaAs Heterostructure 72
Y. Ochiai, K. Ishibashi, M. Mizuno, M. Kawabe, Y. Aoyagi, K. Gamo and S. Namba

18. Magnetism of Metal Superlattice 76
H. Fujimori

Appendix Program of the seminar and abstract (in Japanese) 77

目　　次

1. タンデム加速器とブースターの現状 …… 1
小林　千明（原研）
2. 照射したSi単結晶のX線トポグラフィによる研究 …… 4
富満　　広（原研）
3. シリコン結晶中の点欠陥と2次欠陥 …… 6
阿部　孝夫（信越半導体）
4. 中性子照射したSiの陽電子寿命測定 …… 8
岩田　忠夫（原研）
5. 荷電粒子と固体表面の相互作用に関する最近の話題 …… 9
飯高　敏晃（早稲田大）
6. Glancing Collision 下での Convoy Electron 生成 …… 15
小山　昭雄（理研）
7. イオンビームを用いた固体物理の研究 …… 20
万波　通彦（京大）
8. ビームの物理 …… 24
森　　義治（高エネルギー研）
9. 高エネルギー原子衝突の理論 …… 25
戸嶋　信幸（筑波大）
10. 高エネルギー原子衝突の実験 …… 27
金井　保之（理研）
11. 高温超電導物質の照射効果 …… 29
数又　幸生（原研）
12. ＦＣＣ金属の高エネルギー重イオン照射損傷 …… 45
岩瀬　彰宏（原研）
13. 宇宙用半導体デバイスの重イオン照射効果 …… 53
五家　建夫（宇宙センター）
14. 核融合炉セラミックス増殖材の照射効果 …… 58
野田　健治（原研）
15. ウラン化合物の物性 …… 63
松井　尚之（名大）
16. 人工格子（半導体） …… 67
青柳　克信（理研）
17. 量子細線の電気伝導 …… 72
落合　勇一（筑波大）

１８. 金属人工格子 …… 76
藤森 啓安（東北大）
付録 タンデム加速器研究会プログラム及び要旨集 …… 77

1. PRESENT STATUS OF THE JAERI TANDEM ACCELERATOR AND TANDEM BOOSTER

Chiaki KOBAYASHI

Department of physics, JAERI

Introduction

Installation of the JAERI tandem accelerator[1], manufactured by National Electrostatics Corporation USA, started 1987 and the operation for the experiments began 1980. First two years, half of the running time had to shared for the voltage conditioning to get 20MV. The continuous operation for the experiments started at August 1982 and main experimental apparatus completed by 1985. Since then, the tandem accelerator has been operating smoothly and used for nuclear physics, solid state physics, atomic physics, material research, nuclear chemistry, neutron physics and other basic researches. To increase the energy of the heavy ions from the tandem accelerator by approximately four times, the the tandem booster construction started 1988.

Outline of the tandem accelerator

The JAERI tandem accelerator is a 20MV design voltage with folded column structure. The pressure vessel is 8.2 meters in diameter and 26.5 meters high. The high voltage terminal has a large 180 degree bending magnet and an internal ion source and nanosecond bunching and pulsing system for intense proton and deuteron beams. Fig.1 shows main specifications and layout of the accelerator. The control system is two computers-based digital control with CAMAC system. We are developing a new control system because the present system which was used even for more than 16 years and malfunction has increased. The new system will be used a parallel processing computer.

The machine time is 3～4 months with a continuation for 24 hours/day. Regular maintenance that takes 4～5 weeks is set up an interval of the every machine time. Fig.2 and Fig.3 show the operation time distribution and distributions by the activities.

Tandem booster

The tandem booster project[2] started at 1988. The booster linac will consist of 40 super-conductive resonators made of niobium and copper and resonators are housed in ten cryoststs four by four. The fabrication of the booster components are in progress. The result of the tests with few resonators, a field level of 5～6MV/m obtained which corresponds to the acceleration voltage of 30～36MV for the booster linac. This acceleration voltage will have the energy performance as shown Fig.4. The booster building construction also in progress and the beam acceleration test will start end of 1992. Fig.5 shows the layout of the booster and the building.

References

1) M. Maruyama, The third international conference on electrostatics accelerator technology April 1981

2) S. Takeuchi, T. Ishii, H. Ikezoe, Y. Tomita, Nucl. Instr. and Meth. A289(1990)257.

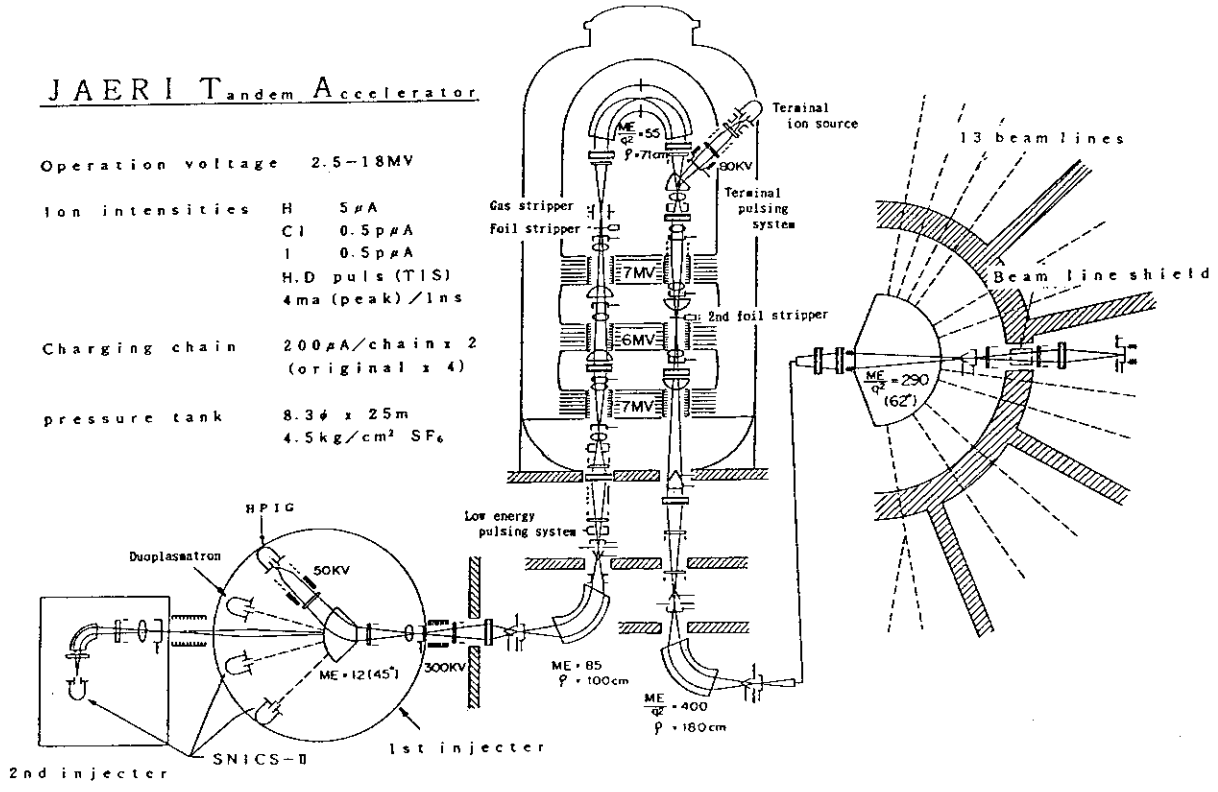

Fig. 1 Main specification and layout of the JAERI tandem accelerator

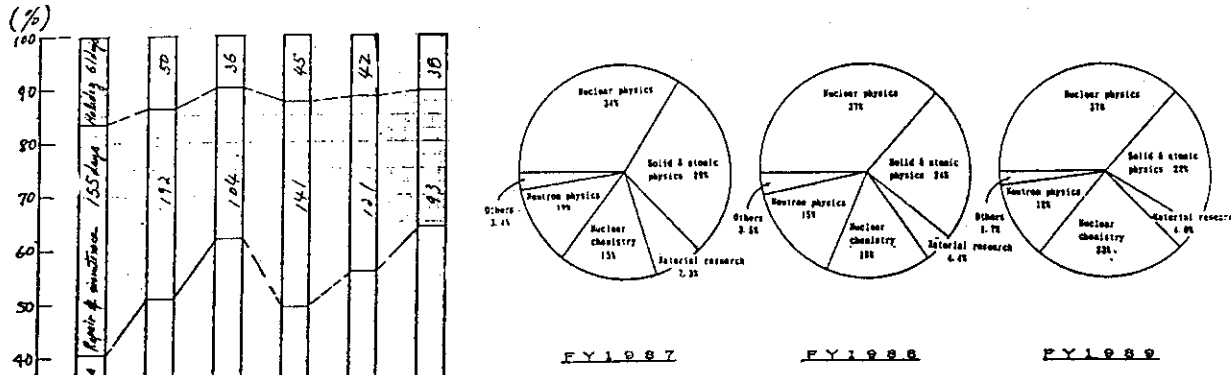

Fig. 2 The operation time distoribution by years

Fig. 3 Distribution by the activities

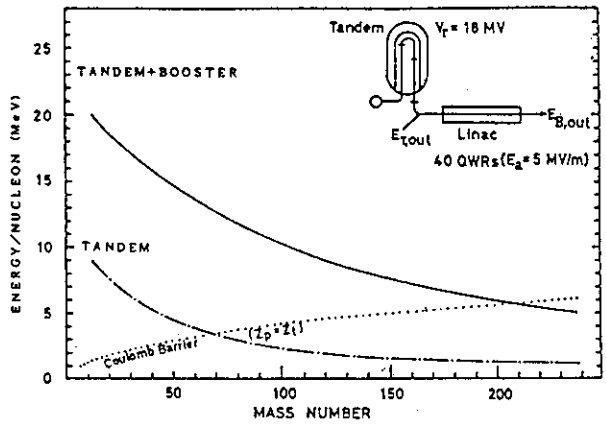

Fig. 4

Energy performance of the JAERI tandem booster

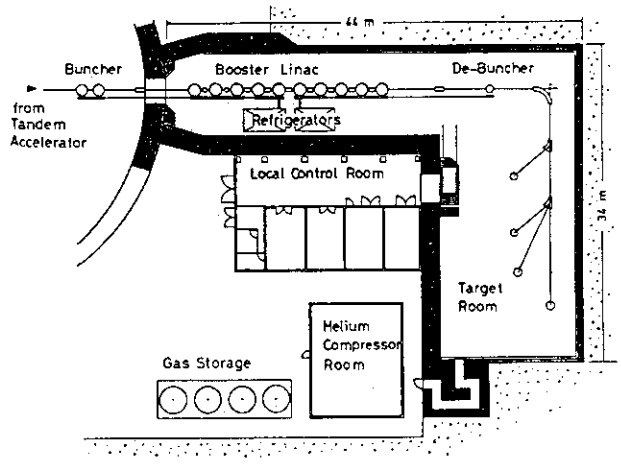

Fig. 5

Layout plan of the JAERI tandem booster

2. X-RAY OBSERVATION OF SILICON SINGLE CRYSTALS IRRADIATED WITH ENERGETIC HEAVY IONS

Hiroshi TOMIMITSU

Solid State Physics 1, Department of Physics, JAERI

By conventional X-ray diffraction topographic observation of Si single crystals irradiated with various energetic ions (Li~Au, 20~200 eV) with the dose from 10^{13} to 10^{15}ions/cm^2, the following results were obtained[1];

1) Specimens were only partly imaged in a topograph, suggesting that they were deformed macroscopically. The deformation in a specimen was concluded to be a kind of convex, the curvature being typically estimated around 14~33m. But any other kind of defects such as dislocations or cracks were not observed.

2) Heavy black-and-white contrast was observed at the boundary between the irradiated- and non-irradiated areas on the specimen surface, suggesting that very heavy lattice-strain was generated at the boundary and the strain seemed so heavy that it reached to the another surface of the specimen.

3) Irregular images were sometimes observed within the irradiated area, suggesting that lattice was more or less damaged.

4) Regularly arrayed fringe patterns were sometimes observed in the irradiated area, suggesting that some kind of interference was occurred.

The results mentioned above seem to depend on the irradiation conditions, i.e. on ion-species, on their energies, especially on the homogeneity of the beam-

distribution, and it was clear that they depend on the experimental conditions such as reflecting planes.

Almost all of the above results of the observation are corresponds to those by previous authors[2~4], but an important part of the result of 4) does not agree with the result in ref.4. So the present author started to study further on the origin of the beautiful interference fringes, making use of the so-called double crystal X-ray diffraction method to measure precisely the change of the lattice-constant within the specimens. In the preliminary results of the measurement, the rocking curve of the Cl-irradiated specimen showed rather complicated profile compared with the non-irradiated specimen.

Further investigation is in progress.

The author is much indebted to Dr.T.Abe of Shin-Etsu Handotai, Co. for his kind offering the Si wafers for the present experiment.

References

1)-H.Tomimitsu; Jpn.J.Appl.Phys. 22 (1983), L674.
-H.Tomimitsu; Acta Crystallogr. A43 (1987), Suppl. C207.
-H.Tomimitsu; JAERI TANDEM, LINAC & V.d.G. Report, 1982-1988.

2)-G.H.Schwuttke, K.Brack, E.E.Gardner & H.M.DeAngelis; Proc.Santa Fe Conf.Radiation Effects in Semiconductors, ed. F.Vook, (Plenum Press, N.Y., 1968) p.406.
-U.Bonse, M.Hart & G.H.Schwuttke; Phys.Status Solidi 33 (1969), 361.
-U.Bonse & M.Hart; Phys.Status Solidi 33 (1969), 351.

3) A.R.Lang & V.F.Miuscov; Appl.Phys.Lett. (1965), 214.

4) D.Simon & A.Authier; Acta Crystallogr. A24 (1968), 527.

3. THE PERFECTION OF SILICON CRYSTALS REQUIRED ULSI DEVICE PROCESSING

Takao ABE

Shin-Etsu Handotai Co., Ltd. Isobe R&D Center

Three important topics[1] regarding the use of silicon crystals for applications in the electronics industry are reviewed in this paper. These are: (1) the perfection of silicon crystals required for ULSI device processing, (2) issues related specifically to large diameter crystal (Fig.1) growth, and (3) the use of bonded wafers with SOI structures.

There is no single silicon crystal specification that is ideal for all device processes. This is due to the facts that different processes have different thermal cycles and that contamination levels can vary from one facility to another. In Japan, lower oxygen concentrations are being chosen for specification of 200 mm silicon wafers compared to what is being used presently 150 mm specifications. This indicates that technology for cleaner device processing is considered more important than the use of internal gettering (IG) methods.

It is believed that it is necessary to further reduce the concentrations of carbon and heavy metals (Fig.2) in silicon crystals since they can serve as nucleation centers for harmful defects. In particular, control of point defects[2] in large diameter crystals (Fig.3) will be an important subject in the near future.

After the 64M bit DRAM generation of device processing, it is expected that an SOI structure may be used due to the high speed and high density requirements. A wafer bonding process technology (Fig.4) such an SOI need is introduced. An understanding of the bonding mechanism is also described .

Reference

1) T. Abe : Nihon Ketsusho Seicho Gatsukai shi Vol. 17 (1990) 146 in Japanese

2) T. Abe : Oyo Buturi Vol. 59 (1990) 272 in Japanese

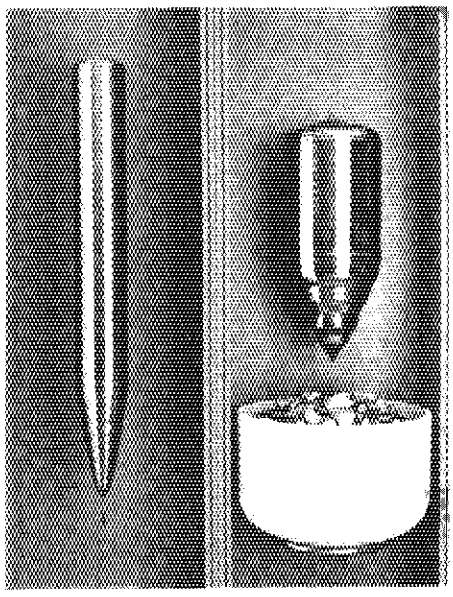

Fig. 1 6 inch FZ crystal with necking part and seed (left), 12 inch CZ crystal and 22 inch fused quartz crucible contained with polysilicon (rigth).

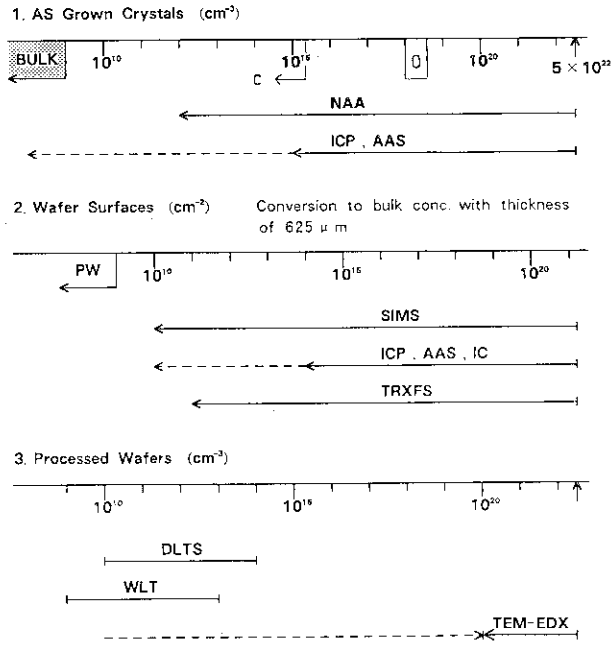

Fig. 2 Sensitivities of various analytical methods on Cr, Fe, Ni and Cu in Silicon. Dotted lines are obtained by each condensation of heavy metals.

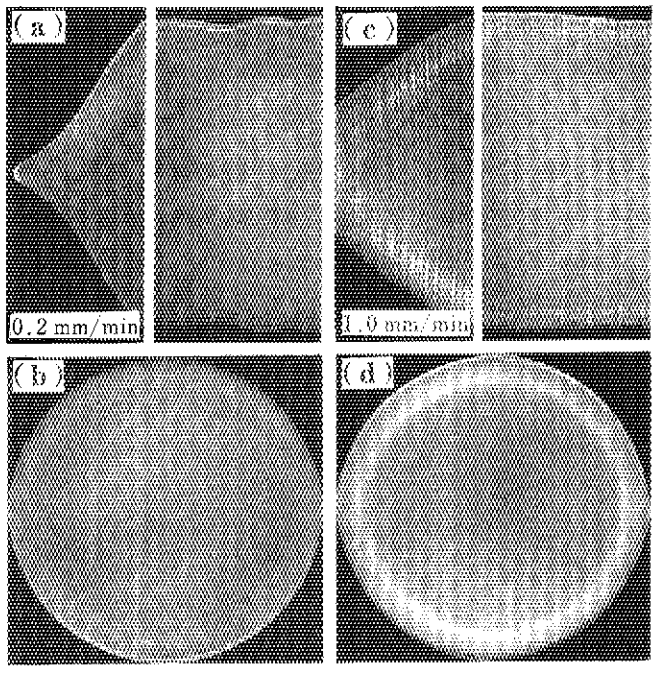

Fig. 3
Inhomogeneity of oxygen precipitation on growth rate. X-ray topographs of specimens with 1 mm in thickness annealed at 1000°C, 16 hrs in dry O_2. p-type, 10 Ω·cm, ⟨100⟩ orientation, 75 mm in diamiter.

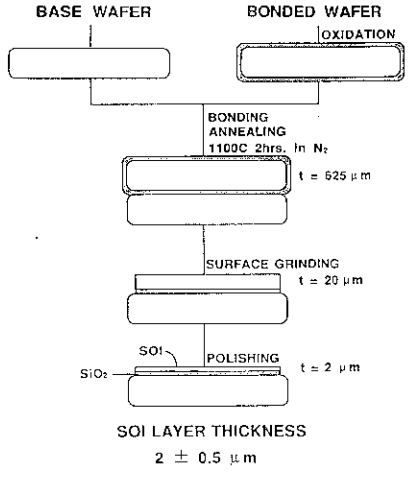

Fig. 4 Schematic of silicon wafer-bonding process with SOI structure.

4. A POSITRON LIFETIME STUDY OF DEFECTS IN NEUTRON-IRRADIATED Si

Anli LI*, Shengnan ZHENG*, Hanchen HUANG*
Donghong LI*, Hongshan DU*, Shengyun ZHU*
and Tadao IWATA

Solid State Physics Laboratory II
Department of Physics
Tokai Research Establishment, JAERI

Positron lifetime measurements in neutron-irradiated Cz silicon crystals have been performed at room temperature after annealings at different temperatures between 100°C and 800°C. Two-component fitting of the positron lifetime spectra is carried out. It is suggested that the short lifetime component is a weighted average lifetime of the positrons in the bulk and those trapped at monovacancy-substitutional oxygen complexes, while the long lifetime component is an average lifetime of the positrons trapped at divacancies or divacancy-substitutional oxygen complexes and those trapped at quadrivacancy-substitutional oxygen complexes. The two-component data are analyzed using an extension of the trapping model to obtain the positron trapping rates at these vacancy-type defects. The annealing of these defects is discussed.

* China Institute of Atomic Energy

5. CHARGED BEAM INTERACTION WITH SOLID SURFACES

Toshiaki IITAKA and Yoshi-Hiko OHTSUKI

Department of Physics, Waseda University,

INTRODUCTION

We review our study about the interaction of charged beam with solid surfaces, especially in the small angle incidence case, in which the interaction time of the ion and the surface becomes extremely long and the effect of the surface becomes very important.

This review treats two important phenomena concerning the effect of the image charge. The first is the skipping motion, a curious motion of ions near the surface which was proposed theoretically ten years ago[1] and observed recently by experiment of Snowdon et al. [3] and Stolzle et al. [19]. The second is the acceleration of convoy electrons produced at glazing angle incidence of fast ions. We studied it by using Classical Trajectory Monte Carlo (CTMC) calculations [26] and explained the experimental results of Hasegawa et al. [28] and Koyama et al. [23].

SKIPPING MOTION

Ions incident on the surface with a grazing angle have thousand times smaller energy in the normal-to-surface direction than in the parallel direction. Some of the ions loose their transverse energy near surface by elastic or inelastic collisions and they are trapped into the surface potential well, which is composed of the repulsive part due to crystal atomic potential and the attractive part due to the dynamical image charge. Then the motion of the ions becomes sinuous, bounded along normal-to-surface direction and nearly free along the parallel direction. This kind of adsorption of particles with its large parallel

momentum is named skipping motion[4].

Numbers of mechanism of transverse energy loss have been discussed: elastic collision with the corrugation of surface potential[12], the excitation of electron-hole pairs, plasmons, phonons, some kind of chemical reaction etc.[3-15]. The possible surface attractive potentials are classified into three types: 1). static image potential, 2). dynamical image potential and 3). chemical binding. Our study has revealed that the most important mechanism of skipping motion of "high energy" (about 30 keV) proton is the corrugation of surface potential and the attraction potential due to the dynamical image charge[12]. Our theories and computer simulations [1,4-8,12] have revealed the two important effects that would enable the observation of the skipping motion i.e., the destruction of the specular reflection peak in the exit angle distribution and the discrete structure of the energy loss spectrum. In order to predict the discrete peaks in the energy loss spectrum, stopping power of fast ions near metal surface has been intensively studied[7,10,11,13,18] and we have confirmed that skipping motion is observable by measuring the discrete energy loss spectrum which has peaks at the multiple (1:2:3:...) of the energy loss of the specular reflected particles.

Snowdon et al.[3] observed "low energy" skipping motion by by using very slow (E_0=2keV) silicon ions incident on copper surface. The skipping motion was identified by measuring the energy loss spectrum of reflected particles. However the observed spectrum has peaks at the multiple (1:3:5:...) of the energy loss of the specular reflected particles. This quantitative difference cannot be explained by our study of skipping motion. The spectrum is rather similar to the spectrum due to surface steps[16] though Snowdon et al. has confirmed that the surface is step free[3]. Our results are not directly applicable to this case because the energy region is different from ours. Thus the mechanism of this skipping motion is not clear by now. Snowdon et al. have suggested the chemical binding mechanism and performed computer simulation [15] using the stopping power formula of Nunez et al.[17]. They are successful

to get the peaks at (1:3:5:...) in energy spectrum but not the correct magnitude of the energy loss.

Recently, Stolzle et al.[19] observed "high energy" skipping motion by by using fast protons (E_0=15keV-75keV) incident on the (0001) surface of Highly Oriented Pyrolytic Graphite (HOPG). The observed spectrum has peaks at the multiple (1:2:3:...) of the energy loss of the specular reflected particles. Both the incident energy and the energy loss peaks are the same as that of our calculation. Thus this skipping motion can be regarded as the one we have proposed. We are now studying the Stolzle experiment by using computer simulation [20].

In conclusion, the origin of Snowdon's "low energy" skipping motion is considered as a new type skipping motion different from our original idea, while Stolzle's is the original type skipping motion. Many points concerning skipping motions remain not clear and further experimental and theoretical studies should be performed in order to testify, for example, the potential ability of skipping motion to probe chemical reactions and adsorption phenomena at surface [14].

ACCELERATION OF CONVOY ELECTRONS

The velocity distribution of the electrons ejected from gases or metal foils by fast ions has a peak at the velocity of the incident ions. The production of these "convoy electrons" can be accounted for in terms of the final state interaction, i.e. the Coulomb attraction between the convoy electron and the ion after the electron was capture into the continuum state of ion. The cross section of this process is given by

$$\sigma_{ba} = | \langle b|T|a \rangle |^2 \frac{d\sigma}{d\underline{v}} d\underline{v} \qquad (1)$$

where the first factor $\langle b|T|a \rangle$ is the matrix element of the electron capture only and the second factor $d\sigma/d\underline{v}$ is the cross section for electron-ion scattering with the relative velocity $\underline{v}$.

This second factor determines the $\underline{v}$-dependence of $_{ba}$. In the low velocity limit ($\underline{v}$ -> 0), the cross section diverges as 1/v for Coulomb potential and a cusp peak appears at the relative velocity v=0.

In the scattering of fast ions incident almost parallel to the surface, the image potential of the ion must be included into the final state interaction as well as Coulomb potential of the ion because the interaction time with the surface becomes very long[21]. The final state interaction should be calculated with this dipole-like potential. In the limit of $\underline{v}$ -> 0, the cross section will show a strong anisotropy[22] because most of the electrons directed to the image charge are reflected by the repulsive image force to the opposite direction, i.e. the direction of the dipole vector pointing from the image charge to the ion. While the dipole vector is normal to the surface when the ion is at rest, the vector is oblique to the surface when the ion is moving fast parallel to the surface because the response of the electron gas cannot follow the ion's motion completely (the retardation effect). Thus the final velocity distribution of the electrons in the ion-rest frame has a peak shifted in the direction of the dipole vector, and this shift causes the acceleration of convoy electrons in the laboratory frame, $E=m\underline{v}_I \cdot \underline{v} + v^2$ where $\underline{v}_I$ is the ion velocity. This model explains the experimental value of the acceleration energy of convoy electrons for heavy ions[23].

Hasegawa et al. [28] measured energy spectra of electrons emitted from a SnTe single-crystal surface following the impact of grazing angle incident H^+ and He^+ ions. For H^+ ions, the convoy peak energy was smaller than $E_i=0.5\ mv^2$. However, for He^+ ions, the peak energy was larger than E_i.

Koyama et al. [23] explored electron excitation by fast heavy ions (N^{6+},Ar^{12+},Xe^{27+},...) and measured projectile dependence of energy distribution of excited electrons. They found that the larger the mean charge of the projectile is, the larger the acceleration is.

We calculated the electron velocity distribution in the field of Coulomb force and image force. [24] to explain Koyama's

work by using CTMC method [26], because in this case we can neglect the electron's image charge. In CTMC, one choose an adequate classical representation of the initial quantum-mechanical state and then solves the classical equations of motion of the involved particles taking into account all interactions in the system. The initial distribution of the electrons is taken as the uniform distribution in the sphere of radius R_0 with its origin at the ion. The energy distribution is uniform in the interval $(0, \epsilon_{max})$ and the distribution of the momentum directions is isotropic. We get the final velocity distribution of electrons by calculating the trajectories with the Runge-Kutta methods. The agreement between the calculated results and the experimental data was very good.

In conclusion, the observed acceleration for heavy ions was explained as the image charge effect. We are now studying the light ion case and quantum theoretical calculation of the acceleration.

REFERENCES

[1] Y.H.Ohtsuki, Rep. Annual Meeting Phys. Soc. Japan (1978)
[2] Dr. R.Sizmann, private communication (1988)
[3] K.J.Snowdon, D.J.O'Connor and R.J.MacDonald, Phys.Rev.Lett. 61 (1988) 1760.
[4] Y.H.Ohtsuki, K.Koyama and Y.Yamamura, Phys.Rev. B20(1979) 5044.
[5] Y.H.Ohtsuki, Nucl.Instr.&Meth.B2(1984) 280.
[6] Y.H.Ohtsuki, R.Kawai and K.Tange, Nucl.Instr.&Meth. B13(1986)193.
[7] M.Kato, T.Iitaka and Y.H.Ohtsuki, Nucl.Instr.&Meth. B33(1988),432
[8] Y.H.Ohtsuki, Charged Beam Interaction with Solids (Taylor & Francis, London, 1983).
[9] V.V.Beroshitskii,M.A.Kumakhov,V.A.Muralev, Rad.Eff.20(1973) 95
[10] M.Kato and Y.H.Ohtsuki, Phys.stat.sol.(b)133 (1986),267
[11] M.Kato, J.Phys.Soc.Japan,55 (1986), 1011
[12] Y.Ono, T.Miyamoto, T.Iitaka and Y.H.Ohtsuki, Rad. Eff.Exp., 2(1988),63.

[13] R.Kawai,N.Itoh and Y.H.Ohtsuki, Surf.Sci.114(1982) 137.
[14] K.J.Snowdon, Nucl. Instr.&Meth., B33(1988)365.
[15] K.J.Snowdon,D.J.O'Connor and R.J.MacDonald, (preprint)
[16] K.Kimura, M.Hasegawa, Y.Fujii, M.Suzuki, Y.Susuki and M.Mannami, Nucl.Instr.&Meth. B33(1988) 358.
[17] R.Nunez, P.M.Echenique,R.H.Ritchie, J.Phys. C13(1980) 4229.
[18] M.Kitagawa, Nucl.Instr.&Meth. B33(1988) 409.
[19] F.Stolzle and R.Pfandzelter, (1990) preprint.
[20] H.Sakai, T.Iitaka, and Y.H.Ohtsuki, (1991), in preparation.
[21] H.Winter, P.Strohmeier and J.Burgdoerfer, Phys. Rev. A39 (1989) 3895.
[22] T.Iitaka, Y.H.Ohtsuki, A.Koyama, and H.Ishikawa, Phys. Rev. Lett. 65(25) (1990) 3160.
[23] A.Koyama, H.Ishikawa, Y.Sasa, T.Iitaka, Y.H.Ohtsuki and M.Uda, Phys. Rev. Lett. 65(25) (1990) 3156.
[24] T.Iitaka,Y.H.Ohtsuki,H.Hizawa,A.Koyama, and H.Ishikawa, Rad.Eff.&Deff. (to be published).
[25] P.M.Echenique, F.Flores, and R.Ritchie, Solid State Physics 43 (1990) 229.
[26] R.Janev, L.Presnyakov, and V.P.Shevelko. Physics of Highly Charged Ions, volume 13 of Springer Series in Electrophysics. (Springer-Verlag, Heidelberg, 1985)
[27] L.F. de Ferraliis and R.A.Baragiola, Phys. Rev. A33 (1986) 4449.
[28] M.Hasegawa, K.Kimura, and M.H.Mannami, J.Phys. Soc. Jpn. 57 (1988) 1834.
[29] M.Hasegawa, T.Fukuchi, T.Mizuno, K.Kimura, and M.H.Mannami, (1990) Rad.Eff.&Deff. (to be published).

6. ACCELERATION OF CONVOY ELECTRONS BY DYNAMIC SURFACE IMAGE CHARGE

AKIO KOYAMA

The Institute of Physical and Chemical Research, Hirosawa-2-1, Wako-shi, Saitáma, 351-01, Japan

It is well known that an atom or molecule near a solid surface induces static image charge due to polarization of surface electrons, and this polarization takes an important role in the physical adsorption.

When a moving charged particle is near a solid surface, it induces dynamic image potential(DIP)[1,2] and when it penetrates a solid medium, it emerges accompanied by electrons which move with the same velocity as the ion; these electrons captured in the continuum states of the projectile are called convoy electrons(CE).[3] The force due to DIP may accelerate CE. Burgdorfer calculated the DIP-induced energy increase of CE which were emitted normal to the surface.[4] However,

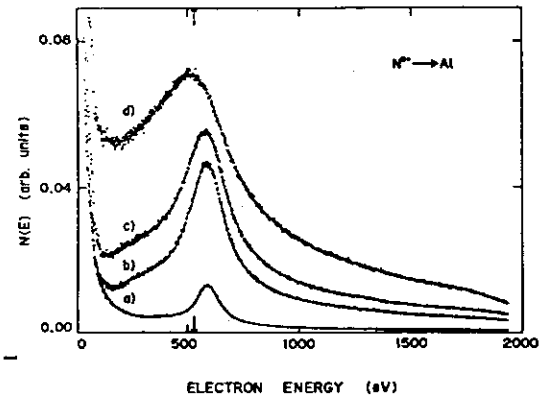

FIG. 1. Energy spectra of electrons emitted from an Al surface induced by N^{6+} ions of 0.98 MeV/amu incident at 1° with respect to the surface. Detection angles, with respect to the incident beam direction, are curve *a*, 3°; *b*, 6°; *c*, 8°; and *d*, 15°.

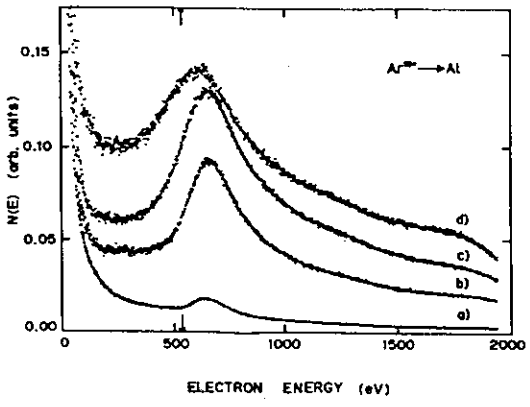

FIG. 2. Same as in Fig. 1, but for projectiles of Ar^{12+} ions isotatic with the N^{6+} ions.

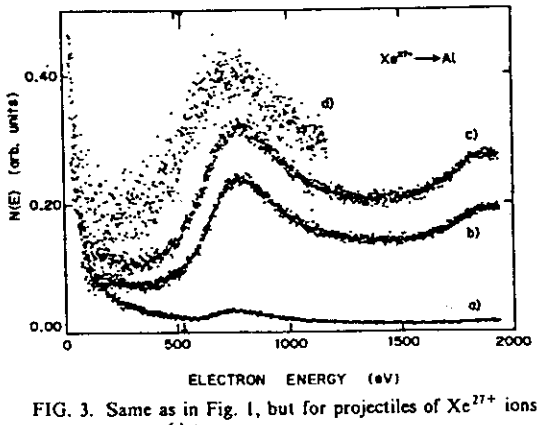

FIG. 3. Same as in Fig. 1, but for projectiles of Xe^{27+} ions isotatic with the N^{6+} ions.

hitherto any evidence of DIP acceleration has not been obtained for such normal-emitted CE,

If the particle is incident or emerges almost parallel to the surface, the interaction time between the surface and the projectile is very long, and the interaction time between CE and DIP should also be long, and acceleration of CE may be significant and observed. De Ferralis and Baragiola measured the energy spectra of electrons ejected from an Al surface due to grazing angle incident H^+ ions.[5] A broad peak was observed and no description was given for the influence of DIP on the CE spectra.. Hasegawa et al. measured energy spectra of electrons emitted from a SnTe single crystal surface following the impact of grazing angle incident H^+ and He^+ ions.[6] For H^+ ions, the most probable energy of the peak was not larger than $E_I=(1/2)mv_I^2$, where m is the mass of an electron and v_I is the velocity of the projectile. However, for He^+ ions, the peak energy was larger than E_I, and the DIP acceleration was evoked to explain this energy increase. Winter et al. measured the energy spectra of electrons emitted from a Si(111) surface, for grazing incident angle H^+ ions, and also observed significantly broadened cusp shaped lines.[7] They attributed this broadening to a deviation from the Coulombic final-state interaction near the surface due to DIP。 In the present review, experimental results obtained by Koyama et al.[8] are mainly discussed related to the DIP-acceleration model.

Fig. 1 shows the energy spectra of electrons induced by N^{6+} ions(energy of 0.98 MeV/amu) incident at an angle of 1° with respect to the target surface and emitted at various angles with respect to the incident beam direction; (a) at 3°, (b) at 6°, (c) at 8°, and (d) at 15°. The ordinate is proportional to the number of electrons induced by a projectile into the unit energy interval N(E). The arrow shows E_I, the energy of electrons isotatic to the projectile. Figs. 2 and 3 show similar spectra for Ar^{12+} and Xe^{27+} ions at the same grazing incident angle and electron emission angles as in Fig. 1. Velocities of these ions are also the

same as that of N^{6+} ions. It is well known that energies of electrons produced in atomic-collisions are representative of respective excitation mechanisms,[9] such as low energy secondary electrons, target or projectile Auger electrons, convoy electrons, loss electrons, and binary electrons. Each spectrum obtained here shows a large peak of low energy secondary electrons. Binary peaks are clearly seen for Xe^{27+} ions due to their large cross sections at energies higher than 1500 eV. The peak with the most probable energy of 500~ 800 eV cannot be explained by any of hitherto identified mechanisms.

Following results are obtained from the figures.
(I) The energy difference between the highest E_e and E_I is 60 eV for N^{6+}, 120 eV for Ar^{12+}, or 250 eV for Xe^{27+}, and is approximately proportional to the projectile charge q.
(II) The peak width increases with increasing q. The values of FWHM at the emission angle 6° are about 200 eV for N^{6+}, 300 eV for Ar^{12+}, and 400 eV for Xe^{27+}.
(III) The emission angle at which Ee is largest increases with q.
(IV) The peak intensity increases steeply with increasing emission angle from 3° to 6°.

These results can be explained in terms of the DIP acceleration of CE. CE may be mainly produced by projectiles emerging from the surface, because the outgoing part of the projectile trajectory plays the important role in the CE excitation.[7] These CE should be accelerated by DIP. The potential is retarded from the projectile by a distance of abcut $0.1v_I/\omega_s$, where ω_S is the surface plasmon frequency.[10] This retardation causes the acceleration of CE. The potential also repells CE from the surface towards vacuum, and makes them deviate from the projectile trajectory. When v_a is the velocity increased by the potential, its value is proportional to q, because the height of the potential is proportional to q. Its direction with respect to the outgoing part of the ion trajectory, θ_a, is independent of projectile species; based on classical mechanics, it

depends approximately only on the initial phase space coordinates of CE. The velocity of accelerated electrons is given by the vector sum of v_a and v_I. The energy increase is given by $E_e - E_I \sim v_I \Delta P \cos\theta_a$, where $\Delta P (=mv_a)$ is the impulse due to this potential.

The energy increase is expected to be proportional to projectile charge q, because the impulse ΔP is proportional to q. This is supported by the experimental results(I). The line width shcuild increase with increasing q, because line broadening is a result of the energy variation for different trajectories of electrons, which are emitted at the same emission angle, and because the energy difference will increase with q. This is also consistent with the result(II). Results(III) and (IV) are explained, because for a large charge q, v_a is also large and the deviation of emission angles of electrons from v_I will be larger than 3°, and the deviation will increase with q. Thus DIP acceletation model is well consistent with the above experimental results. Furthermore, based on the DIP acceleration model, Iitaka et al. carried out a numerical calculation of energy increase of CE.[11] They calculated, using a Monte Carlo method, trajectories for a large number of CE which were induced by a projectile moving parallel to the surface and accelerated by DIP approximated by a simple dypole potential, as used by Winter et al., in which retardation of polarization was taken into account. The calculated energy increases were almost equal to the experimental results from Koyama et al.. Recently, Hasegawa et al. calculated analytically incident energy-dependence of energy increase by DIP, and obtained results qulitatively well consistent with their experimental results.[12] Therefore, it is concluded that when a projectile is incident at a grazing angle to a surface, CE are accelerated by DIP.

References

1) Y。H。Ohtsuki, Charged Beam Interactions with Solids (Taylor & Francis, London, 1983)。
2) . M. Echenique, R.H.Ritchie, N.Barberan, and J.Inkson, Phys. Rev. B23, 6486 (1981).
3) Y。Yamazaki, and N. Oda, Phys. Rev. Lett. 52, 29 (1984).
4) J. Burgdorfer, Nucl. Instrm. Methods., Sect. B24/25, 139 (1987).
5) L. F. de Ferrariis and R. A. Baragiola, Phys. Rev. A33, 4449 (1986).
6) M. Hasegawa, K. Kimura, and M. Mannami, J. Phys. Soc. Jpn. 57, 1834 (1988).
7) H. Winter, P. Stromeier, and J. Burgdorfer, Phys. Rev. A39, 3895 (1989).
8) A. Koyama, Y. Sasa, H. Ishikawa, A. Misu, K. Ishii, T. Iitaka, Y. H. Ohtsuki, and M. Uda, Phys. Rev. Lett. 65, 3156 (1990).
9) N. Stolterfoht, D. Schneider, D. Burch, H. Wieman, and J. S. Risley, Phys. Rev. Lett. 33, 59 (1974).
10) P. M. Echenique, F.Flores, and R. H. Ritchie, Solid State Phys. 43, 229 (1990).
11) T. Iitaka, Y. H. Ohtsuki, A. Koyama, and H. Ishikawa, Phys. Rev. Lett. 65, 3160 (1990).
12) M. Hasegawa, T. Fukuchi, T. Mizuno, K. Kimura and M. Mannami, Nucl. Instr. Methods., Sect. B, in press.

7. ION BEAM AND SOLID STATE PHYSICS

Michi-hiko MANNAMI

Department of Engineering Science, Kyoto University,
Yoshida, Sakyo-ku, Kyoto 606

§1. Application of ion beam to the studies of solid

Industrial application of ion beam is developing rapidly and many small accelerators are now used in production lines. Analytical methods using ion beam irradiation are now commonly used, e.g., SIMS, RBS, INS, PIXE. All these methods are called by acronyms and sound like the methods based on new physical concepts, however, they are mostly based on fundamental physical concepts, except INS. The outcome of the progress has not only enriched and widened our scope in solid state physics, but also brought us new interesting states of solids produced by ion beams, for instance, metastable alloys produced by ion implantation, sub-micron electronic devices, clusters produced by sputtering, which offer new scope in the studies of solid states.

One of the new concepts discovered during the last thirty years in this research field with ion beam is ion channeling. This was first found in a computer simulation of radiation damages in solid by Robinson and Oen which showed that some exceptionally long trajectories result from atoms travelling within the open channels between close-packed rows of atoms. Experimental verifications of channeling were reported 1965 from Chalk River, Harwell and München.

Channeling has been applied in various fields related to the studies of crystals since the late 60's. There are two important contributions of the channeling in the studies of solids: Lattice site determination of foreign atoms by channeling is a unique methods which cannot be done by any other methods. Determination

of surface atomic arrangement by RBS/channeling, including ISS or ICISS, is also worth mentioning. It must be noted, however, that the information obtainable by these methods is of atomic and not of electronic level. Except for the ion neutralisation spectroscopy (INS), where the electron transfer between projectile ion and surface is studied, it is not easy to study the electronic state of solid by ion scattering. In most of ion-solid interaction processes, the primary processes are more or less related to electronic excitation in solid. However, the cross sections of the collisions in solid are large, and elementary scattering process is embedded in the multiple scattering and the details of the elementary process is difficult to extract from the observable quantities.

Ions at channeling are steered by rows (planes) of atoms within open channel by correlated series of small angle multiple scattering and cannot approach to the rows (planes) closer than the distance of the order of Thomas Fermi screening distance. Results of these large impact parameter collisions, which are mostly affected by the outershell or valence band electrons, are embedded in the multiple scattering. This situation is not different from that at ion scattering in an isotropic solid. Successful applications of channeling to the studies of solid as mentioned above are based on the detection of rare collisions with small impact parameters, which are superposed on multiple scattering of large impact parameters collisions, e.g., large angle scattering of channeling ion with atoms displaced in the channel in the lattice site determination of interstitial atoms.

This is the reason why we cannot study electronic states of solid by the methods based on ion scattering. In ion neutralisation spectroscopy, however, experimental conditions are so arranged that the projectile slow ion interacts only with surface in vacuum and the change in their states after being reflected from the surface without penetrating the surface is observed, thus

the state of solid electrons near the surface can be studied.

In comparison with ion-gas collisions, the characteristics of atomic collisions in solid lie in the ion scattering caused by valence or outershell electrons. One of the important phenomena in this respect is the dynamic response of valence electrons to the energetic ion during the passage in solid. Valence electrons respond to the charge of fast moving ion and the density oscillation of conduction electrons is produced along the ion trajectory. This is known as the "wake" which trails behind the projectile ion. This has been extensively studied both theoretically and experimentally. Experimental observation of the "wake" was done in the studies of dissociation of molecular ions in solid, where the one of the fragment ions is trapped in the potential field caused by the wake of the foregoing fragment.

§2. Surface study

Dynamic response of solid electrons in the ion-surface interaction plays an important role in the inelastic scattering of slow projectile ion at the surface. When the velocity of ion in vacuum is smaller than the Fermi velocity of valence electrons, solid electrons respond to the external charge and induce a potential distribution in the vacuum similar to that of image charge. The electronic states of the projectile ion are modified by the field and this modification depends on the distance of ion from the surface. This change in states affects inelastic scattering process that takes place at the surface as observed in INS. Response of surface electrons to ion in vacuum with velocity faster than those of solid electrons is similar to the wake in the bulk of solid. A periodic potential field is induced in vacuum near the surface and affects both elastic and inelastic scattering events of the ion. However, the material parameters in the dynamic response of valence electrons are only the plasma frequencies, either bulk or surface, and lifetmes of the plasmons.

We have been studying glancing angle scattering of MeV ions at clean crystal surfaces, for the purpose to study inelastic scattering of ions with surface electrons. The glancing angle scattering at surface is similar to that at planar channeling; ion is reflected away by a plane of surface atoms by a series of small angle scattering into the angle of specular reflection, and its trajectory is well described by the continuum planar potential which has been successfully applied to planar channeling.

As in the case of channeling, most of the inelastic scattering events of ions with surface are governed by the multiple small angle scattering during the specular reflection. Stopping power for the reflecting ions and the charge states of the reflected ions are explained in terms of position dependent probabilities and we cannot derive the elementary scattering process from the states of reflected ions. Effects of "surface wake" have been observed in the stopping power of surface for the reflecting ions and in the angular and energy distributions of the reflected fragment ions at the dissociation of molecular ions. Superposed on the multiple small angle scattering, we found collisions of ions with surface steps, where the impact parameters of the collisions are small. Density and distribution of steps on the surface can be obtained from the inelastic scattering of ions when the situation is favourable.

Although no epock making discovery worth Nobel prize has been made during the past thirty years in the physics of ion-solid interaction, many accelerators are now in daily use in research and technology. As it can be seen from the fact that several international conferences on application of accelerators being held every year, we are in need of better understanding of the passage of charged particles through matter, which has been studied since the discovery of atomic structure by Rutherford.

8. PHYSICS OF ION BEAM

Yoshiharu Mori

(No paper was submitted)

9. THEORY OF HIGH-ENERGY ION-ATOM COLLISIONS

Nobuyuki TOSHIMA

Institute of Applied Physics, University of Tsukuba

When ions collide with atoms, various kinds of physical processes can be expected to occur depending on the magnitude of collision energy. Several MeV are required for nuclear reactions, while even a few eV energy can easily induce some chemical reactions. On the other hand, transitions between electronic states can take place over an extremely wide energy region spreading from a few eV to several GeV. This report surveys recent progress of the theoretical research for electronic transitions. The collisional energies usually are classified into three ranges referring to the ratio of the projectile velocity and the average orbital velocity of the active electron. When this ratio is much larger than unity, we may expect that the electronic states are not perturbed seriously during the collision because of the short collision time and the perturbation theory that is peculiar to high-energy collisions can be applied successfully. However, some exceptional cases are known to exist in which traditional perturbative treatments break down even at extremely high energies.

One of the most typical example is the problem of the Thomas double scattering in electron-capture processes. The first Born cross section for 1s-1s transitions decreases rapidly in proportion to E^{-6} (E: collision energy) while the second Born cross section shows slightly weaker energy dependence as $E^{-5.5}$, and the latter eventually becomes dominant in the high-energy limit.[1] Drisko has shown that this second-order term contains a contribution of the double scattering process proposed originally by Thomas in the framework of the classical mechanics. After this discovery many theoretical approaches have been developed for the study of this double scattering mechanism. The inversion of the first- and the second-order terms implies the essential failure of the perturbation theory. Nevertheless most of the existing theories are based on the traditional perturbation theory. Recently the author has succeeded for the first time in the analysis of this problem using non-perturbative procedures, the classical trajectory Monte Carlo method[2] and the coupled-channel calcula-

tions.[3] These calculations confirm that the Thomas double scattering process also plays a decisive role even after the inclusion of the all-order terms but the higher-order terms modify the idealized picture considerably in some cases. An interference effect between the projectile and the target continuum states are found and this causes an oscillatory structure in the differential cross sections that are totally absent in the perturbative treatment.

For the relativistic collisions, the criterion of the velocity ratio becomes unclear since all the velocities have the ceiling limit of the light velocity. K-shell electrons of a heavy nucleus such as uranium have an average orbital velocity that is nearly equal to the light velocity and the condition of high-energy collisions can never be satisfied. This indicates that the perturbative treatment may not work even for ultra-relativistic collisions. Fully relativistic coupled-channel equations based on two-center atomic expansions are solved[4] and the results are compared with other existing perturbation theories and experimental data. In these calculations extremely long-ranged couplings are found that arise purely from the relativistic effect related to the Lorentz transformation. The appropriate consideration of this long-range nature is inevitable and it makes the cross sections change by a factor of two.[5] Some theoretical approaches that are simply extended from their original non-relativistic version show unphysical spin-flip cross sections. A warning has been given to the easy extension of the symmetrization procedure for distorted-wave formalism.[6] Any relativistic theory should merge into the nonrelativistic limit from which it is constructed as an extension.

References

1) R. Shakeshaft and L. Spruch, Rev. Mod. Phys. 51 (1979) 369.
2) N. Toshima, Phys. Rev. A42 (1990) 5739.
3) N. Toshima and J. Eichler, Phys. Rev. Lett. 66 (1991) in press.
4) N. Toshima and J. Eichler, Phys. Rev. Lett. 60 (1988) 573; Phys. Rev. A38 (1988) 2305.
5) N. Toshima and J. Eichler, Phys. Rev. A42 (1990) 3896.
6) N. Toshima and J. Eichler, Phys. Rev. A41 (1990) 5221.

10. CHARGE STATE DISTRIBUTION MEASUREMENTS OF 25.3 AND 77MeV／U ARGON IONS WHICH HAVE PASSED THROUGH A CARBON FOIL

Yasuyuki Kanai, Tadashi KAMBARA, Yohko AWAYA, Akira HITACHI, Takashi NIIZEKI, Yaming ZOU, and Kunihiro SHIMA*

The Institute of Physical and Chemical Research(RIKEN),
* Tandem Accelerator Center, University of Tsukuba

We measured the charge-state distributions of 25.3 and 77 MeV/u Ar ions which have passed through a carbon foil with varying the foil thickness(10 μg - 4.27 mg/cm^2) and incident charge states(16+ - 18+). The study aims to get (1) the equilibrium charge distribution of Ar ions which have passed through a carbon foil and (2) the charge changing cross sections(capture and loss cross sections) of Ar ions which collide with carbon atoms. Projectiles of 25.3 and 77 MeV/u Ar ions were obtained from RIKEN Ring Cyclotron. Projectiles of $Ar^{16+,17+,18+}$ ions were produced by using Al or C foils and then selected by a magnet. The experiment was performed at the atomic physics beam line(E2B); the targets were placed in the general purpose experimental chamber on the E2B beam line. The charge states of the Ar ions which have passed through the target were analyzed with a charge analyzing magnet and a position-sensitive parallel-plate avalanche counter(PPAC).

When the target was thicker than about 1 mg/cm^2, the charge-state-distributions did not depend on the target thickness. We concluded therefore that the distribution is equilibrated as shown in Table 1. Shima proposed a semi-empirical formula for the equilibrium charge-

Energy (MeV/u)	Mean charge $\bar{q}$	Charge state fraction 16+	17+	18+
25.3	17.98	1.2 (-4)	2.0 (-2)	9.80 (-1)
77	17.9994	5 (-7)	5.6 (-4)	9.994 (-1)

Table 1. Equilibrium charge-state distributions of 25.3 and 77 MeV/u Ar ions after passing through carbon targets. Numbers in parentheses stand for the power of ten.

state-distribution of high energy ions(> 10 MeV/u) after passing through the carbon foil.[1] Our results for 25.3 MeV/u Ar ions are in good agreement with the values obtained from Shima's formula. However, the Ar^{17+} fraction of our results for 77MeV/u is larger than the value obtained from Shima's formula. This difference may be due to the difference in a dominant process of the electron capture of the Ar ions between 25.3 and 77 MeV/u. From our recent measurements of a radiative electron capture(REC) cross section of Ar^{18+} collide with carbon atoms, we found that the ratio betweem the REC cross section and total electron capture cross section of 25.3 and 77 MeV/u Ar^{18+} ions were 3% and 58%, respectivly.[2,3]

Using the charge-state distributions for thin targets(10 - 38.5 $\mu g/cm^2$), we obtained the electron capture and loss cross sections of 77 MeV/u Ar ions which collide with carbon atoms. Preliminary results are shown in Table 2(including our recent results of REC measurements). Precise analysis is in progress.

Initial charge state	Final charge state	Cross section(cm^2) 25.3 MeV/u	77 MeV/u
16+	17+	16 (-20)	5.9 (-20)
17+	18+	7.8 (-20)	2.9 (-20)
17+	16+	2.7 (-21)	1.3 (-23)
18+	17+	4.5 (-21)	3 (-23)
(Radiative electron capture)			
18+	17+	1.6 (-22)	1.8 (-23)

Table 2. Preliminary charge changing (electron capture and loss) cross sections of 25.3 and 77 MeV/u Ar ions collide with carbon atoms. Numbers in parentheses stand for the power of ten.

References

1) K. Shima, N. Kuno, and M. Yamanouchi: Phys. Rev. **A40** (1989)3557.
2) Y. Awaya, A. Hitachi, T. Kambara, Y. Kanai, K. Kuroki, and T. Mizogawa: RIKEN Accel. Prog. Rep., **23**(1989)46.
3) Y. Kanai, T. Kambara, Y. Awaya, A. Hitachi, T. Niizeki, Y. Zou, and K. Shima: to be published in RIKEN Accel. Prog. Rep., **24**(1990).

11. A BRIEF REVIEW OF RADIATION EFFECT OF HIGH Tc SUPERCONDUCTING MATERIALS

Yukio KAZUMATA

Japan Atomic Energy Research Institute,
Tokai-mura, Naka-gun, Ibaraki-ken, 319-11, japan

Radiation effects of high T_c superconductors will be briefly reviewed. It is the principal problem of radiation effects on high T_c materials to study the correlation between the various parameters for superconductivity and lattice defects. The following examples will be the characteristic parameters of superconductivity;

T_c (critical temperature)
J_c (critical current density)
H_{c2} (upper critical field)
H_{c1} (lower critical field)
ξ (coherence length)
λ (penetration depth)

To date radiation effects on the three parameters for superconductivity T_c, J_c and H_{c2}, have been reported in the literature. The last parameter, H_{c2}, has received the least attention of the three, due to this we will restrict our review to the other two. Two methods we usually used to introduce lattice defects into solids; these are with and without irradiation. Quenching and impurity doping are the typical examples of the latter. As for the former , all of the available irradiation sources are used to study the radiation effects on high T_c materials. These sources are (1) X- and γ-rays, (2) electrons, (3) neutrons and (4) various ions. In these sources, X- and γ-rays are distinct, because only electron excitations are effective to displace lattice atoms, which is a rather indirect process for displacement. The other sources are particles and the direct collisions to lattice atoms govern defect formation.

As for γ-ray irradiation, three quite different results

are reported. All of these experiments are done with ^{60}Co γ-rays; photon energies of 1.17 and 1.33 MeV. Vasek et al[1] report the decrease of T_c from the measurements of resistivity and ac susceptibility. Boiko et al[2] observe the increase of T_c in $Y_{0.2}Sn_{0.2}Ba_2Cu_3O_{7-y}$ by electrical resistivity measurements, but our results[3] show no change of T_c. Therefore, we have not come to a firm conclusion as yet.

As for particle irradiations, electrons, neutrons and ions produce their respective characteristic defects. The first displaced atoms by incident particles are called the primary knockon atoms (abbreviated as PKA). When these PKA have large energies far beyond the threshold energy (the energy required to displace lattice atoms), the second displaced atoms have large energies enough to displace 3rd atoms, and so on as shown in Fig.1. These consecutive collisions, cascade collisions, will form clustered defects. Therefore, a general idea of defects such as a size and structure will be outlined from PKA spectrum. Fig.2 represents schematic PKA spectrum[4]. The peak of the PKA energy by 0.8 MeV electrons lies at about 60 eV and only a few atoms are possibly displaced by the PKA on assuming 30 eV threshold energy. As a consequence, point defects will be dispersed in the specimen by the 0.8 MeV electron irradiation. On the contrary, neutron irradiation will produce large energy PKA with 10^5 eV and the collision cascade by these PKA will form clustered defects. As for ion irradiation such as 1 MeV P or 100 MeV Br ions, these PKA show broad spectra, which predict formation of various kinds of defects from points to clustered defects. These consideration suggest that neutron irradiation is the most suitable to low T_c materials for flux pinning because the coherence lengths of the materials are the order of several hundred A and the defects of the same size will be the most effective. However, in high T_c materials the coherence lengths lie in the range from several to a few tens of A, and consequently point defects produced by electrons and ions are also effective for flux

pinning.

Next, we will describe the results by electron, neutron and ion irradiation. As for electron irradiations, the decreases of T_c reported up to now are listed in Table 1 [5-12] and a glance of the Table gives the estimation of at most 1 K/10^{18} e/cm^2. Further, a linear relation between degradation of T_c and an increase of the resistivity above T_c is given by Rullier et al[12] for La compounds as shown in Fig.3. This relation is quite general and holds also in Y and Bi compounds. The comparison between single crystals and sintered materials was done for the Y compounds by Vichery et al[9] as shown in Fig.4. In this Fig., the x and y axes show T_c of before the irradiation and the decrement of T_c divided by 10^{18} e/cm^2, respectively. Single crystals with higher T_c are resistive to the irradiation but sintered specimens are very sensitive.

Two methods are usually used to measure J_c; one is the transport method which measures an actual current density by the four probe method and the other is the magnetic method which measures a hysteresis loop, M-H curve and J_c is calculated from the loop on the assumption of Bean's model. The change of J_c by the magnetic method (magnetic current density) is shown in Fig.5 as a function of irradiation dose[13-14]. The increase by the irradiation is higher at higher magnetic field and linearly increases with an increase of the dose up to 1.5x10^{18} e/cm^2 and turns to decrease above the dose. In next section we will give our results in more details.

The rate of T_c decrease by neutron irradiation is listed in Table 2[15-23]. The decrease of T_c is estimated to be 3 K/10^{18} n/cm^2 for Y compound and the similar value is given for La compounds, but in Bi compounds a value a few times larger is indicated. As for J_c, the transport method shows a decrease after irradiation as listed in Table 3(J_c=160 A/cm^2 drops to below tenth after a dose of 8.7x10^{17} n/cm^2, and very weak magnetic fields give remarkable effects to the J_c's decrease.). On the contrary to the transport method,

the magnetic method shows an increase by the irradiation. For sintered Y compounds, the J_c after a dose of $1x10^{17}$ n/cm^2 is 2.1 times at 4.2 K as large as that before the irradiation. The results for single crystals of the Y compound is shown in Fig.6[27]. The increase in J_c for the applied field being parallel to a or b axis is much larger than that for the field in c-axis, and consequently the anisotropy of the J_c disappears with an increase in the dose.

The results by ion irradiations are similar to those for neutron irradiations, but one characteristic feature is observed in a resistivity - temperature curve. For sintered specimens, ion irradiations leave the onset temperature unchanged, but shift the offset one to lower temperature, and as a result a broadening of the transition temperature is observed as shown in Fig.7[28]. For high quality thin films, however, without broadening shifts the curve to lower temperature as shown in Fig.8[29], which means the same change of the onset and offset temperatures by the irradiation. A general rule for ion irradiations is derived by Summers et al[30]. As shown in Fig.9, the reduction of T_c is linearly proportional to the nonionizing energy loss (nuclear collision). Furthermore, the comparison of the reduction of T_c between high and low T_c materials is done by Rummel et al as shown in Fig.10[31]. High T_c materials are much more sensitive to irradiation which compared with low T_c materials. As for J_c, a slight increase is observed in a certain magnetic field, 3 T in Fig.11, by the transport method, although without the field such an increase is not found[29]. The magnetic method shows an increase of J_c as shown in Fig.12[32]. However, it is noteworthy that the specimen used in the transport method is thin film, but the sintered bulk materials are used in the magnetic method.

In summary :

1.One displaced atom per 10^4 lattice atoms yields 1 K decrease of T_c for the Y compound, but for the Bi compound a more radiation sensitive value, three times or more larger

value, is observed.

2.The decrease of T_c will be determined only by the number of displaced atoms, but will be independent of detailed structure of defects.

3.The transport J_c decreases, but the magnetic J_c increases by irradiation. This fact indicates the decrease of intergrain J_c and the increase of intragrain J_c by irradiation.

References

1.P.Vasek, L.Smrcka, J.Dminec, M.Pesek, O.Smrckova and D.Sykorova; Solid State Commun. 69 (1989) 22-25.
2.B.B.Boiko, F.P.Korshunov, G.V.Gatalskii, A.I.Akinov, V.I.Gatalskaya, S.E.Demyyanov and E.K.Stribak; Phys. Stat. Sol.(a) 107 (1988) K139-144.
3.T.Kato, M.Watanabe, Y.Kazumata, M.Naramoto, T.Iwata, Y.Ikeda, H.Maekawa and T.Nakamura; Jpn.J.Appl.Phys. 27 (1988) L2097-2099
4.A.Iwase; Private commun.
5.A.Hofmann, H.Knonmuller, N.Moser, R.Reisser, P.Schule and F.dworshak; Physica C156 (1988) L2339-2341.
6.B.Stritzker, W.Zander, F.Dworchak, U.Poppe and K.Fischer; Mat.Res.Soc.Symp.Proc. 99 (1988) 491-495.
7.V.F.Zelenski, I.M.Neklyndov, Yu.T.petrusenko, A.N.Sleptsov and V.f.Finkel; Physica C153-155 (1988) 850-851.
8.M.Watanabe, T.Kato, H.Naramoto, H.Maeta, K.shiraishi, Y.Kazumata, A.Iwase and T.Iwata; Advances in Superconcutivity (Proc. 1st Inter. Symposium on Superconductivity, eds. Kitazawa and Ishiguro) p469-474.
9.H.Vichery, F.Ruller-Albenque, M.Konczykowski, H.Pascard, R.Korman, G.Collin and D.Favrot; Physica C162-164 (1989) 749-750.
10.Y.Kazumata, S.Okayasu and T.Kato; to be published.
11.K.Shiraishi, H.Itoh and O.Yoda; Jpn.J.Appl.Phys. 27 (1988) L2339-2341.
12.F.Ruller-Albenque, J.Provost, F.Studer, D.Groult and B.Raveau; Solid State Commun. 66 (1988) 417-420.
13.K.Shiraishi, T.Kato and J.Kuniya; Jpn.J.Appl.Phys. 28 (1989) L807-809.
14.T.Kato, K.Shiraishi and J.Kuniya; Jpn.J.Appl.Phys. 28 (1989) L766-768.
15.J.O.Willis, J.R.Cost, R.D.Brown, J.d.Thompson and D.E.Peterson; Mater.Res.Soc.Symp.Proc. 99 (1988) 391-394.
16.P.Przyslupski, A.Wisniewski, S.Kolesnik, W.Dobrowolski, A.Pajaczkowska, K.Pytel and B.Pytel; Physica C153-155 (1988) 345-346.
17.A.Umezawa, G.W.Crabtree, J.Z.Liu, H.W.Weber, W.K.Kwok, L.H.Nunez, T.J. Moran, C.H. Sowers and H.Claus; Phys.Rev. B36 (1987) 7151-7154.
18. Kupfer, I.A. Apfelstedt, W.Schauer, R.Flukiger, R.Meier-Hirmer, H.Wuhl and H.Scheurer; Z.Phys. B- Condensed Matter 69 (1987) 167.
19.B.A.Aleksashin, I.F.Berger, S.V.Verkhovskii, V.I.Voronin, B.N.goshchitskii, S.A.Davydov, A.E.Karkin, V.L.Kozhevnikov, A.V.Mirmelshtein, K.N.Mikhalyov, V.D.Parkhomenko, S.M.Cheshnitskii; Physica C153-155 (1988) 339-340.
20.P.Muller, H.Gerstenberg, M.Fischer, W.Schinder, J.Strobel, G.Saemann-Ischenko and H.Kammerneier; Solid State Commun. 65 (1988) 223-225.
21.J.R.Cost, J.O.Willis, J.D.Thompson and D.E.Peterson; Phys.Rev. B37 (1988) 1563-1568.
22.S.T.Sekula, D.K.Christen, H.R.Kerchner, J.R.Thompson,

L.A.Boatner and B.C.Sales;
Jpn.J.Appl.Phys. 26 Supplement 26-3 (1987) 1185-1186.
23.Y.Herr, K.Lee, C.Kim, H.Lee, C.Kim. G.Hong and O.Won;
Jpn.J.Appl.Phys. 28 (1989) L1561-1563.
24.K.V.Rao, R.Puzniak, D.X.Chen, NKarpe, M.Baran,
A.Winiewski, K.Pytel, H.Szymzek, K.Drybye and J.Bottiger;
Physica C153-155 (1988) 347-348.
25.A.Wisniewski, M.Baran, P.Przyslupski, H.Szymszak,
A.Pajaczkowska, B.Pytel and K.P.Pytel;
Solid State Commun. 65 (1988) 577-580.
26.J.O.Willis, J.R.Cost, R.D.Brown, J.D.thompson and
D.E.Peterson; Mater.Res.Soc.Symp.Proc.99 (1988) 391-394.
27.F.M.Sauerzopf, H.P.Wiesinger, H.W.Weber, G.W.Crabtree,
and J.Z.Liu; Physica C162-164 (1989) 751-752.
28.A.Iwase, M.Masaki, T.Iwata, T.Nihira and S.Sasaki;
Jpn.J.Appl.Phys. 27 (1988) L2071-2074.
29.B.Roas, B.Hensel, G.Saemann-Ischenko and L.Schultz;
Appl.Phys.Lett. 54 (1989) 1051-1053.
30.G.P.Summers, E.A.Burke, D.B.Chrisey, M.Nastasi and
J.R.Tesmer; Appl.Phys.Lett. 55 (1989) 1469-1471.
31.J.Remmel, J.Geerk, G.Linker, O.Meyer, R.Smithey,
B.Strehlan and G.C.Xiong; Physica C165 (1990) 212-220.
32.J.O.Willis, D.W.Cooke, R.D.Brown, J.R.Cost, J.F.Smith,
J.L.Smith, R.M.Aikim and M.Maez;
Appl.Phys.Lett. 53 (1988) 417-419.

Table 1. Change of T_c by electron irradiation

Specimen	T_{co} (Before irrd.)	Change of $T_c/10^{18}e/cm^2$	Energy of electrons	Irrad Temp.	Ref.
1. $YBa_2Cu_3O_7$ (poly)	92K	~−0.3K	2.7 MeV	<40K	(5)
2. $YBa_2Cu_3O_7$ (poly)	97K	~−0.5K	3.0 MeV	<20K	(6)
3. $YBa_2Cu_3O_x$	89K	~ 2K	30 MeV	5K	(7)
		~−0.5K	〃	185K	(7)
		~−2.2K	〃	375K	(7)
4. $YBa_2Cu_3O_x$					
$x=6.9$	89K	~−1.0K	3.0 MeV	RT	(8)
$x=6.6$	70K	~−1.0K	〃	〃	
5. $YBa_2Cu_3O_x$					
single	81K	~−0.45K	2.5 MeV	−20K	(9)
single	90.2K	~−0.21K	〃	〃	
Poly	91.8K	~−0.25K	〃	〃	
Poly	89.8K	~−0.27K	〃	〃	
6. $YBa_2Cu_3O_x$					
$x=6.9$	90K	~−1.5K	3.0 MeV	RT	(10)
$x=6.6$	60K	~−7.0K	〃	〃	(10)
$x=6.4$	35K	~−4.6K	〃	〃	(10)
7. $YBa_2Cu_3O_7$	92.5K	~−0.3K	3.0 MeV	RT	(11)
8. $La_{1.85}Sr_{0.15}CuO_4$	35.5K	~−0.3K	2.5 MeV	20K	(12)
9. $La_{1.8}Sr_{0.2}CuO_4$	35.1K	~−0.5K	〃	〃	(12)

Table 2. Change of T_c by neutron irradiation

Specimen	Change of $T_c/10^{18}$ n/cm^2	Ref.
1. $YBa_2Cu_3O_x$ (poly)	−2.7 K	(15)
2. $YBa_2Cu_3O_x$ (poly)	−1.3 K	(16)
3. $YBa_2Cu_3O_x$ (single)	−2.6 K	(17)
4. $YBa_2Cu_3O_x$ (poly)	−2.1 K	(18)
5. $YBa_2Cu_3O_x$ (poly)	−5.0 K	(19)
6. $YBa_2Cu_3O_x$ (single)	−38.0 K (Low Temp. Irrad.)	(20)
7. $YBa_2Cu_3O_x$ (poly)	−2.5 K	(21)
1. $La_{1.85}Sr_{0.15}CuO_4$ (poly)	−2.3 K	(22)
1. Pb-doped BiSrCaCuO	−10.5 K	(23)

Table 3. Change of transport J_c by neutron irradiation

- Przyslupski et al. (Physica C 153-155 (1988) 345)[16]

Before irrad.	160 A/cm at 77K
2.4 x 10^{17} n/cm^2	73.4
8.7 x 10^{17} n/cm^2	14.5

- Rao et al. (Physica C 153-155 (1988) 347)[24]

Transport critical current at 4.2K (A/cm)

Field (O)	60	80	100	120
Before irr.	1220	870	600	120
$2 \cdot 10^{16}$ neutr. /cm^2	210	140	100	80
$1 \cdot 10^{17}$ neutr. /cm^2	42	35	26	20

Table 4

Critical magnetzation current

- Wisniewski et al.
  Solid state commun. 65 (1988) 577
  Polycrystal : $YBa_2Cu_3O_x$

Critical current densities in A/cm at H=10 kOe

T (K)	4.2	42	77
sample			
Before irrad.	1×10^4	0.5×10^3	29
2×10^{16} n/cm^2	1.4×10^4	1.7×10^3	2.4×10^2
1×10^{17} n/cm^2	2.1×10^4	4.2×10^3	5.2×10^2

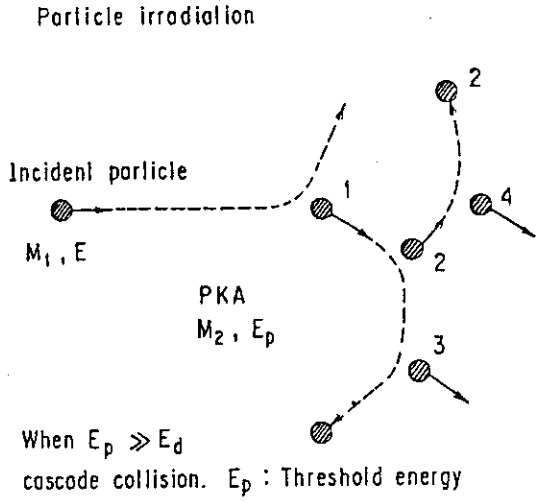

Fig. 1 Schematic diagram for displacement of lattice atoms by particle irradiation

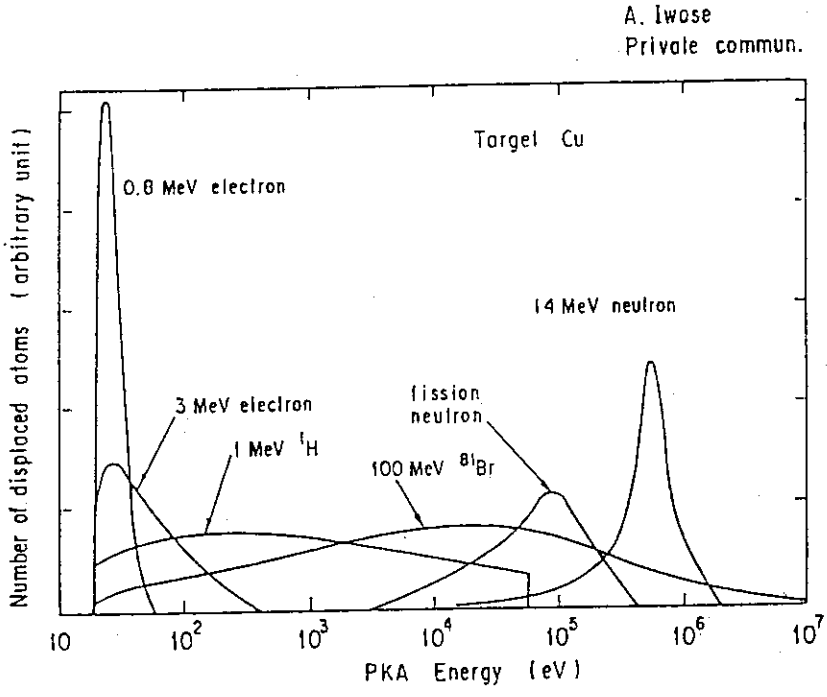

Fig. 2 PKA spectra

Correlation between (T_c/T_{co}) and $R(40K)/R_0(40K)$

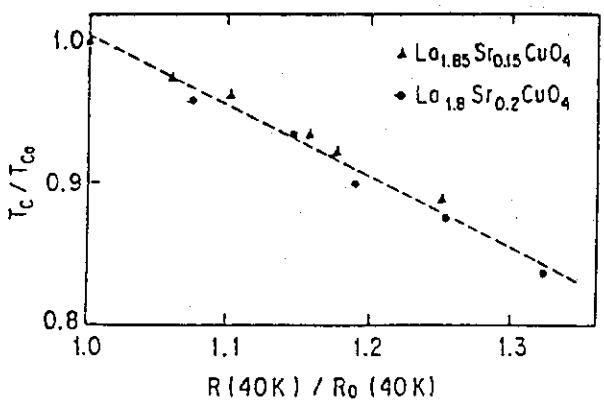

Rullier-Albengue et al.
Solid State Commun. 66 (1988) 417

Fig.3 Correlation between (T_c/T_{co}) and $R(40K)/R_0(40K)$

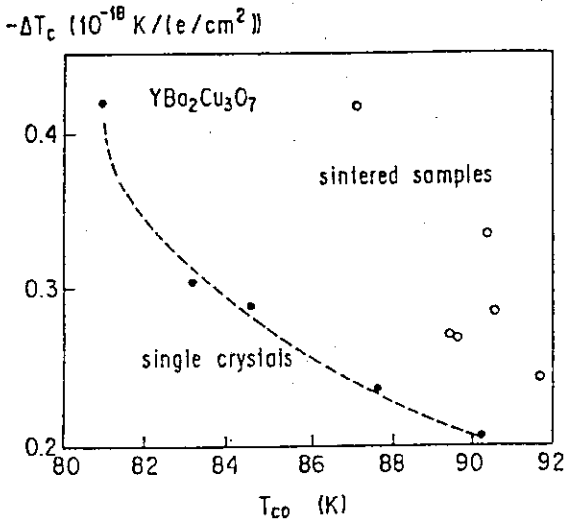

H. Vichery et al.
Physica C 162-164 (1989) 749

$\Delta T_c = dT_c/d(\phi t)$

2.5 MeV electrons
20 K Irrad.

Fig.4 Change of T_c in various T_{co} specimens.
X-axis : T_c before irrad. (T_{co})
Y-axis : Change of T_c per a dose of 10^{18}e/cm^2

Change of J_c by 3 MeV electron irradiation

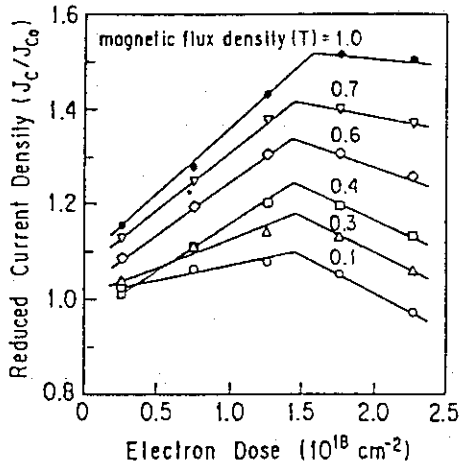

$YBa_2Cu_3O_{7-x}$

K. Shiraishi et al.
Jpn. J. Appl. Phys. 28 (1989) L807

3 MeV electrons.
Irrad. temp. ~ 370K

Fig.5 Dose dependence of reduced J_c (J_c/J_{co})

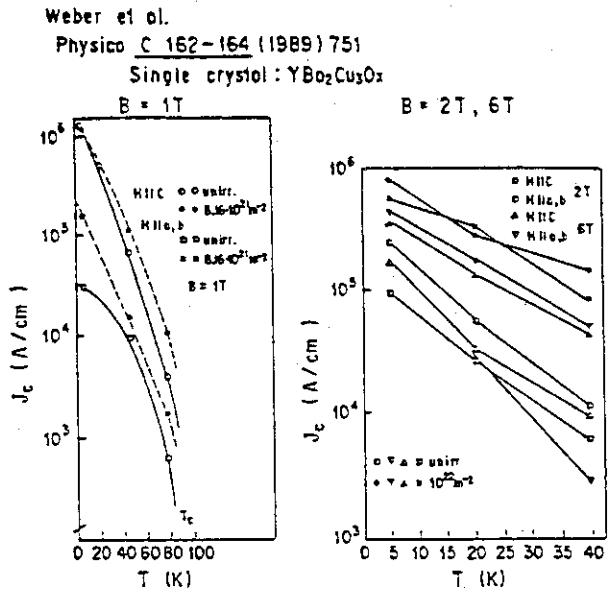

	Anisotropy Ratio $J_c(c)/J_c(ab)$		Enhancement Ratio J_c/J_{co}	
	Irradiated sample	Unirradiated sample	H∥a,b	H∥C
6K	6.75	43.60	5.00	1.00
45K	7.27	7.25	1.67	1.67
77K	5.49	6.48	2.83	2.40

Fig. 6 Change of J_c in single crystals by neutron irradiation

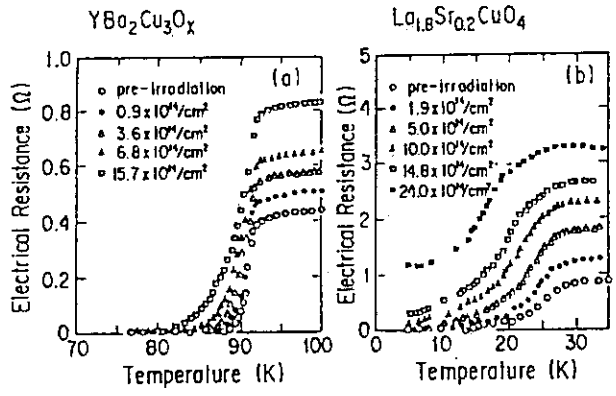

120 MeV ^{16}O Irradiation
$YBa_2Cu_3O_x$ LNT : $La_{1.8}Sr_{0.2}CuO_4 < 10$ K
A. Iwase et al. Jpn. J. Appl. Phys. 27 (1988) L2071

Fig. 7 ρ-T curves for $YBa_2Cu_3O_x$ and $La_{1.8}Sr_{0.2}CuO_4$ irradiated by 120 MeV ^{16}O ions
Irradiation temperature: $YBa_2Cu_3O_x$ at NT. $La_{1.8}Sr_{0.2}CuO_x$ below 10K

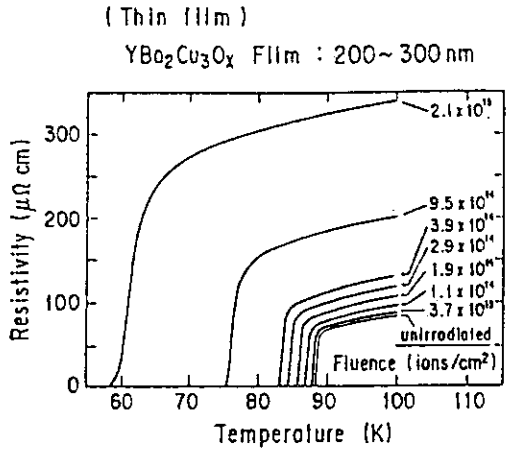

B. Roos et. al.
Appl. Phys. Lett 54
(1989) 1051

25 MeV ^{16}O
77 K

Fig.8 ρ-T curves for $YBo_2Cu_3O_x$ thin film irradiated by 25MeV ^{16}O ions at 77K

Empirical rule for the change of T_c by irradiation

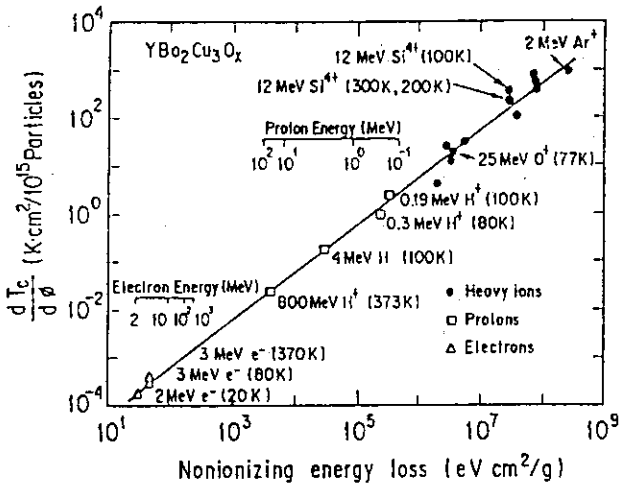

G. P. Summers
et al.
Appl. phys. Lett
55 (1989) 1469

Fig.9 Empirical rule for the change of T_c by ion irradiation
X axis : Energy loss by nuclear collision
Y axis : Decrease of T_c per the dose of $10^{15}/cm^2$
The gradient of the line : 0.95 ±0.2

The change of T_c in superconducting materials by irradiation

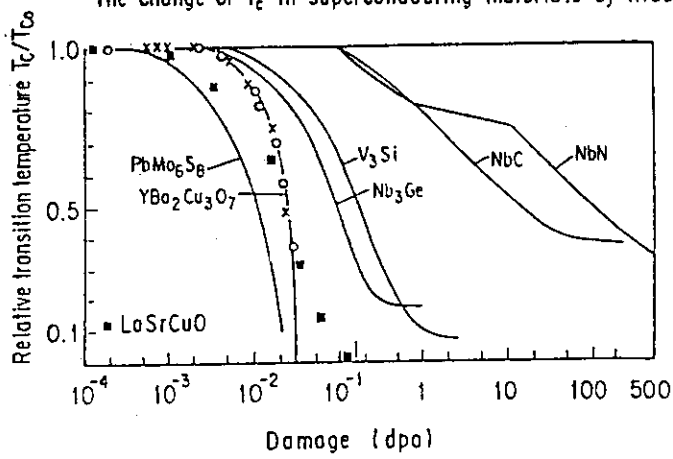

J. Remmel et al.
Physica C 165
(1990) 212

Fig.10 Comparison of the change of T_c of several superconducting materials by irradiation

$$dpa = \frac{\text{The number of displaced atoms}}{\text{The atomic density of target}}$$

○ Transport critical current
$YBa_2Cu_3O_x$ Film.

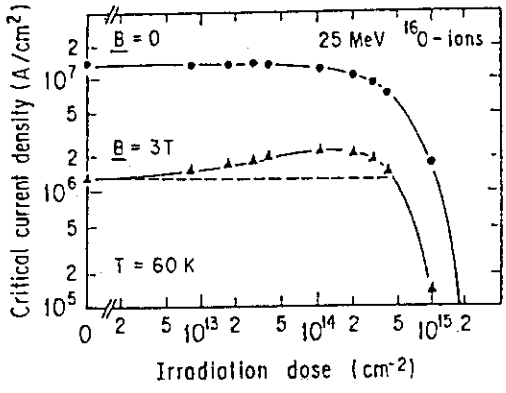

B. Roas et al.
Appl. phys. Lett 54
(1989) 1051

10^{14} ^{16}O / cm^2

Fig.11 Change of J_c by 25 MeV ^{16}O ion irradiation measured by the transport method

○ Magnetization critical current
Pellets : 1 x 1.5 x 8 mm^3

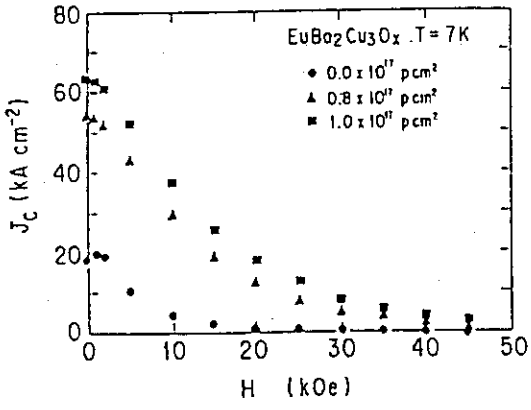

J.O. Willis et al.
Appl. Phys. Lett. 53
(1988) 417

800 MeV P
～85 K

Fig.12 Change of J_c by 800 MeV P irradiation, measured by the magnetic method

12. EFFECT OF ELECTRON-EXCITATION ON HIGH ENERGY ION IRRADIATION IN NICKEL AND COPPER

Akihiro IWASE*, Tadao IWATA*, Takeshi NIHIRA** and Shigemi SASAKI*

*Department of Physics, Japan Atomic Energy Research Institute, Tokai-Mura, Naka-Gun, Ibaraki, 319-11, **Faculty of Engineering, Ibaraki University, Hitachi Ibaraki 316.

§1. Introduction

When charged particles traverse solid, they lose their energy through collisions with electrons (inelastic interactions) as well as through direct nuclear collisions(elastic collisions). Through the elastic collisions, the particle energy is transferred directly to target atoms, and lattice atoms are permanently displaced from their regular positions, or the transferred energy leads to lattice agitations around the already existing defects and causes the annihilations of them. The latter phenomenon is called "radiation annealing". On the other hand, in some materials, atomic displacement or irradiation damage originates from the electron excitation caused by the inelastic interactions. For example, it is well known that nuclear tracks are formed in insulators bombarded with high energy heavy ions.[1] This phenomenon has been explained as due to the energy transfer from excited electrons to lattice atoms through a strong electron-phonon interaction. In the case of metals, however, as the electron-phonon interaction is much weaker than in insulators, it has been considered that the process of irradiation damage can be described only within the framework of elastic collisions.

Recently, however, we have found that inelastic interactions (electron excitations) play an important role on irradiation damage in some FCC metals irradiated with high energy heavy ions. In this paper, we report the effect of electron excitation on ion-irradiation in FCC metals with emphasis on the radiation annealing in Ni and Cu.

§2. Anomalous reduction of stage-I recovery in Ni irradiated with high energy heavy ions[2]

Nickel foils were irradiated with 0.5-1.8 MeV H, He, N and Ar ions,

and 84-120 MeV C, F, Si, Cl, Br and I ions. The temperature of the specimens during irradiation was held < 10 K. After the irradiations, the annealing experiments were performed up to 300 K with use of electrical resistivity measurements. Figure 1 shows the recovery curves and their temperature derivatives as a function of annealing temperature. As can be seen in the figure, with increasing the mass and the energy of irradiating ions, the recovery peaks disappear gradually from the lower temperature region. Moreover, for high-energy(∿100 MeV) heavy ion irradiations, the amount of the stage-I recovery is greatly reduced or nearly completely disappears. We also measured the stage-I recovery in Cu under the same experimental condition. Figure 2 shows that in Cu, anomalous reduction or disappearance of stage-I recovery cannot be observed even for high-energy heavy ion irradiations.

In Fig. 3, The amount of the stage-I recovery in Ni and Cu is plotted as a function of PKA median energy $T_{1/2}$. PKA median energy is one of the parameters which well characterize the PKA energy spectrum in the elastic collisions. Figure 2 and Fig. 3 show that in Cu the structure and the amount of the stage-I recovery change systematically with increasing $T_{1/2}$. Since the amount of the stage-I recovery is a measure of a concentration of single interstitials which can migrate freely in a lattice in the low temperature region (these defects are called "stage-I defects"), the above behavior of the stage-I recovery in Cu can be interpreted as due to the radiation annealing effects by elastic collisions.

On the contrary, in the case of Ni, the amount of stage-I recovery cannot be scaled by $T_{1/2}$, and the anomalous reduction or the disappearance of stage-I recovery cannot be explained within the framework of elastic collisions. Another mechanism besides the elastic collision should enhance the annihilation of stage-I defects during irradiation.

High-energy heavy ions cause high-density electron excitations along their ion beam path in solid. In order to study the effect of high-density electron excitation on the stage-I recovery, we plotted the amount of stage-I recovery in Ni as a function of electronic stopping power. Electronic stopping power gives the energy transferred from the irradiating ion to electrons in the specimen per unit length of the ion-path. Figure 4 shows that the amount of the stage-I recovery can be well scaled by the electronic stopping power S_e , and decreases with increasing

S_e. This result means that the energy of excited electrons is transferred to the lattice system and contributes to the annihilation of stage-I defects.

As mentioned above, anomalous reduction or disappearance of stage-I recovery is not found in Cu. The difference of the behaviors of stage-I recovery between two metals can be explained as a difference of electron-phonon interaction strength. In the case of Ni, energy of excited electrons can be effectively transferred to the lattice through a strong electron-phonon interaction, and lattice agitations are induced along the ion beam path. With increasing the energy of excited electrons, lattice agitation becomes more violent, and can cause the annihilation of stage-I defects. But in Cu, as a result of weak electron-phonon interaction, the lattice agitation along the ion path is insufficient for the annihilation of stage-I defects.

§3. Radiation annealing in Ni and Cu by 100 MeV iodine ions[3)]

As shown in §2, the inelastic interaction(electron-excitation) causes the radiation annealing of stage-I defects in Ni irradiated with high-energy heavy ions. In Cu, on the contrary, the radiation annealing of these defects is dominated only by elastic collisions.

In order to study the radiation annealing by high energy ions in Ni and Cu more quantitatively, we performed the following experiment: first, Ni and Cu foils were doped with simple defects using 84 MeV C-ion irradiations. Subsequently, the specimens were irradiated with 100 MeV I-ions. For reference, undoped Ni and Cu specimens were also irradiated with 100 MeV I-ions. The electrical resistivity change $\Delta\rho$ was measured as a function of C-ion and I-ion fluence. The specimens were held below 10K during irradiations. Next, to study what types of defects were annihilated by 100 MeV I-ion irradiation, thermal annealing experiments were performed up to 300 K after C-ion and I-ion irradiations. For reference, the same experiments were carried out also in the specimens irradiated only with C-ions.

Figure 5 illustrates the irradiation induced electrical resistivity change $\Delta\rho$ as a function of ion fluence Φ for Ni and Cu. In the case of I-ion irradiation of pre-doped Ni, about a half of doped-in defects are annihilated at the initial stage of I-ion irradiation. On the other hand, in Cu, the defect concentration continues to increase even during I-ion

irradiation. In the figure, are also shown the resistivity changes of undoped specimens during I-ion irradiation.

Figure 6 shows the results of the annealing experiments performed after C-ion irradiation plus I-ion irradiation and after only C-ion irradiation. In Ni, the peak of stage-I recovery is strongly reduced by the I-ion irradiation, and the reduction of other recovery peaks is also observed up to 200 K. On the contrary, in Cu, only the defect recovery below ∿35 K is slightly reduced by I-ion irradiation, but the total amount of stage-I recovery is little affected.

The result of the thermal annealing experiments shows that during the I-ion irradiation some configurations of defects are preferentially annihilated and the others are not. In other words, selective defect annihilations occur during the irradiation. Then, we have analyzed the present result by using a new model which describes the production and the selective annihilation for several types of defects. The detail of the model and the method of analysis have been shown in refs. 3 and 4. The main results of the analysis are as follows; in Ni, the defect annihilation corresponding to the stage I_{B+C} annealing occurs during the I-ion irradiation with the cross section of $6.5\times10^{-12}cm^2$, and the stage I_{D+E} defects are annihilated with the cross section of $1.4\times10^{-12}cm^2$. On the other hand, in Cu the stage-I defects are annihilated by I-ion irradiation with the cross section of $4.6\times10^{-13}cm^2$. The extraordinarily large cross sections for the annihilation of stage-I defects as compared with Cu show quantitatively the radiation annealing due to the electron excitation and the subsequent electron-phonon interaction in Ni.

§4. Concluding remarks

Our recent experimental results on the defect recovery and radiation annealing in Ni and Cu showed for the first time the effect of electron-excitation on the radiation annealing in metals. This effect has been also observed as a decrease of the defect production cross section and an increase of the effective recombination volume in Ni irradiated with high energy heavy ions.[5)]

References

1) R. L. Fleischer, P. B. Price and R. M. Walker, in Nuclear Tracks in Solids(Univ. of California Press, Berkeley, 1975).

2) A. Iwase, S. Sasaki, T. Iwata and T. Nihira, Phys. Rev. Lett. 58, 2450(1987).

3) A. Iwase, T. Iwata, S. Sasaki and T. Nihira, J. Phys. Soc. Jpn, 59, 1451(1990).

4) T. Iwata and A. Iwase, Rad. Eff. and Defects in Solids, 113, 135(1990).

5) A. Iwase, S. Sasaki, T. Iwata and T. Nihira, J. Nucl. Mater. 155-157, 1188(1988).

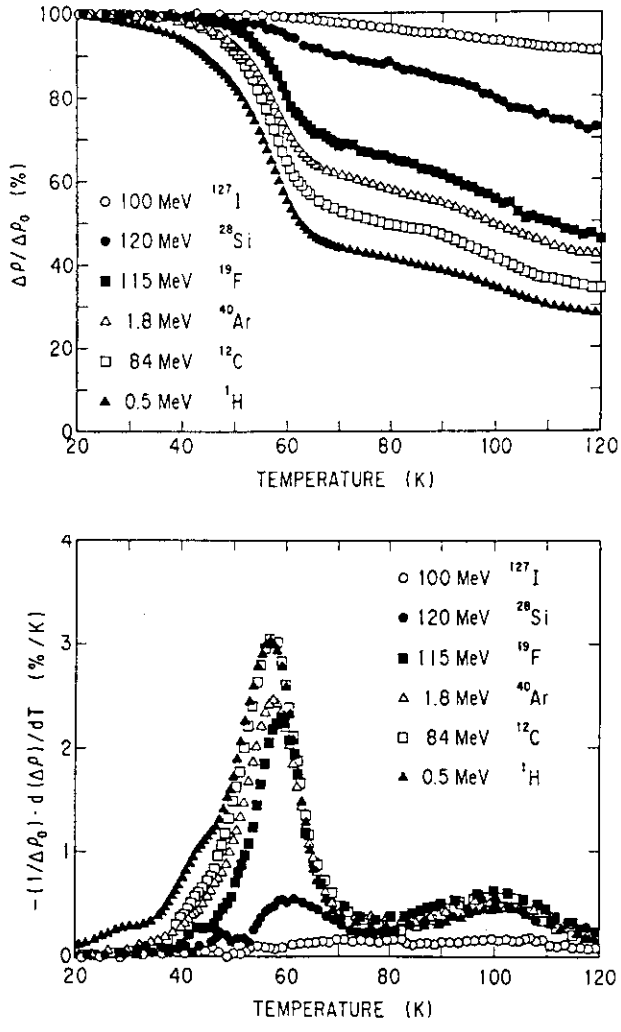

Fig. 1 Recovery curves (above) and temperature derivatives of recovery curves (below) in Ni as a function of annealing temperature.

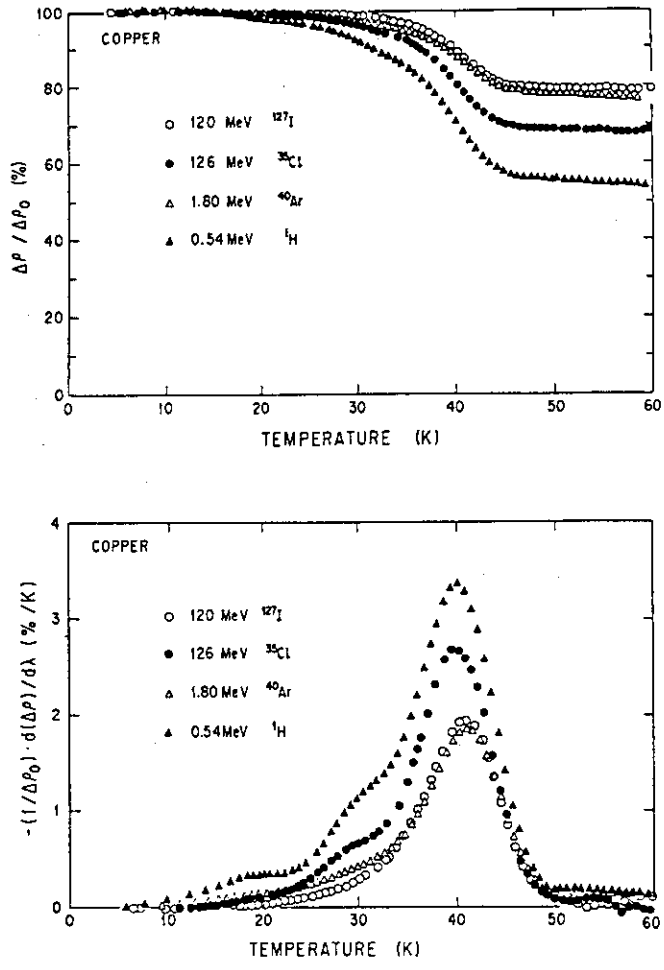

Fig. 2 Same as Figure 1, except in Cu.

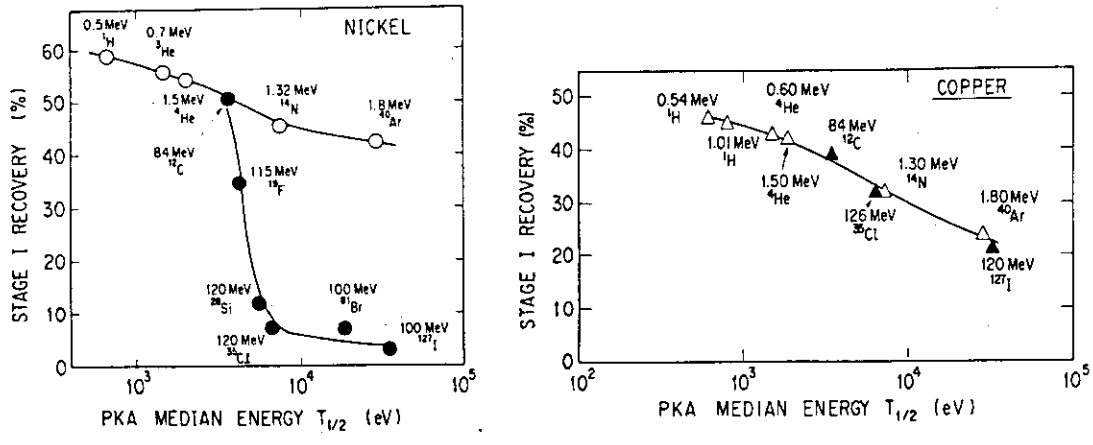

Fig. 3 Amount of stage-I recovery in Ni (left) and Cu (right) for low-energy ion irradiations(open circles and open triangles) and for high-energy ion irradiations (solid circles and solid triangles) as a function of PKA median energy $T_{1/2}$.

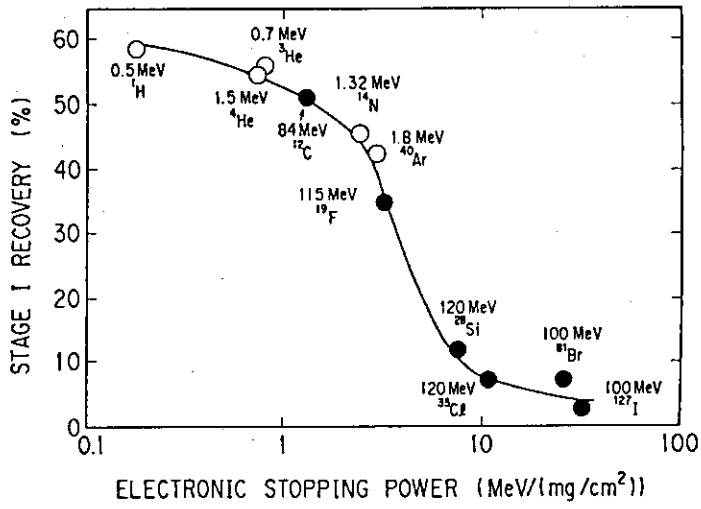

Fig. 4 Amount of stage-I recovery in Ni for low-energy ion irradiations(open circles) and for high-energy ion irradiations(solid circles) as a function of electronic stopping power.

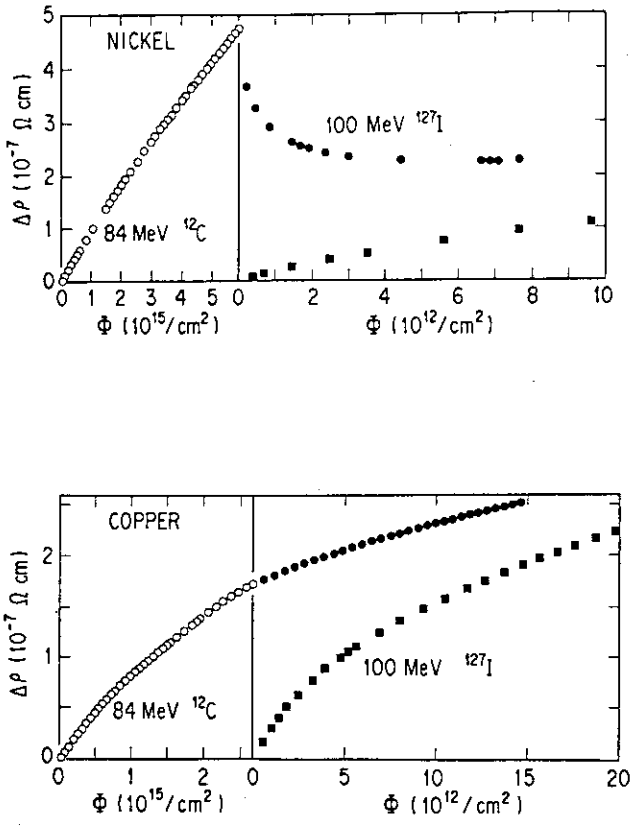

Fig. 5 Electrical resistivity change versus ion-fluence in Ni (above) and Cu (below) during 84 MeV C-ion irradiation(open circles) and during subsequent 100 MeV I-ion irradiation(solid circles). Solid squares present the electrical resistivity change of undoped specimens during I-ion irradiation.

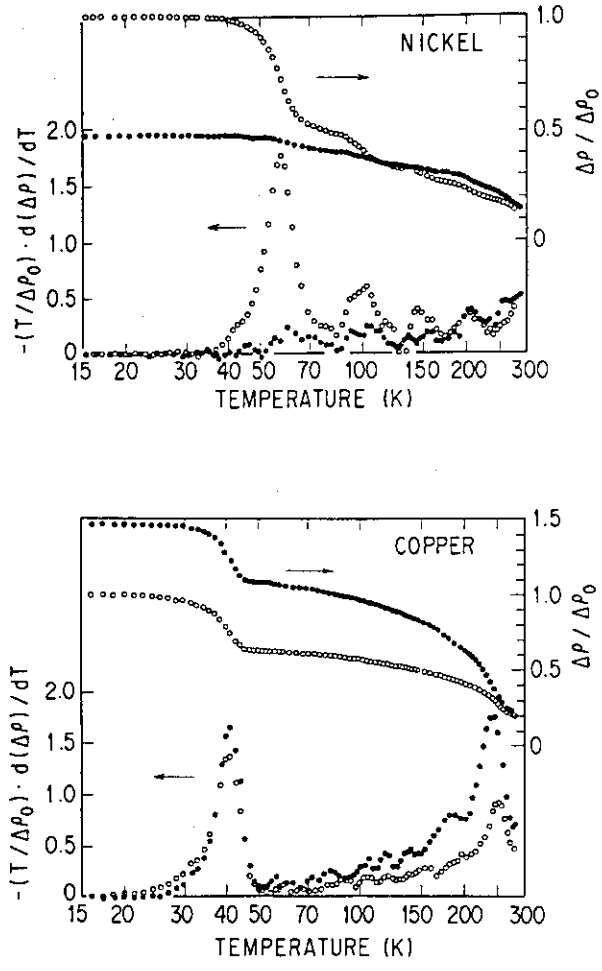

Fig. 6 Recovery curves of electrical resistivity and their temperature derivatives in Ni (above) and Cu (below) after 84 MeV C-ion irradiation(open circles) and after 84 MeV C-ion irradiation plus subsequent 100 MeV I-ion irradiation(solid circles).

13. THE APPROACH TO HEAVY ION IRRADIATION EFFECT (SINGLE EVENT PHENOMENA) FOR THE SEMICONDUCTOR DEVICES FOR SPACE USE

Tateo. GOKA, Satoshi. KUBOYAMA, Yosuke. SHIMANO

Tsukuba Space Center
National Space Development Agency of Japan
2-1-1 Sengen, Tsukuba-shi, Japan

Introduction Single event phenomena are the well known interactions between the high-energy particles in the space environment and the electronic devices on the space crafts. This phenomena can be classified into SINGLE EVENT UPSET (SEU), SINGLE EVENT LATCHUP (SEL) and SINGLE EVENT BURNOUT(SEB). SINGLE EVENT UPSET is a phenomena that the informations which are maintained in the memory or the microprocessor of the space craft are made upset by the particles in the space. This phenomena are caused by proton or heavier particles such as helium, carbon, nitrogen, oxygen, iron and so forth. Especially, the upset caused by proton is termed as PROTON UPSET, and that occurs even in the low-altitude orbit owing to the protons trapped by the magnetic field of the earth. These protons are most abundant above the South-Atlantic Ocean, so called SOUTH-ATLANTIC ANOMALY. LATCHUP and BURNOUT are irreversible hard errors which are caused by the heavy particles to the electronic parts of the CMOS technology and the POWER MOS FET respectively.

History of Single Event for the Space Crafts of NASDA Our first experience of SEU was in 1971. Four upsets were observed at the 1 kbits memory on the Geostationary Meteorological Satellite (GMS-2). After that several upsets were found in the memory on the GMS-3 and so on. Most serious experience was for Marine Observation Satellite-1 (MOS-1) in 1987. One or more upsets were observed in the memory of TTL technology almost every day in the SOUTH-ATLANTIC ANOMALY. Namely, this was apparently PROTON UPSET.

Prediction of Single Event Rate The prediction of the in-orbit single event rate is the most significant theme of our study. It is a basic information that should be input to the system design review and an important means to determine whether the parts can be used for the mission. The irradiation Test and comprehensive data of the space environment are necessary for the precise prediction. For this purpose, we established the SINGLE EVENT TEST FACILITY last year, where californium-252 is used as an fission fragment source. As the space environment data, we are using the NASA AP8 for the trapped proton and the CREME (COSMIC RAY EFFECTS ON MICROELECTRONICS) programs (NAVAL RESEARCH LABORATORY) for the cosmic ray or the solar-flare particles. In addition to the prediction for the spacecraft, the prediction of the upset rate for the microprocessor of the launcher is increasing its importance recently. Since in the polar-orbit missions in Japan, the launcher should mostly pass the SOUTH-ATLANTIC ANOMALY, we cannot neglect the possibility of the PROTON UPSET.

Irradiation Test At the SINGLE EVENT TEST FACILITY, mentioned previously, californium-252 can be used up to 740 kBq. So far, 3.7 kBq and 37 kBq sources are available. Using these sources, we can make test as to the UPSET for heavy particles, LATCHUP and BURNOUT. For the Proton Upset, however, an appropriate test cannot be made in this facility. Moreover, californium has a limited energy or mass spectrum, so a facility possessing the accelerator such as cyclotron, van de graaff and so forth is necessary to investigate the energy (or LET) dependence characteristics. For this purpose we are making tests in collaboration with NATIONAL INSTITUTE OF RADIOLOGICAL SCIENCES (NIRS) OR UNIVERSITY OF TSUKUBA, PARTICLE RADIATION MEDICAL SCIENCE CENTER (PARMS), for PROTON UPSET, and INSTITUTE OF PHYSICAL AND CHEMICAL RESEARCH (RIKEN) or JAPAN ATOMIC ENERGY RESEARCH INSTITUTE (JAERI) for the single event by the heavy particles.

Development of the Single Event Tolerant Device It is comparatively easy to develop a device of latchup free by adopting the epitaxial layer or the twin well technology. On the other hand, it is very difficult to develop a device of upset free. The problem exists mainly in the tradeoff between the requirement of upset tolerance and that of larger scale integration or higher speed of the devices. Therefore, as a general rule, we require the latchup free for the devices of CMOS technology and do not require the upset free for the memory or microprocessor devices. We cope with this phenomena by the system design such as error correction, redundancy and so on. However, as to some custom ICs or the gate array devices, upset free was confirmed by the californium test.

Quest of Basic Mechanism　A lot of studies have been done in quest of the basic mechanism of single event phenomena in the United States and Europe. The quantitative comprehension for the single event, however, cannot be obtained so far, mainly because the phenomena are of high speed (about several picoseconds). To observe the instance of the occurrence of UPSET, we are developing a wide-range measurement system and we are planning to make an experiment using the helium microbeams at ELECTROTECHNICAL LABORATORY (ETL). For the PROTON UPSET, we are also making an basic experiment at TOKYO UNIVERSITY.

The On-orbit Measurements of Single Events by ETS-V　The on-orbit data of single event phenomena were obtained for the static RAMs equipped in Engineering Test Satellite-V (ETS-V) in a geostationary orbit. The data were acquired for a period of about 3 years, and the effects of solar flares were observed. A comparison with Marine Observation Satellite-1 (MOS-1: a medium-altitude satellite) was also conducted.

National Space Development Agency of Japan (NASDA) has launched Engineering Test Satellite-V on August 27, 1987, and has been put into the orbit at Long.150°E (Fig.1). This space craft has a Technical Data Acquisition Equipment (TEDA) aiming at obtaining the technical data which is necessary to develop spacecrafts. TEDA includes a RAM Soft-error Monitor (RSM) that makes a measurement of the SEU or SEL occurring at eight 64 kbits static RAM devices (NEC, μPD4464D-20). This monitor has been developed by NASDA in collaboration with NTT, Japan and has functions as follows,

1) Measurement of the frequency of SEU occurring at the RAM devices.
2) Measurement of the frequency of SEL by monitoring the current supplied to the RAM devices. When SEL occurs, the RSM turns off the current, turns it on again and resets the state of RAMs.
3) Measurement of the number of bits which lose the memory function by a hard-error.
4) Measurement of the total current supplied to the RAM devices aiming at the detection of any deterioration of the devices owing to the total-dose effect.
5) Telemetering of the data acquired by the above measurements, the RAM identification and the state of RAM devices.

Fig.2 indicates a schematic diagram of the measurement. The RSM alternates '0'writing/reading and '1'writing/reading approximately every 256 seconds. The RSM discriminates SEU from other hard-error by the comparison of the result of reading in each adjoining cycle. Namely, when there is a bit error in a cycle and no bit error is found in the next cycle, the RSM judges it to be SEU. On the other hand, if there is no bit error in the next cycle, the RSM identifies it with a hard-error.

Fig.3 shows the SEL data acquired by the ETS-V TEDA RSM. In this figure, the abscissa and the ordinate axis indicate passing days and the number of SEL occurred in a week. The period of data acquisition is about 140 weeks from November 22, 1987 to August 31 ,1990.
The solar activity became intensive since September, 1989 and the 4B-class solar flares were observed on September 29 and October 19. The number of SEL drastically increased by these solar flare. The number of SEU measured by RSM each week is also plotted in Fig.4. From this figure one can see that the number of SEU is not so much as that of SEL and it increased remarkably when the solar flare occurred as well as SEL.

Fig.5 and Fig.6 indicate the details as to the increase of the cumulative number of SEL and SEU owing to the solar flare on September 29 and October 19 respectively. The time-lag between the occurrence of the solar flare and that of SEL and SEU proved to be about 2.5 and 3 hours as a result of a minute investigation. Fig.6 shows a rapid increase of the number of SEL on October 20. However, that is supposed to be due to the bit error during the transmission and one should remove 64 bit errors when one investigates this figure. As a reference of the data mentioned above, Fig.7 shows the number of SEU occurred at the stored command memory used in the command decoder of Marine Observation Satellite-I (MOS-I). This memory consists of three TTL RAM devices (93419, 64x9 bit RAM, Fairchild). At this memory, about one SEU was caused every day by the high-energy protons trapped in the radiation belts. Though MOS-I, different from ETS-V, is a medium-altitude satellite (909 km altitude and 99 deg inclination), one can see from this figure that the number of SEU increased apparently by the effect of solar flare on October 19. These SEUs are assumed to be due to not only the protons but also the heavy particles included in the flare.

References

(1) J. H. Adams, Jr NRL Memorandum Report 5901, 1989
(2) N.Shiono, Y.Sakagawa et al. "Single Event Effects in High Density CMOS SRAMs", IEEE Trans. Nucl. Sci. NS-33, p1632-1636, 1986
(3) Y.Shimano, T.Goka et al. "The Measurements and the Prediction of Proton Upset", IEEE Trans. Nucl. Sci. NS-36, p2344-2348, 1989

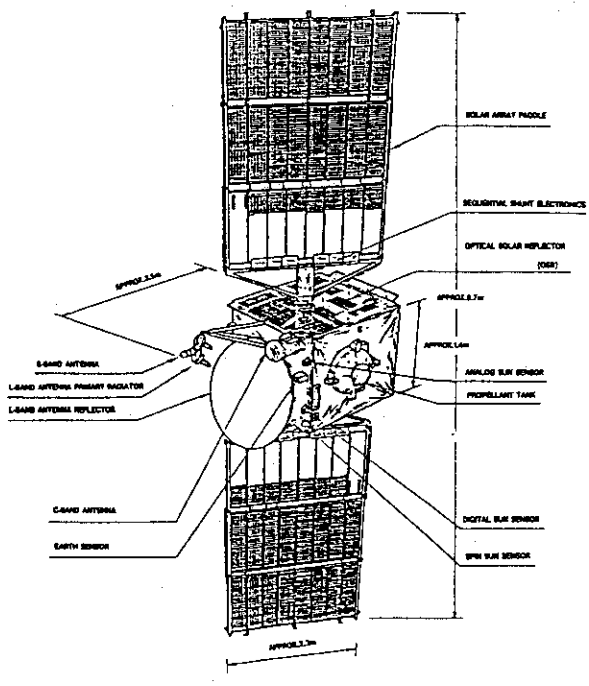

Fig. 1. Configuration of ETS-V

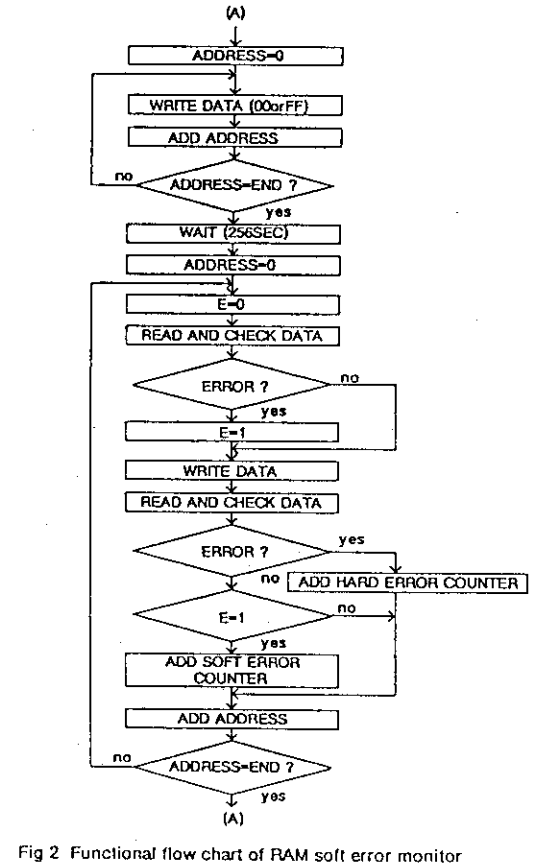

Fig 2 Functional flow chart of RAM soft error monitor

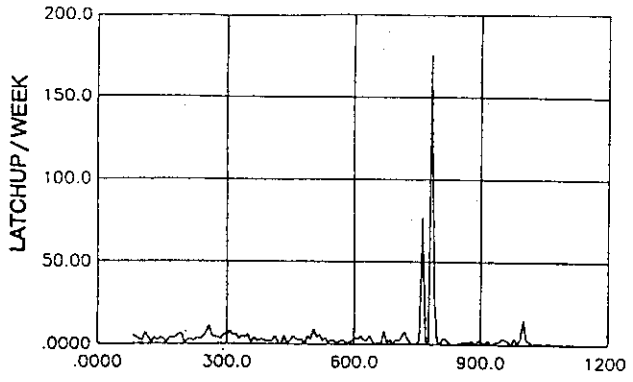

Fig.3 Measured Latchup rate as a Function of Time (ETS-V)

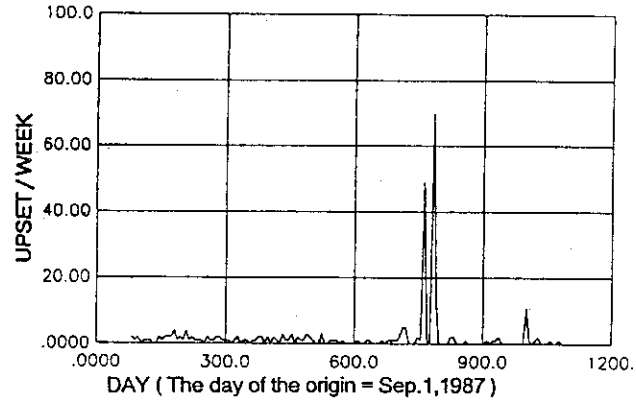

Fig.4 Measured Upset rate as a Function of Time (ETS-V)

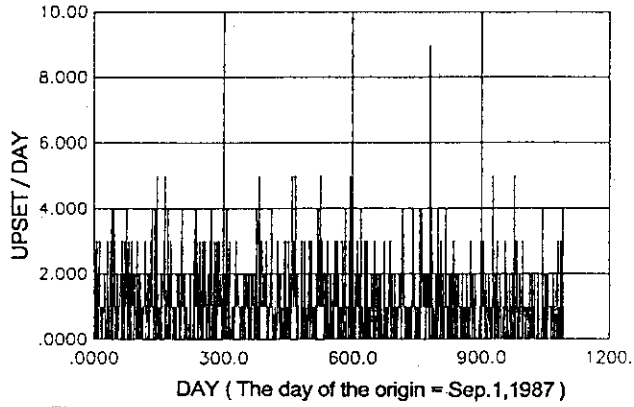

Fig. 7. Measured Upset rate as a Function of Time (MOS-1)

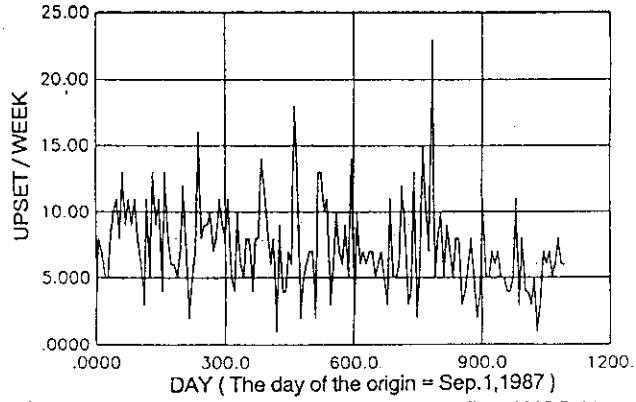

Fig. 7 a. Measured Upset rate as a Function of Time (MOS-1).

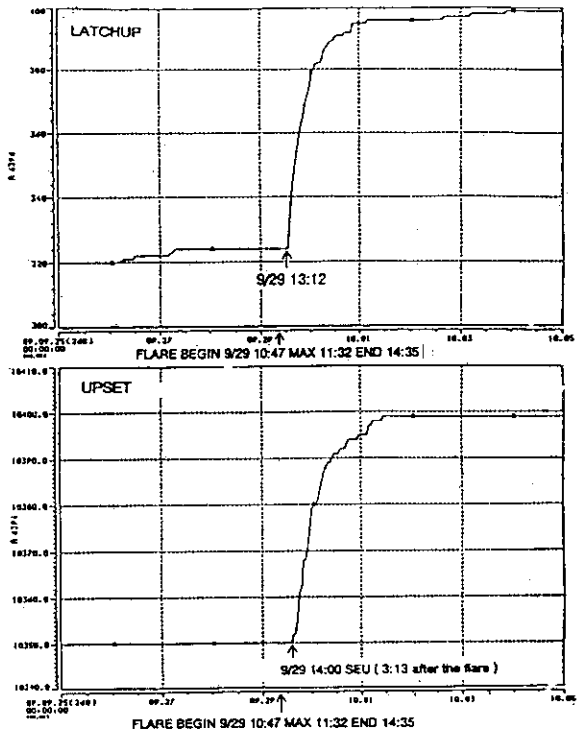

Fig.5 Measured Cumulative Number of SEL&SEU (Sep.29,1989)

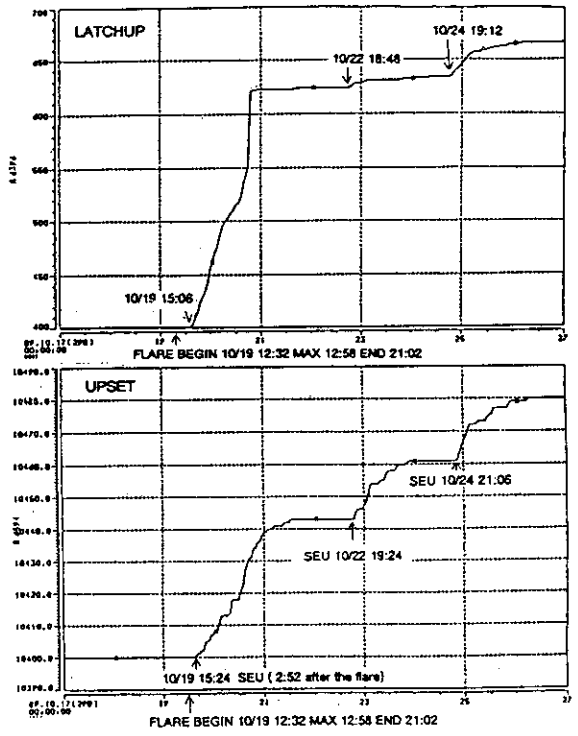

Fig.6 Measured Cumulative Number of SEL&SEU (Oct.19,1989)

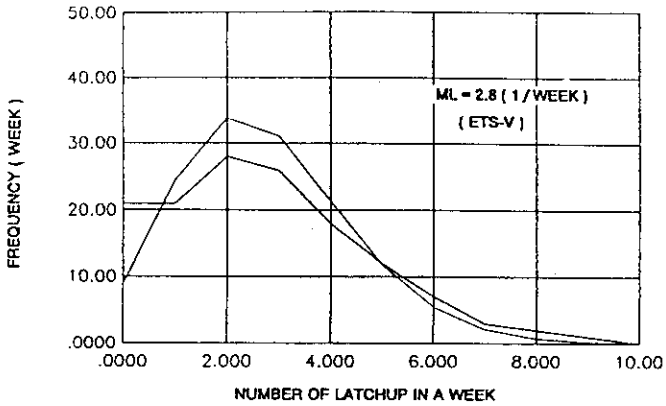

Fig. 8. The Distribution of the Frequency Versus the Number of SEL (Total Period)

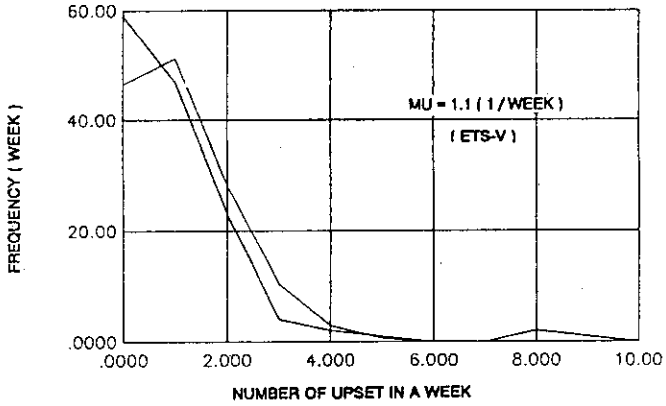

Fig. 9. The Distribution of the Frequency Versus the Number of SEL (Total period)

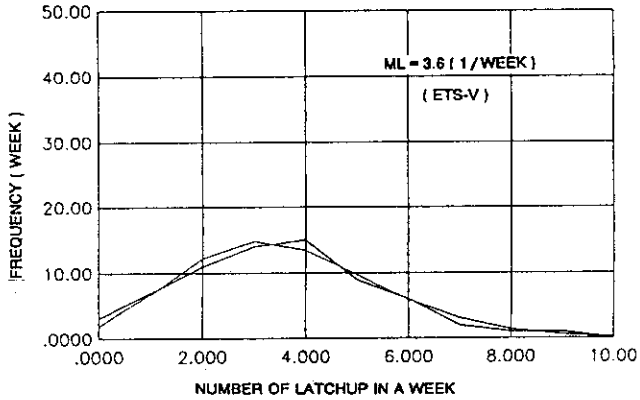

Fig. 10 a. The Distribution of the Frequency Versus the Number of SEL (First half period)

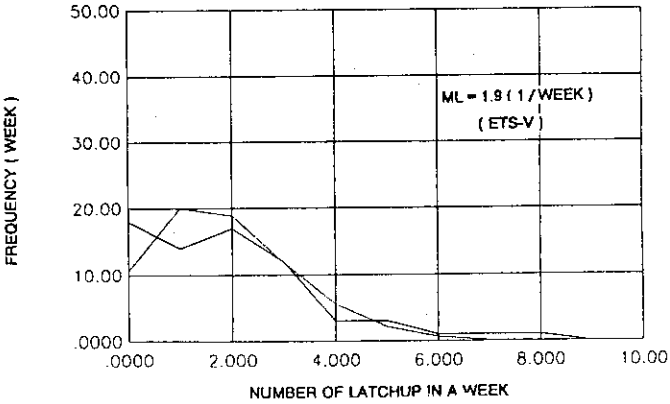

Fig. 10 b. The Distribution of the Frequency Versus the Number of SEL (Latter half period)

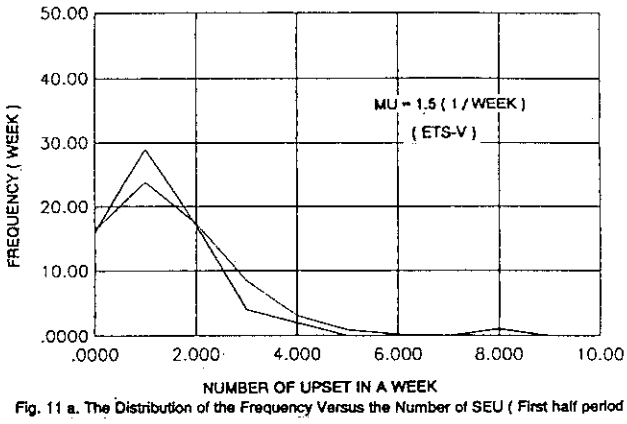

Fig. 11 a. The Distribution of the Frequency Versus the Number of SEU (First half period)

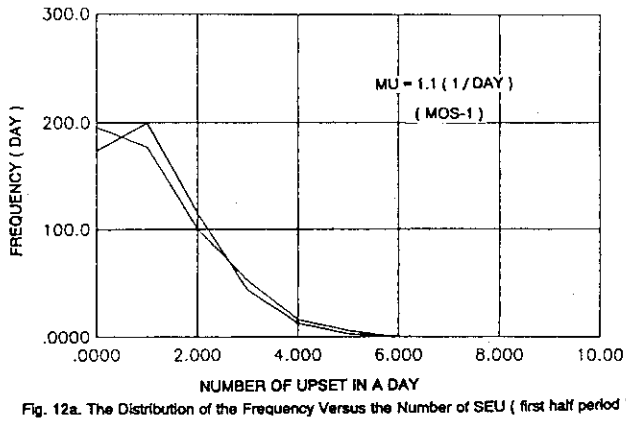

Fig. 12a. The Distribution of the Frequency Versus the Number of SEU (first half period)

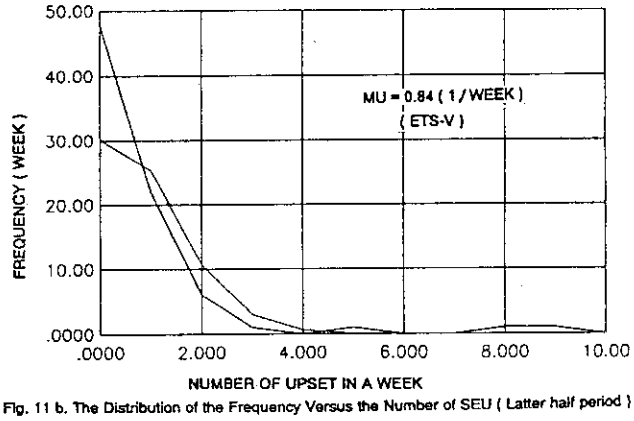

Fig. 11 b. The Distribution of the Frequency Versus the Number of SEU (Latter half period)

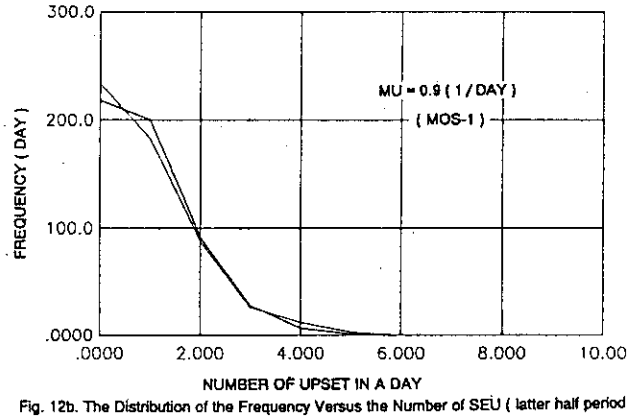

Fig. 12b. The Distribution of the Frequency Versus the Number of SEU (latter half period)

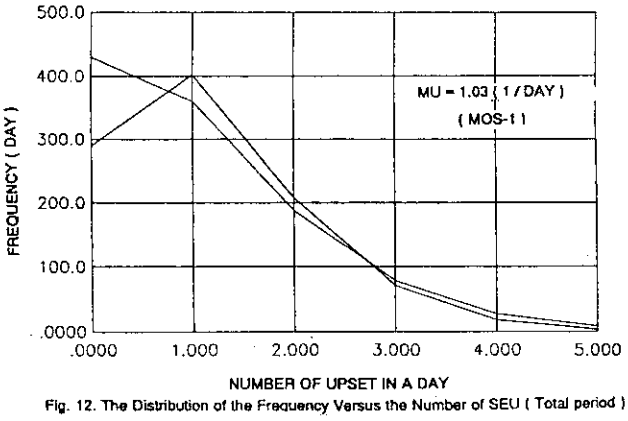

Fig. 12. The Distribution of the Frequency Versus the Number of SEU (Total period)

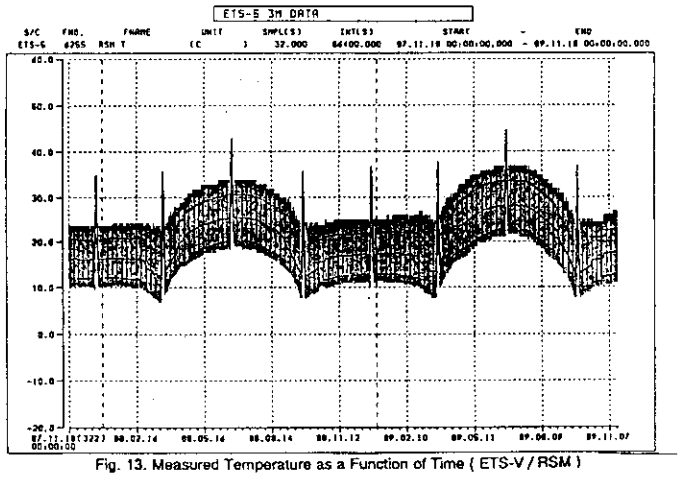

Fig. 13. Measured Temperature as a Function of Time (ETS-V / RSM)

14. IRRADIATION EFFECTS ON CERAMIC BREEDERS FOR FUSION REACTORS

Kenji NODA*, Yoshinobu ISHII*, Hisayuki MATSUI**,
Tetsuya NAKAZAWA*, Hitoshi WATANABE*

*Department of Fuels and Materials Research, Japan Atomic Energy Research Institute, **Faculty of Engineering, Nagoya University

1. Introduction

Ceramic breeder materials for D-T fusion reactors will be subjected to severe neutron irradiation during operation of the reactors. Defects will be introduced by neutrons with the energies up to 14 MeV, as well as tritons (2.7 MeV) and helium ions (2.1 MeV) produced from $^{6}Li(n,\alpha)^{3}H$ reactions. These defects not only induce swelling and degradation of mechanical integrity but also affect tritium transport and compatibility with structural materials through changes in the diffusivity of the component atoms.

Studies of radiation damage and irradiation effects on ionic conductivity in ceramic breeder materials especially Li_2O have been carried out using thermal neutron and ion irradiation to obtain fundamental knowledge on radiation defects and the irradiation effects on transport phenomena of Li ions and tritium.[1-9] In this paper, studies of radiation-induced defects in Li_2O with the electron spin resonance and optical absorption methods, and studies of irradiation effects on the ionic conductivity in Li_2O and Li_4SiO_4 are reviewed.

2. Radiation-induced defects

In electron spin resonance (ESR) studies, F^+ centers were observed to be introduced in Li_2O single crystals and the sintered pellets irradiated by thermal neutrons (10^{20}-10^{23} $n.m^{-2}$) and by 100-120 MeV oxygen ions (10^{20} $ions.m^{-2}$).[2-4] The F^+ center is an oxygen ion vacancy trapping an electron and has positive charge. A schematic diagram is shown in fig. 1. Fig. 2 shows ESR spectra of a Li_2O single crystal irradiated to $4.5X10^{21}$ $n.m^{-2}$ by thermal neutrons along with the hyperfine line-intensity rations predicted for the F^+ centers.[3] Each spectrum shows a hyperfine structure

(HFS) consisting of more than 20 peaks which depends on the crystal orientation in the applied magnetic field, H. Such spectra can be attributed to the F^+ centers, because agreement is found between the characteristic features of the observed spectra and the hyperfine line-intensity ratios calculated for the F^+ centers.

In optical absorption measurements, the F^+ centers were also observed as a predominant absorption band at 310 nm (3.90 eV) for thermal neutron and oxygen-ion irradiation.[1,5] In addition, bands at 375 nm (3.23 eV) and 570 nm (2.12 eV) which were thought to be F aggregate centers appeared at the higher fluence.

For Li_2O sintered pellets irradiated to 10^{23} $n.m^{-2}$ by thermal neutrons, a narrow and sharp ESR spectrum was superimposed on the spectrum due to the F^+ centers.[2] This was attributed to colloidal lithium metal centers. The colloidal lithium metal centers were not observed for Li_2O single crystals irradiated to the same level of neutron fluence and, so they observed for the pellets may be associated with grain boundaries. In case of oxygen-ion (120 MeV) irradiation, the colloidal lithium metal centers were observed for Li_2O single crystals irradiated to $3X10^{20}$ $ions.m^{-2}$, in which the concentration of F^+ centers was higher than that for thermal neutron irradiation of 10^{23} $n.m^{-2}$.[4]

Thermal recovery behavior of F^+ centers and colloidal lithium metal centers was investigated by isochronal annealing experiments. The number of F^+ centers decreased in the range 420 to 570 K and almost all F^+ centers disappeared above 630 K.[3] On the other hand, the intensity of ESR spectra for the colloidal lithium metal centers increased in the range 400-600 K and then began to decrease around 700 K, disappearing completely at 870 K.[2]

3. Irradiation effects on ionic conductivity

The ionic conductivity of ceramic breeder materials is controlled by the concentration of defects, solute atoms and impurities, and reflects the diffusion of lithium ions. Furthermore, the conductivity is related to tritium diffusion because tritium diffusion is thought to depend on lithium diffusion.[10] Ionic conductivity of Li_2O and Li_4SiO_4 during and after oxygen-ion (120 MeV) and lithium-ion (24 and 60 MeV) irradiation was studied by "in-situ" measurements using the AC two terminal method.[6-9]

Fig. 3 shows the post-irradiation ionic conductivity at 443 and 489 K

as a function of oxygen-ion fluence.[6] The conductivity at 443 K increased with the fluence, flattening to a constant value above $6X10^{19}$ ions.m^{-2}. At 489 K, the conductivity decreased with the fluence.

The thermal recovery of ionic conductivity was investigated by isochronal annealing experiments. The conductivity at 443 K decreased with the annealing temperature in the range 443- 498 K and then increased in the range 498-548 K. On the other hand, the conductivity at 489 K increased in the annealing temperature range 489-570 K. The increase in conductivity occurred at temperatures that were close to those that led to recovery of F^+ centers. Thus, the low values at 489 K in irradiated Li_2O are associated with F^+ centers. On the other hand, the high values at 489 K must be caused by unspecified defects which are recovered in the range 443-498 K.

In other studies, the irradiation effects on ionic conductivity were investigated in the range 393-673 K.[7,8] From these studies, it was seen that the conductivity increased with the fluence below 443 K due to the unspecified defects which were assumed to be lithium vacancies, and that it decreased in the range 453-573 K due to the F^+ centers.

The post-irradiation ionic conductivity of Li_4SiO_4 in the range 423-523 K is shown versus the ion fluence in Fig. 4. The conductivity in this temperature range increased with the fluence. To clarify the cause of this increase, radiation damage studies by electron microscopy and various spectroscopic methods are necessary.

Thus, if the conductivity in Li_2O and Li_4SiO_4 is related to the tritium diffusion, then tritium diffusivity in the post-irradiation tests is as follows: The tritium diffusivity in Li_2O decreases between 453 and 573 K due to the F^+ centers and increases below 443 K due to the unspecified defects. The diffusivity in Li_4SiO_4 increases in the range 423-523 K.

Ionic conductivity of Li_2O during irradiation was larger than that before or after irradiation.[7,8] The conductivity during irradiation increased with the ion flux, as shown in Fig. 5. Similar behavior of conductivity was also observed for Li_4SiO_4 during irradiation.[9] However, before this can be stated unequivocally, direct evidence of the correlation between lithium-ion diffusion and tritium diffusion in the ceramic breeder materials must be experimentally obtained.

References

1) K. Uchida, K. Noda, T. Tanifuji, S. Nasu, T. Kirihara and A. Kikuchi, phys. stat. sol. (a) 58 (1980) 557.

2) K. Noda, K. Uchida, T. Tanifuji and S. Nasu, J. Nucl. Mater. 91 (1980) 234.

3) K. Noda, K. Uchida, T. Tanifuji and S. Nasu, Phys. Rev. B24 (1981) 3736.

4) K. Noda, T. Tanifuji, Y. Ishii, H. Matsui, N. Masaki, S. Nasu and H. Watanabe, J. Nucl. Mater. 122 & 123 (1984) 908.

5) K. Noda, Y. Ishii, H. Matsui and H. Watanabe, J. Nucl. Mater. 133 & 134 (1985) 205.

6) K. Noda, Y. Ishii, H. Matsui, H. Ohno, S. Hirano and H. Watanabe, J. Nucl. Mater. 155-157 (1988) 568.

7) K. Noda, Y. Ishii, H. Ohno, H. Watanabe and H. Matsui, in Advances in Ceramics, Vol. 27 (American Ceramic Society, Westerville, OH, 1990) p. 227-247.

8) K. Noda, Y. Ishii, H. Matsui, H. Ohno and H. Watanabe, J. Nucl. Mater., in press.

9) K. Noda, Y. Ishii, H. Matsui, D. Vollath and H. Watanabe, Proc. 16th Symposium on Fusion Technology, London, Sept. 3-7, 1990, in press.

10) H. Ohno, S. Konishi, T. Nagasaki, T. Kurasawa, H. Katsuta and H. Watanabe, J. Nucl. Mater. 133 & 134 (1985) 181.

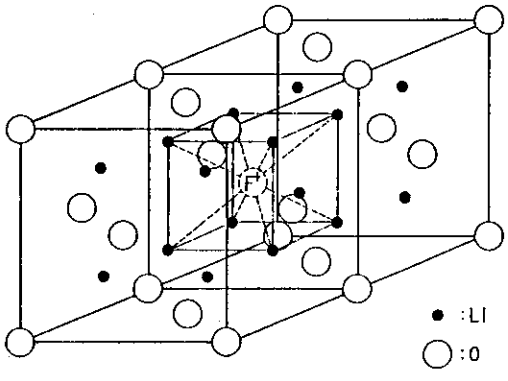

Fig. 1 Schematic diagram of F^+ centers.

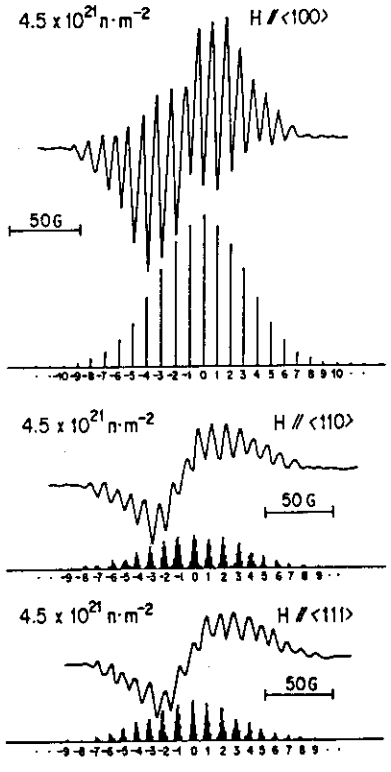

Fig. 2 ESR spectra of Li_2O single crystals irradiated with thermal neutrons.

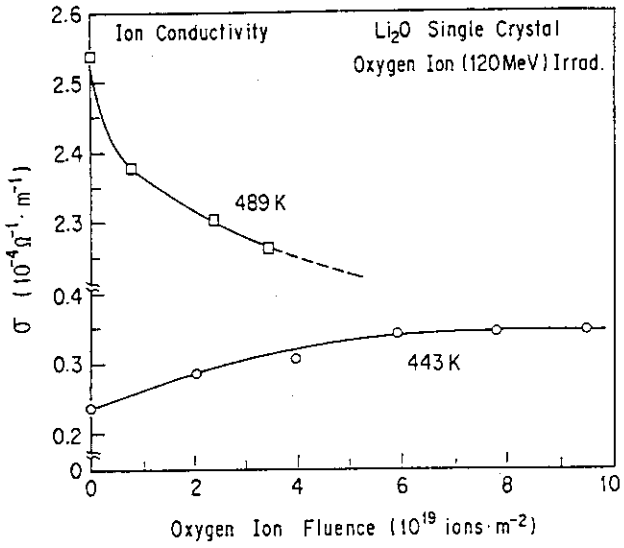

Fig. 3 Post-irradiation ionic conductivity at 443 and 489 K for Li2O irradiated with 120 MeV oxygen ions as a function of the fluence.

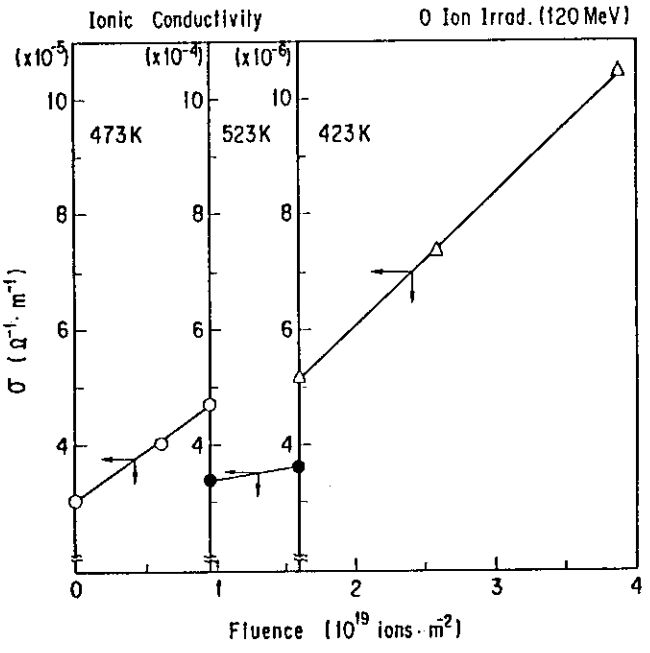

Fig. 4 Post-irradiation ionic conductivity in the temperature range 423-523 K for Li4SiO4 irradiated with 120 MeV oxygen ions as a function of the fluence.

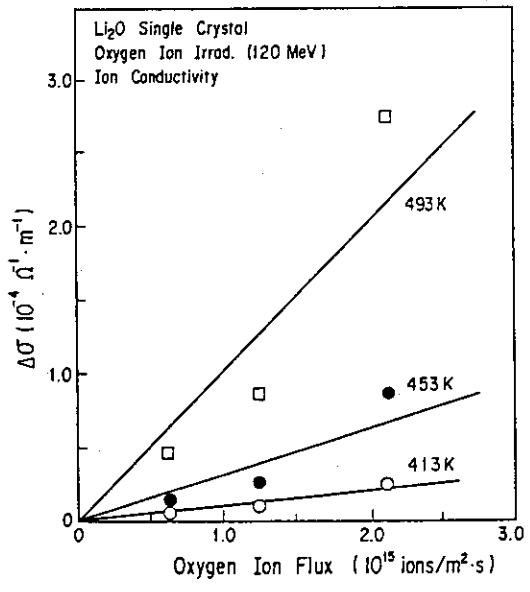

Fig. 5 Ionic conductivity of Li2O during 120 MeV oxygen ion irradiation as a function of the flux.

15. PHYSICAL PROPERTY OF URANIUM COMPOUNDS

Hisayuki MATSUI

Department of Nuclear Engineering, Nagoya University

In a recent development of the "Actinide Research", it has been found that the actinide compounds show a variety of interesting material features. As materials with 5f electrons in the system, they often reveal strange physical behavior, especially in the magnetism, being like as the 4f (lanthanide) containing compounds. After a discovery of "heavy electron" in the 4f -related compounds, a new attempt is going on to investigate the actinide compounds in order to establish a new field of the solid state physics and the so-called "Heavy Fermion Physics". However, a restriction of handling with such high radioactive materials leads to an investigation on only the earlier series of the actinides, such as uranium and thorium, and plutonium as well but in a special procedure. Therefore, the actinide research has been mainly concentrated to the uranium compounds so far, especially in our country. In the present paper, we deal with (1) "anomalous" magnetic character and (2) "heavy fermion" research of uranium compounds which have been conducted in our laboratory, in a collaboration with scientists at the Jpn. Atomic Energy Res. Inst. and the Phys. Dept. of the Nagoya Univ..

[1] Anomalous Magnetic Character

UP (Uranium Monophosphide: T_N=123 K)

An antiferromagnetic UP shows a very anomalous magnetic behavior. It contains five or six "characteristic temperatures" [1], at which the magnetic susceptibility changes drastically (at T_{MJ} and T_N) or slightly (at T_{MIN} T_{MAX} and T_{CWL}), as shown in Fig. 1. All the "characteristic temperatures" in the magnetic measurement are confirmed also in the resistivity measurement [1], as illustrated in that figure. Remarkable features in the physical properties of UP are as follows;

1. A very big "moment jump" and resistivity increase at 23 K (T_{MJ}),
2. Appearences of a minimum (T_{MIN} at 90 K) and a maximum (T_{MAX} at 133 K) in the magnetic susceptibility,
3. A semiconductive-type resistivity found above T_N (to 830 K).

The same NaCl-type uranium pnictide, UAs (T_{MJ}=64 K, T_N=125 K and T_{MAX}=140 K [2]), indicates a magnetic behavior similar to UP. For T_{MJ} at 23 K in UP, it has been found in a neutron diffraction study that the ordered magnetic spins turn the antiferromagnetic coupling from the [100] to [110] crystal direction [3]. However, it is not clearly understood the origins of other magnetic anomalies.

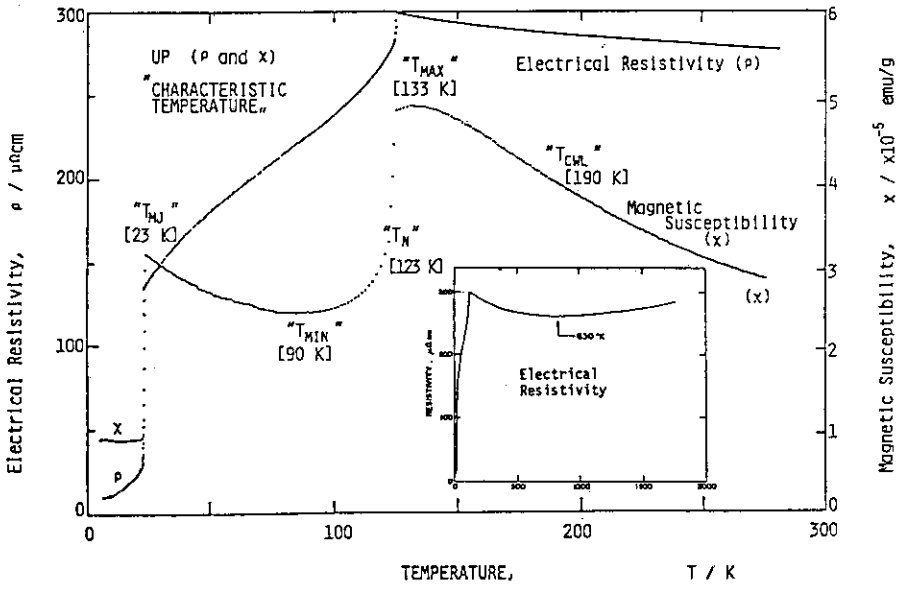

Fig.1 Magnetic Character and Resistivity of UP

β-U_2N_3 (β-Uranium Sesquinitride: T_C=188 K)

Another anomalous finding in the uranium compounds is a strange temperature dependence of the electrical resistivity of β-U_2N_3, a ferromagnet below 188 K in magnetic measurement. The electrical resistivity, however, behaves quite curiously at the Curie point, as shown in Fig.2. A maximum (T_{top} at 163 K) and a minimum (T_{val} at 209 K) are found below and above the Curie point (T_C), respectively [4]. At the magnetic ordering, this substance shows an increase of the resistivity, that is quite strange in a normal sense.

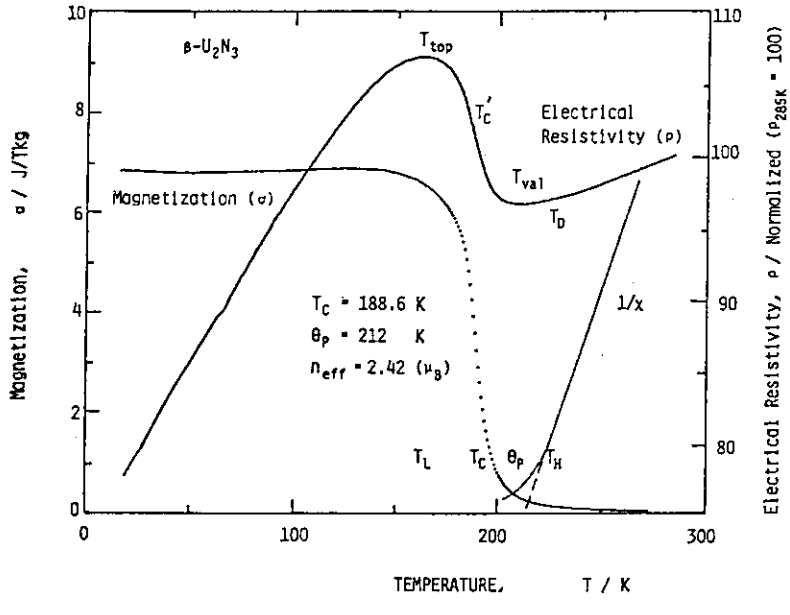

Fig.2 Magnetization and Resistivity of β-U_2N_3

A drastic change of the magnetic character has been observed, when such magnetic uranium compounds are irradiated to thermal neutrons. The origin of the drastic change is an induced magnetic disordering caused by lattice defects, accompanying with a local expansion and distortion of the crystal lattice. It is of interest that a new antiferromagnetic phase, α-U_2N_3 (T_N= ～25 K, depending on N/U ratio), appears after the irradiation [5]. It is suggested, therefore, that a slight change in the crystal structure (e.g., the lattice parameter) plays a significant role to establish the magnetic structure. Other magnetic compounds, such as an antiferromagnetic UP [6,7], UN (T_N=52 K) [8] and a ferromagnetic US (T_C=180 K) [7,9] revealed also big changes of the magnetic characters by the irradiation (fission damage).

[2] Heavy Fermion Materials

An experimental evidence of "heavy Fermion" material is a large temperature-independent electronic specific-heat coefficient, γ, near T=0,

$$C_P = \gamma T + \beta T^3.$$

The coefficient, γ, is related to the density of electronic states at the Fermi level, as

$$\gamma = (2/3) k_B^2 \pi^2 N(E_F).$$

Thus, the large γ suggests a high electron density of state and a heavy electron mass. Such a large γ-value was firstly found in a 4-f related compound ($CeAl_3$). As shown in Fig. 3, the large γ has been found in compounds which have large f-f metal separation. It is noticed that the uranium compounds show either magnetic or superconductive character. This seems an important feature for the "heavy Fermion" material.

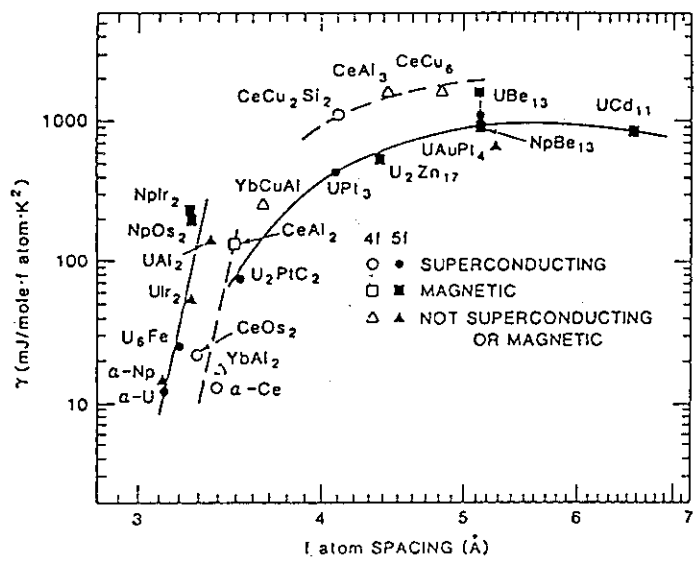

Fig.3 γ-value vs f-f metal separation

Now, many 5-f related (uranium) compounds are investigated to establish the physical meaning of the "heavy Fermion". We focuss the study on binary alloys of uranium with transition metals. In the first attempt, we found that as-cast UAu_3 showed a comparatively large γ (γ=200 mJ/K² mol-U) with an antiferromagnetic transition at about 10 K [10]. However, after anneal at 850 °C for 1 or 2 weeks, the specimen showed another type of magnetic

transition (a ferromagnet below 22 K), as illustrated in Fig. 4. A recently

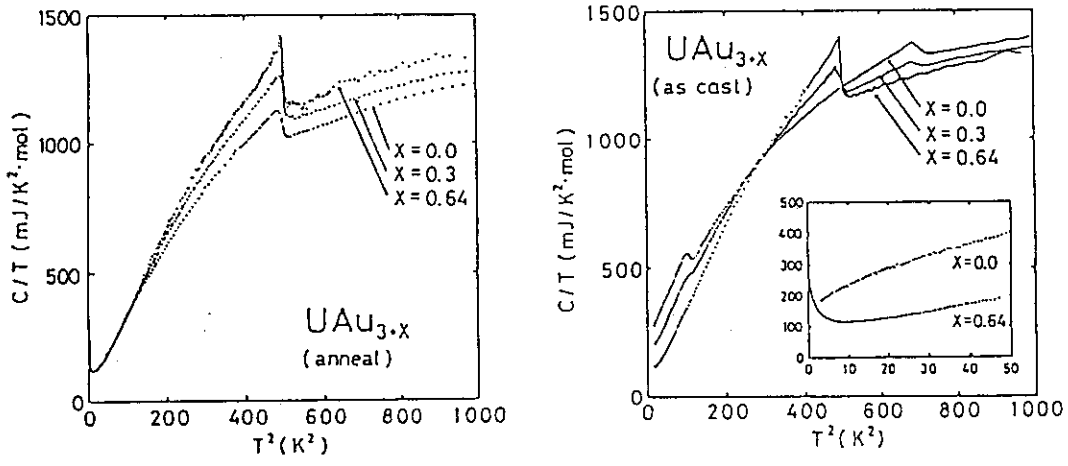

Fig.4 Specific Heat of U-Au alloys (As-melt and Annealed)

reported phase diagram of U-Au alloys [11] claims an existence of $U_{14}Au_{51}$ ($UAu_{3.64}$), instead of UAu_3. In the present study, however, we confirmed the two phases by careful specimen preparation and precise measurements of the specific heat, magnetic susceptibility and electrical resistivity.

We studied a lot of U-T (T: transition metal) systems (e.g., U-Pd(Pt), U-Rh and U-Os). Among them, the U-Pd alloys (UPd and UPd_{4+x} which indicated rather large γ-values around 200 mJ/K² mol-U, thus a type of the "heavy Fermion" material) showed antiferromagnetisms which might be caused by the "itinerant" electrons. Whereas the other systems (paramagnetism) would be able to interpreted by the "localized" electron model.

References

[1] H.Matsui: phys. stat. sol. (a), 104 (1987) 825.
[2] R.Troć and D.J.Lam: phys. stat. sol. (b), 65 (1974) 317.
[3] J.Rossat-Mignod, et al.: 4th Int. Conf. Crystal Field and Structural Effects in f-Electron Systems (Plenum Press, 1982), pp. 501.
[4] H.Matsui, S.Suzuki and M.Tamaki: phys. stat. sol. (a) 103 (1987) 199.
[5] H.Matsui, S.Suzuki and M.Tamaki: J. Mag. Mag. Mat., 70 (1987) 400.
[6] H.Matsui et al.: Inorg. Chim. Acta, 140 (1987) 173.
[7] H.Matsui et al.: J. Radioanal. Nucl. Chem., 143 (1990) 187.
[8] M.Tamaki et al.: Rad. Effects, 91 (1985) 61.
[9] H.Matsui et al.: J. Nucl. Mater., 110 (1982) 208.
[10] M.Kontani et al.: J. Mag. Mag. Mat., 76/77 (1988) 655.
[11] A.Dommann and F.Hulliger: J. Less-Comm. Metals, 141 (1988) 261.

16. QUANTUM SIZE EFFECT ON THE EXCITON POLARITON IN GaAs THIN FILMS

Yoshinobu. AOYAGI, Jun-ichi. KUSANO, Yusaburo. SEGAWA and Susumu. NAMBA

The Institute of Physical and Chemical Research,

Discrete fine structures were observed in a luminescence of the free exciton band in high quality GaAs thin films. The appearance of these structures is explained by the quantum size effect on exciton polariton due to the quantization of the center of mass motion. This experiment is a new approach to the additional boundary condition.

1.Introduction

AN EXCITON has a center of mass motion and moves in real space due to its kinetic energy. Coupling with a radiation field, it forms an exciton polariton [1] and has a spatial dispersion. With decreasing thickness of a crystal, an exciton polariton in a semi-infinite slab is strongly affected by boundaries. The interference effect on the reflectance spectrum and absorption spectrum has been observed [2, 3]. In contrast, an exciton in a quantum well structure [4] provides us with a two-dimensional (2-D) nature, because both the wave functions of the electron and the hole are confined and the exciton consists of a 2-D electron and hole. The center of mass motion perpendicular to the hetero interface (z-direction) is suppressed by potential barriers. In this report, for the first time, the clear evidence of the quantum size effect on the exciton polariton in GaAs thin films is presented. Several discrete luminescence lines were clearly observed in the free exciton luminescence spectrum of high quality GaAs thin films. The thickness of samples was of the order of 1000Å. Also discrete structures related to the luminescence lines were measured using reflectance spectra. Both photoluminescence and reflectance spectra were dependent on the thickness of the GaAs film. The discrete spectra are interpreted by considering the quantization of the spatial dispersion of the exciton polariton. This is a new quantum size effect on the exciton polariton which is quite different from the usual quantum well structure.

2.Experiments

Undoped GaAs thin films whose thicknesses (d) were of the order of 1000 Å, were prepared by a MBE technique. To obtain a high quality GaAs, a GaAs (50 Å)-$Al_{0.19}Ga_{0.81}As$(86 Å) superlattice buffer layer composed of 70 periods was grown on a semi-insulating (100) GaAs substrate. The cap layer consists of the same superlattice structure of 20 periods. The thickness of the GaAs thin film layer was measured by using a scanning electron microscope whose

resolution is 30 Å. The hetero-interface was observed using a treatment of chemical etching and the thickness could be determined with a precision of 50 Å. The thickness of typical samples presented in this report were 990 + 50 Å, 2010 ± 50 Å, and 5200 ± 50 Å.

3.Results and Discussion

Figure 1 shows the photoluminescence spectrum of the free exciton (the exciton polariton) for the three different thickness of GaAs film. The samples were immersed in liquid He and the lattice temperature was 1.8 K. The excitation source was a dye laser (LD 700) excited by a Kr laser (6471 Å) and the wavelength was 7870Å. The excitation intensity on the sample was 5 mW cm-2 . The observation system consisted Of a 126cm spectrometer and a GaAs cooled photomultiplier with a photon counter. The resolution of this system was 0.05 Å.

As shown in Fig. 1(A), in the 5200 Å sample, the dominant peak at 1515meV is the polariton luminescence (Is state) and the excited exciton state (2s) is observed around 1517.8 meV. The weak luminescence with the fine structures around 1512.4meV is due to the radiative recombination of the exciton bound to the acceptor *((A°, X))*[5]. Optical quality is extremely high, because no other luminescence lines related to impurities can be observed. Although a carrier concentration of ~10^{14} cm^{-3} can be measured by our Hall measurement system, the carrier concentrations of undoped GaAs layers could not be measured because of the high resistivity. Fig-

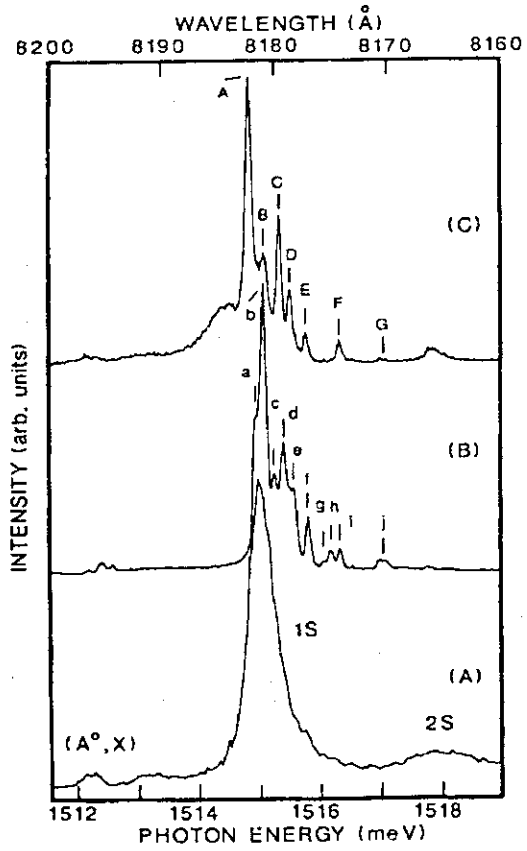

Fig. 1. Photoluminescence spectra of undoped GaAs thin films at 1.8 K. The thicknesses of the GaAs films are (A) 200Å, (B) 2010Å, and (C) 990Å.

ure 1 (B) and (C) present the luminescence spectra of the 2010-Å and the 990-Å samples, respectively. Remarkable changes can be observed in comparison to that of the 5200-Å sample. Sharp luminescence lines appear around the polariton luminescence (1515meV). In the following discussion and as shown in Fig. 1, the luminescence lines of the 990-Å and the 2010-Å samples are referred to as A, B, . . ., G and a, b, . . . , j, respectively. The linewidth (FWHM) of the F-line at 1516.34meV is found to be 0.1 meV. The *E, F,* G-line and the f, g, *h, i,* j-line exist between the Is and the 2s exciton state of the bulk GaAs. The luminescence from the *(A°, X)* state is also observed. This photon energy is the same as that of bulk sample, showing that the band structure of both the 990-Å and the 2010-Å sample is of the 3-dimensional type. Another type of sample whose buffer layer and cap layer were $A_{10.3}Ga_{0.7}As$, were grown and the same discrete luminescence spectra were observed. Therefore these discrete luminescence lines originate in the GaAs thin film layer. The fact that the photon energies of these structures depend on the thickness of the film shows that the appearance of the discrete luminescence spectra is caused by the decrease in thickness of the GaAs film.

The appearance of the discrete luminescence lines is interpreted to be due to the intrinsic nature of an exciton in a confined system. Two physical concepts are proposed; (1) interference effects on polariton branches into the crystal, similar to a Fabry-Perot mode, (2) quantization of the center of mass motion of an exciton and generation of quantized energy states.

A mechanism of an exciton polariton luminescence is considered as following [6]. An exciton polariton propagates in the crystal. At the boundaries, it reflects or transmits according to the probability of escaping from the crystal which is introduced from the Maxwell boundary conditions and the additional boundary condition (ABC). This probability is quite small at the large wave vector region. The exciton polariton with a large wave vector reflects into the crystal and can not go out as the luminescence. After relaxing the kinetic energy, the exciton polariton with a small wave vector can escape the crystal as polariton luminescence.

If the Fabry-Perot interference of polariton branches gives rise to the modulation of the escaping probability, the luminescence spectrum should be dependent on the angle of the observation like the reflectance spectrum. As the luminescence spectra are independent of the angle, the appearance of the fine structures of luminescence is attributed to the quantization of the center of mass motion. Such a size effect on the luminescence in the GaAs film is different from the interference effect on the reflectance spectrum in a semi-infinite slab [2, 3]. In the case of the reflectance spectrum, the exciton polariton with the fixed momentum and direction of propagation, is generated by the incident radiation field. The interference patterns in the reflectance spectrum which satisfies the Fabry-perot interference condition between the incident radiation field and the reflected radiation field, can be observed in a crystal whose size is limited by the length of the polariton propagation. In contrast, the type of photo-excited carrier in our experiment is an electronhole pair and the generated polariton from the electron and the hole distributes thermally and moves in all directions. The exciton state is determined by the film thickness

(d) and the energy distribution in the z-direction is restricted. The exciton in this confined system loses one degree of freedom and becomes 2-dimensional.

In the above mentioned discussions, it has not been clear whether this size effect is explained as the quantum size effect on the exciton or the exciton polariton. If the energy levels are generated by the confinement of excitons [7], the quantized energy levels should appear above the photon energy of the heavy-hole exciton at K= O (E_o = 1515meV). As shown in both the A-line and the a-line of Fig. 1, the lowest levels are observed at 1514.88meV and 1514.95meV, respectively. These levels are below the photon energy of Eo and correspond to the low energy tail of the polariton luminescence of the 5200-Å sample. The quantized energy states are not explained by the total blue shift and should be considered as the exciton polariton.

The spatial dispersion curve of the exciton polariton in GaAs consists of three branches [8] and was determined experimentally by resonant Brillouin scattering [9] with a wave vector less than 1 x $10^6 cm^{-1}$. The dispersion curve which is in good agreement with the experimental result of the resonant Brillouin scattering [9], is presented in Fig. 2. This curve is calculated by using entirely the same method as in [8]. Parameters are as follows; M_h^{-1} = $1.25m_o^{-1}$, M_l^{-1} = $5.46m_o^{-1}$,$\pi\beta_0$= 1.325 x 10-3, = 12.55, εo = 1515 meV, the total energy from the exchange interaction = 7.3 x 10^{-2}meV.

D'Andrea and Del Sole [10]considered the wave function of the exciton to be a propagating wave and an evanescent wave exp (—Pz) at the boundaries. The quantization condition of the center of mass motion is described by Cho [11] as

$$K = (N\pi)/(d-2/P),\ N = 1, 2, 3, \ldots.$$

where **K** is the wave vector, when Pd 1. The dead layer (I/P) is a result of the boundary condition of the exciton wave function and implies that the exciton can not be found at boundaries. This dead layer is the intrinsic parameter for the ABC problem. Only the **K** vector satisfied in the above equation is allowed in the thin films.

The lowest energy levels of both the A-line and a-line correspond to the photon-like part of the lower branch. This is why the lowest energy level appears below the photon energy of E_o and the quantized phenomena is explained by the exciton polariton picture. In the case of the 2010-Å sample, the a-line corresponds to the N= 2 state obtained from the quantization condition. If the depth of the dead layer is zero, this energy level should be observed at 1514.65 ± 0.09 meV as shown by the arrow in Fig.2. The observed photon energy is 1514.95meV. This large discrepancy convinces us of the existence of a dead layer. The depth of the dead layer (I/P) is determined to be 127.5 Å from the experimental result of the a-line and the quantization condition. This value is almost the same as the Bohr radius of an exciton in a bulk sample [11]. Applying this quantization condition to the observed photoluminescence spectra, our results give good agreement with the dispersion curve of the bulk sample, as shown in Fig. 2.

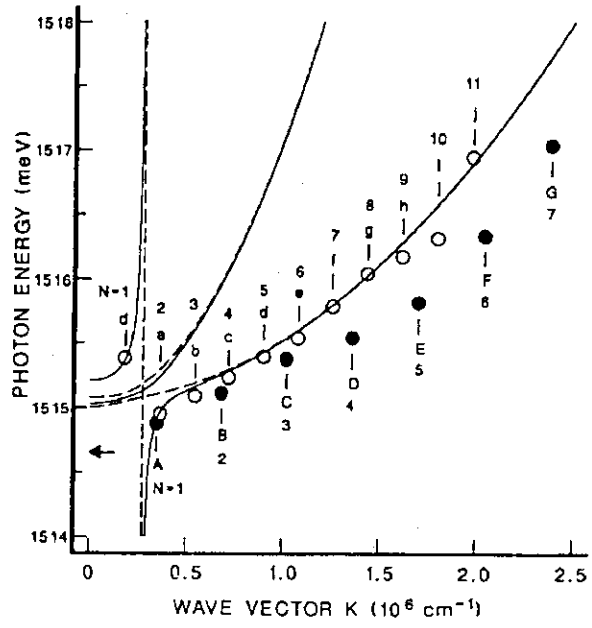

Fig. 2 Exciton polariton dispersion curve (solid lines) obtained by the calculation. Dashed lines are dispersion curves of the heavy-hole exciton, the light-hole exciton and the photon. Open and closed circles represent luminescence photon energies allowed the quantization condition of the 2010-Å and the 990-Å GaAs, respectively.

4.Conclusion

It is concluded that this discrete spectrum indicates the quantization of the spatial dispersion of the exciton polariton. From the same analysis, the (I/P) of the 990-Å sample is found to be 31.6 Å and the lower polariton branch is obtained as shown in Fig. 2. The lower branch of the 990-Å sample is different from that of the 2010-Å sample. The dispersion curve of the 990-Å sample shows that the exciton mass increases in comparison to that of the 2010-Å sample and the deviation from the dispersion curve of the bulk polariton becomes large. With decreasing thickness, the center of mass motion is strongly affected by boundaries and the 2-D character is enhanced.

REFERENCES

1.J.J. Hopfield & D.G. Thomas, *Phys. Rev.* 132, (1963)563.
2.V.A. Kiselev, B.S. Razbirin & I.N. Uraltsev, *Phys. Status Solidi (b)* 72, (1975)161.
3.T. Mita & N. Nagasawa, *Solid State Commun.* 44, (1982)1003.
4.R. Dingle, in *Festkorperprobleme XV (Advances in Solid State Physics),* edited by H.J. Queisser (Vieweg, Braunschweig, 1975).
5.U. Heim & P. Hiesinger, *Phys. Status Solidi (b) 66,* (1974)461.
6.Yutaka Toyozawa, *Prog. Theor. Phys.* 12, (1959) 93.
7.Y. Kayanuma, *Solid State Commun.* 59, (1986)405.
8.G. Frishman, *Solid State Commun.* 27, (1978)1097.
9.Rainer G. Ulbrich & Claude Weisbuch, *Phys. Rev. Lett.* 38, (1977)865.
10.A. D'Andrea & R. Del Sole, *Phys. Rev.* B25, (1982)3714.
11.Kikuo Cho & Masaru Kawata, *J. Phys. Soc. Jpn.* 54, (1985)4431.

17. FOURIER POWER SPECTRA OF APERIODIC CONDUCTANCE FLUCTUATIONS IN NARROW WORES OF GaAs／AlGaAs HETEROSTRUCTURE

Yuichi OCHIAI, Koji ISHIBASHI,[1] Masahiro MIZUNO, Mitsuo KAWABE, Yoshinobu AOYAGI,[1] Kenji GAMO,[2] and Susumu NAMBA[1]

Institute of Materials Science, University of Tsukuba, Tsukuba Ibaraki 305, Japan. [1]Frontier Research Program, Institute of Physical and Chemical Research, Wako, Saitama 351-01, Japan. [2]Department of Electrical Engineering, Faculty of Engineering Science, Osaka University, Toyonaka, Osaka 560, Japan.

1. Introduction

Recently we can obtain one-dimensional narrow wires of Si and GaAs by confining their two-dimensional electron-gas systems. Low temperature magnetoresistance (MR) in narrow GaAs/AlGaAs wires have been measured in order to clarify the quantum interference effects in a mesoscopic system where the dimensions are comparable or less than the phase coherent length of electron transports. Electrons in such a system behave coherently and the phase coherence of the electron wave gives rise to the quantum interference. In high magnetic fields, suppression of quantum interference oscillations due to Aharonov-Bohm effect was observed in the MR for a ring of high mobility GaAs/AlGaAs heterostructures and the period of the oscillation shifts to lower frequency in the field dependence of Fourier spectrum of the MR.(1) A similar low frequency shift of the decay part in the Fourier spectrum has been observed in a wire of GaAs/AlGaAs heterostructure.(2) In this study, magnetic field dependence of aperiodic fluctuations in MR has been studied by means of analysing the Fourier transform.

2. Experiments

The samples in this study are narrow wires with GaAs/AlGaAs double and single heterostructures grown by the molecular beam epitaxy technique and made by using electron beam lithography and dry etching technique. The double heterostructure sample (named DHW-08) has a 800 nm-thich non-doped GaAs buffer layer, a 10 nm-thick cap layer, two 2nm-thick spacers, and a 10nm-thickGaAs layer sandwiched between two Si-doped AlGaAs layers of 60 nm-thickness. The single heterostructure sample (named SHW-02) has a non-doped GaAs buffer layer followed by a 6 nm-thick non-doped AlGaAs spacer layer and the 50 nm-thick Si doped AlGaAs layer. The lithographical width and length of those wires were about 700 nm and 3000 nm for DHW-08 or 1700 nm for SHW-02, respectively. The actual width for electrical conduction is less and about 400 nm for the two samples because of existence of a surface depletion layer. The mean free paths of DHW-08 and SHW-02 are less than 150 and 430 nm, respectively. Mobilities are estimated to be about 8600 cm^2/Vsec for DHW-08 and 25000 cm^2/Vsec for SHW-02 at 4.2 K, respectively.

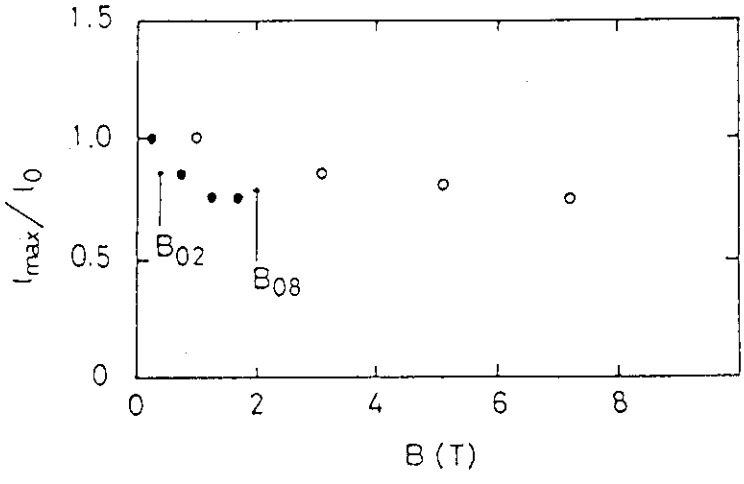

Fig. 1; Magnetic field dependence of Lmax/L0 at 80 mK for DHW-08(open circle) and at 1.2K for SHW-02(closed circle). B02 and B08 stand for the critical fields for SHW-02 and DHW-08, respectively.

The MR measurement at low temperature was carried out under magnetic fields up to 8.5 T in a He3-He4 dilution refrigerator.

3. Results and Discussions

Universal conductance fluctuations (3,4) can be observed in the MR with an amplitude of the order e^2/h for the two samples. Although DHW-08 shows MR fluctuations up to 8 T, such fluctuations in SHW-02 cannot be detected in higher fields above 2 T because of the appearance of Shubnikov-de Haas oscillations. Fourier spectra of the MR in the two samples were analysed in various ranges of the magnetic field and are relevant to the area enclosed by a pair of electron trajectories. If the oscillation is caused by the AB effect in each conduction path in the wire, the period of ΔB in a certain oscillation component of the fluctuations is connected with the enclosed area S by the relation $\Delta BS=h/e$. With increasing magnetic fields we have observed a low frequency shift of the decay part of the fluctuations in the spectrum for DHW-08.(2) A similar shift has been obtained in the case of SHW-02. Here we define a maximum length l_{max} which corresponds to the maximum area where the

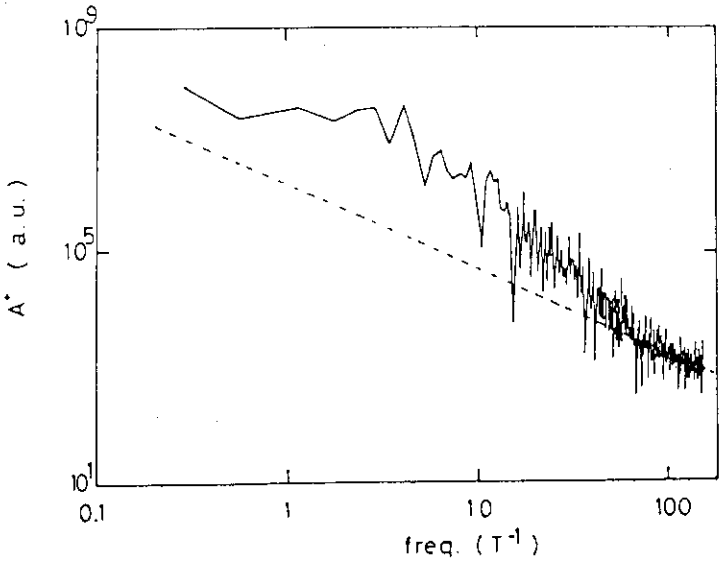

Fig. 2; Fourier power spectrum between 0 and 2 T in DHW-08 at 80 mK. Dotted line shows $f^{-1/2}$ dependence.

quantum interference can be successfully performed. l_{max}/l_o of the two samples are plotted in Fig. 1, where l_o is the effective conduction length at the lowest field range in the Fourier transformation. Near the critical field of $\omega_c\tau=1$, the decay of aperiodic fluctuations, which is observed in the low frequency side of the Fourier spectra, begins to shift to low frequencies. The shift can be explained by reduction of the effective area for the interference. We consider that the reduction comes from the formation of a certain conduction channel which does not affect quantum interference.

Figure 2 shows Fourier power spectrum at the lowest field range between 0 to 2 T from the MR in DHW-08 at 80 mK. It is noted that the spectrum has a back ground component whose slope is almost $f^{-1/2}$ as indicated with a dotted line. If the back ground does not originate in quantum interferences, the band spectrum from 5 to 40 T^{-1} must correspond to the component due to the network of the actual conduction paths in a wire. Since in the case of DWH-08 the lowest field range is in $\omega_c\tau < 1$, the reduction of effective area, as mentioned above, does not occur. It means that using a precise analysis of the interference of the electron waves, we will be able to resolve each conduction path in a mesoscopic wire. As for the $f^{-1/2}$ component in Fig. 2, we can not determine the origin from our transport results. We think that it may come from a certain process in measurement system.

References

(1) G.Timp, P.M.Mankiewich, P.deVegvar, R.Behringer, J.E.Cunningham, R.E.Howard and H.U.Baranger: Phys.Rev. B39 (1989) 6227.

(2) M.Mizuno, K.Ishibashi, S.K.Noh, Y.Ochiai, Y.Aoyagi, K.Gamo, M.Kawabe and S.Namba: Jpn.J.Appl.Phys. 28 (1989) L1025.

(3) B.L.Altshuler: JETP Lett. 41 (1985) 648.

(4) P.A.Lee and A.D.Stone: Phys.Rev.Lett. 55 (1985) 1622.

18. MAGNETISM OF METAL SUPERLATTICE

Hiroyasu Fujimori

(No paper was submitted)

APPENDIX　タンデム加速器研究会プログラム及び要旨集

平成３年１月２２日（火）
１月２３日（水）

東海研　第７会議室

タンデム加速器研究会プログラム

平成３年１月２２日（火）

		講演開始時間 （講演時間）
開会の挨拶	石井三彦（原研）	９：２５
１．タンデム加速器とブースターの現状		
	小林　千明（原研）	９：３０ （２０分）

セッション（Ａ）－半導体の欠陥－
座長　前田　裕司（原研）

１．照射したＳｉ単結晶のＸ線トポグラフイによる研究		
	富満　広（原研）	９：５５ （３０分）
２．シリコン結晶中の点欠陥と２次欠陥		
	阿部孝夫（信越半導体）	１０：３０ （３５分）
３．コメント		
中性子照射したＳｉの陽電子寿命測定		１１：１０
	岩田忠夫（原研）	（１５分）

＊＊＊＊＊　昼　　食：１１：３０～１３：１５　＊＊＊＊

セッション（Ｂ）－イオン・固体衝突－
座長　俵　博之（核融合科学研）

１．荷電粒子と固体表面の相互作用に関する最近の話題		
	飯高敏晃（早稲田大）	１３：１５ （４０分）
２．Glancing Collision 下でのConvoy Electron 生成		
	小山昭雄（理研）	１４：００ （４０分）
３．イオンビームを用いた固体物理の研究		
	万波通彦（京大）	１４：４５ （４０分）

＊＊＊＊＊　休　　憩　：１５：３０～１５：４０　＊＊＊＊

セッション（Ｃ）－高エネルギー原子衝突－
座長　渡部　力（国際基督大）

１．ビームの物理
森　義治（高エネルギー研）　１５：４０
（４０分）
２．高エネルギー原子衝突の理論
戸嶋信幸（筑波大）　１６：２５
（４０分）
３．高エネルギー原子衝突の実験
金井保之（理研）　１７：１０
（４０分）

＊＊＊＊＊＊＊　懇親会（１８：１５から）＊＊＊＊＊＊＊＊

平成３年１月２３日（水）

セッション（Ｄ）－照射効果－
座長　岩田　忠夫（原研）

１．高温超電導物質の照射効果
数又幸生（原研）　９：３０
（３０分）
２．ＦＣＣ金属の高エネルギー重イオン照射損傷
岩瀬彰宏（原研）　１０：０５
（３０分）

＊＊＊＊＊　休　　憩　：１０：４０～１０：５０　＊＊＊＊

３．宇宙用半導体デバイスの重イオン照射効果
（シングルイベント現象）
五家建夫（宇宙センター）　１０：５０
（４０分）
４．核融合炉セラミック増殖材の照射効果
野田健治（原研）　１１：３５
（３０分）

＊＊＊＊＊　昼　　食　：１２：１０～１３：１５　＊＊＊＊

セッション（Ｅ）－ウラン化合物及び人工格子－
座長　数又　幸生（原研）

１．ウラン化合物の物性		
	松井尚之（名大）	１３：１５ （４０分）
２．人工格子（半導体）		
	青柳克信（理研）	１４：００ （４０分）
３．量子細線の電気伝導		
	落合勇一（筑波大）	１４：４５ （４０分）
４．金属人工格子の磁性		
	藤森啓安（東北大）	１５：３０ （４０分）
閉会の挨拶	数又幸生（原研）	１６：１５

原研タンデム加速器とブースターの現状

日本原子力研究所
加速器管理室　小林千明

概要

原研タンデム加速器は米国National Electrostatics Corpration（ＮＥＣ）製で、１９７８年組立が開始され１９８０年１０月最初の実験を行った。１９８２年８月より実験体勢が整い、本格的に使用を開始した。以来現在に至るまで順調に運転され、核物理、固体物理、原子分子、材料物性、核化学、放射線化学、中性子物理等の研究に使用されている。研究領域拡大のため１９８８年よりタンデム後段ブースターの建設を開始した。

タンデム加速器

加速電圧１８ＭＶで世界第３番目の大型静電加速器である。折り返し構造のため低エネルギー加速管と高エネルギー加速管が並列に配置されている。高電圧端子内には１８０度偏向電磁石やイオン源を装備しているので、通常のタンデム加速器と比べ構造は非常に複雑である。使用分野が広いので加速元素の種類も多い。静電型加速器としては世界最初の計算機による制御システムを採用した機種である。順調に作動中で５０００時間以上／年の運転を行っている。

タンデム後段ブースター

タンデム加速器からの重イオンのエネルギーを約４倍に増強し、重イオンを用いた研究が広い分野で可能となることを建設の目的とした。完成後は広い分野において最先端の研究ができるようになる。

加速器の方式としては性能に優れた超電導加速空洞で構成するリニアックにとした。このため数年をかけてニオブによる１／４波長型超電導加速空洞を開発した。現在量産中の加速空洞の性能は８００ＫＶ／ｍ程度が得られている。これは世界第一級の性能である。下表にブースター建設の日程を示す。

タンデム後段ブースター建設日程

項目＼年度	１９８８	８９	９０	９１	９２	９３
リニアック製作						
Ｈｅ冷凍器製作						
建家増設						
加速器組立						
試験調整運転						

(A) － 1

重イオン照射したSi単結晶のX線観察

原研・固体物理第1研究室　富満　広

種々の重イオン（Li～Au）を、高エネルギー（20～200MeV）で照射した（照射量 10^{13}～10^{15} ions／cm^2）Si単結晶試料に関して、その結晶完全性の変化を、X線回折トポグラフィ法（XDT）で観察して、以下のような事柄が見出された[1]。

① 試料結晶が巨視的に変形・弯曲することがあるが、転位線の発生や、試料の溶融・破壊等は見出されていない。

② 照射～非照射境界に非常に大きな格子歪みが集中し、それが、試料裏面にまで達することがある。

③ 照射領域に、特異な欠陥像が観察されることがある。

④ 照射領域に規則的な干渉縞が観察されることがある。

また、上記の観察事実は、照射条件（照射イオン種、エネルギー、特にビームの均一性など）にも依存するらしいこと、及びXDT観察条件（反射面の種類など）に依存すること、等が明らかになった。

他方、上記の観察事実は一部、先人の観察結果[2-4]に共通する部分はあるが、重要な点で不一致の部分がある[2]ので、観察を深めている所である。
最近では、上記の観察事実の物性的理解を更に深める目的で、二結晶精密X線回折法による精密測定をも試みている。特に上記 ④ の干渉縞に関して、その成因・由来を明らかにするために、試料中の格子定数を精密測定する実験を行なっている。

当日は、上記の研究により現在までに明らかになった事柄を報告する。

[参考文献]
1)-H.Tomimitsu; Jpn J.Appl.Phys. 22 (1983) L674.
-H.Tomimitsu; Acta Crystallogr. A43(1987) Suppl. C207.
-H.Tomimitsu; JAERI TANDEM, LINAC & V.D.G Annual Report, 1982-1988.
2)-G.H.Schwuttke,K.Brack,E.E.Gardner & H.M.DeAngelis; Proc.Santa Fe Conf. Radiation Effects in Semiconductors ed. F.Vook, (Plenum Press, N.Y., 1968) p.406.
-U.Bonse, M.Hart & G.H.Scwuttke; Phys.Status Solidi 33 (1969) 361.
-U.Bonse & M.Hart; Phys.Status Solidu 33 (1969) 351.
3) A.R.Lang & V.F.Miuscov; Appl.Phys.Lett. 7 (1965) 214.
4) D.Simon & A.Authier; Acta Crystallogr. A24 (1968) 527.

(A)－2

シリコン結晶中の点欠陥と二次欠陥

阿　部　孝　夫

信越半導体(株)磯部研究所　〒379-01　安中市磯部 2-13-1

21世紀の初めには 1G（ギガ）DRAM メモリーが予測され，そのときの出発結晶の直径が 300 mm といわれる．現在，結晶の完全性を乱す重金属不純物の低減化が進み，次は「不純物」としての点欠陥が注目されている．本稿ではまず，成長中の結晶格子が膨張か収縮かによって発生する点欠陥の種類が変わることを，ウエハー表面の酸化と窒化現象，共有結合半径の異なる不純物の添加および，結晶内温度こう配の解析により説明する．それによって，一見大きく異なる FZ 結晶と CZ 結晶中の微小欠陥の発生を統一して記述できることを示す．また，大直径化とともに半径方向の温度こう配が増大するので，酸素誘起の積層欠陥（OSF）の制御が困難になることを明らかにする．さらに今後の課題として，完全結晶を得るための計算機シミュレーション研究の方向について触れる．

(B)−1

荷電粒子と固体表面の相互作用の理論

早稲田大学物理学科
飯高敏晃

表面とイオンの動的な相互作用の研究は、さまざまな応用分野での基礎過程として重要である。従来、このような研究は高速軽イオンを使って為されてきたが、近年、高速多価重イオンによる表面研究の重要性が注目されはじめた。多価重イオンは軽イオンに比べて電荷がはるかに大きいため、今まで軽イオンでは弱すぎて観測が困難であった表面の動的な応答の影響を明確に見ることができるからである。最近、我々はＸｅ$^{+27}$など高速重イオンによる二次電子放出スペクトルの実験結果を説明する理論を展開して成果をあげつつあるが、未解明の問題が多数ある。この分野の実験的および理論的研究はこれからの課題である。

今回は、多価重イオンによるコンボイ電子の加速を中心に話しをする。コンボイ電子とは、イオンを固体に入射したときにイオンとほぼ同じ方向にほぼ同じ速さで出てくる二次電子のことで、気体標的の実験やイオンの薄膜透過型の実験では広く研究されている。表面にすれすれ角で入射する実験では正の電荷を持ったイオンがつくる負の鏡像電荷によって電子が反発されて加速することが予想される。従来、水素・ヘリウムを用いて実験が行われてきたが(1)、最近の多価重イオンの実験で鏡像電荷で加速されたらしい二次電子が明確に観測された(2)。我々は、固体表面の誘電応答を考慮したシミュレーション・コードを開発し、このコンボイ電子の加速エネルギーを理論的に説明することに成功した(3,4)。

荷電粒子による表面の誘電応答の理論は我々の研究室で長年研究してきたテーマであるが、多価重イオンによる実験によって新しい展望が開かれたと言えよう。多価イオンと表面の相互作用は、これから理論的にも実験的にも大変興味深い分野である。

(1) M. Hasegawa et al., J. Phys. Soc. Jpn. 57 1834(1988)
(2) A. Koyama et al., Phys. Rev. Lett. 65(25) 3156 (1990)
(3) T. Iitaka et al., Phys. Rev. Lett. 65(25) 3160 (1990)
(4) T. Iitaka et al., the 4th Japan-USSR Symposium on the Interaction of Fast Charged Particles with Solids (Tsukuba)

(B)－2

Glancing Collision 下でのConvoy Electron の生成

理研　　小山　昭雄

荷電粒子が固体を通り抜ける時、イオンと同じ方向に、同じスピードを持った電子が励起される。このような、入射粒子の連続準位に捕獲された電子はコンボイ（ＣＥ）と呼ばれる。荷電粒子が固体表面の近傍にある時、表面電子は分極され、それによって、動的な鏡像ポテンシャルが誘起される。この鏡像ポテンシャル（ＤＩＰ）はこれらのＣＥを加速することが出来る。

Brugdorferは表面に対して垂直に出射する荷電粒子により励起されるＣＥのＤＩＰによる加速を考察した（１９８７）。しかしながら現在のところ、これら垂直出射イオンにより励起されたＣＥのＤＩＰによる加速は実験的に見出されていない。

もしイオンが表面にすれすれに入射し、かつＣＥがすれすれに出射するならば、表面とイオン及び表面とＣＥとの相互作用の時間が長くなり、ＤＩＰの作用は強く現れることになり、従ってＣＥの加速も検証可能になるかも知れない。実際、万波グループはHe^{+}をＳｎＴｅに入射させた時、イオンのスピードより速いＣＥが放出される事を初めて見出した（１９８８）。

理研では、このＤＩＰ加速メカニズムを検証するため、多荷チャージのイオンを用いて、Ａ１表面から放出されるＣＥのエネルギー角度分布を調べた。測定結果はＤＩＰ加速モデルと定性的によく一致するものであった(１９９１)。さらに飯高らは、このモデルに基づいて、加速エネルギーのモンテ・カルロ計算を行ない、定量的にも本実験とよくあう結果を得た（１９９０）。本講演ではこれらの実験結果と共に、最近得たターゲット依存性についても述べる。

(B)－3

イオンビームを用いた固体物理の研究

京都大学工学部物理工学　　万波通彦

1.　近年，イオンビームを利用した半導体素子の製造，新素材の開発，加工等の工業的利用が盛んである．更に，イオンビーム技術により作られた特殊な半導体素子，新素材，メゾスコピック状態は固体物理の最先端と関わる新しい展開を始めている．また，イオンビームを用いた多くの固体の分析法が利用されている．このような進歩の背後には，イオンと固体の相互作用についての研究の成果が大きな役割を果している．しかし，イオンビームを用いた固体物理の研究そのものについて見る限り，この３０年間の進歩は工業的利用の進展に比べ非常に見劣りするように思える．

例えば，１９６０年代前半にイオンチャネリングが発見され，これを利用して不純物原子の格子内位置決定が出来るようになつた．これは他の分析方法に替え難いものである．これと同じ原理によりイオンビームによる固体表面原子構造の新しい決定法が開発され，従来のＬＥＥＤ構造解析を補うものとして利用されている．しかし，固体電子状態についてはイオン中性化スペクトロスコピー等による表面電子状態についての研究があるのみである．イオンと固体の相互作用として特徴的現象としてイオンの下流に生じる航跡（wake）の存在が見いだされているが，固体電子の詳細には依存しない現象のように思える．

ｋｅＶからＭｅＶのイオンは固体内原子衝突において，電子励起，原子弾き出しの断面積等は大きい．したがつて，イオンにより固体内で引き起こされる現象およびイオン状態の変化の多くは非弾性多重衝突に支配され，散乱素過程そのものを知ることは容易でない．単結晶でイオンチャネリングが起こると，イオン軌道は結晶原子間に制限されThomas-Fermi遮蔽距離（約0.2Ａ）以下の衝突径数でのイオン・原子衝突が起こり難くなる．この様な状態で小さな衝突径数のイオン原子衝突が起こると，その衝突は容易に検出できる．不純物格子間原子の位置決定，表面原子構造決定はイオンチャネリングのこの特徴を利用したものである．

2.　チャネリングしているイオンは原子と小角多重散乱しながら運動する．１回の衝突はソフトで（衝突径数が大きい）その非弾性散乱の素過程は重要な情報をもたらす筈であるが，この場合も多重散乱により覆い隠されてしまう．面チャネリングと同様な現象として結晶表面における斜入射イオンの散乱がある．斜入射角がある臨界角以下のとき，イオンは表面原子との小角多重散乱により結晶内に入ることができず，鏡面反射される．この場合も小さな衝突係数による散乱は容易に検出されるが，衝突径数の大きなイオン励起過程は多重散乱に支配されている．表面斜入射散乱が面チャネリングと異るのはイオンが表面付近の価電子の集団振動を励起する点にある．これは固体内を運動するイオンのつくる航跡(wake)に対応するものである．面チャネリング，表面斜入射散乱におけるイオンの散乱励起過程について最近の我々の研究について述べる．

(C)－2

高エネルギー原子衝突の理論

筑波大学物理工学系　戸嶋信幸

一般に、原子と原子が衝突すると核反応から化学反応にいたるまで様々な現象が起こるが、ここではその内電子状態の遷移に話を限って報告する。入射粒子の速度が十分大きいと衝突時間が短く電子状態の変化は小さいと期待されるから、１次ボルン近似に類する摂動的手法が有効であると考えるのは自然な発想であるが、実際にはこれに反したり、それを越えた特別の扱いを要する場合が多々存在する。１次ボルンが破綻する最も顕著な例は、電荷移動におけるトーマス過程である。1s-1s間の１次ボルンの電荷移動断面積は入射エネルギーの６乗分の１に比例して急激に減少するのに対して、２次ボルンの断面積は５.５乗分の１に比例し僅かながら遅い減少を示し、高エネルギー極限では２次が１次を上回るという逆ざやが起こる。1955年にDriskoがこのことを示して以来、多種多様の理論が提唱され活発な研究が行われてきたが、その全てが量子論、古典論ともに摂動論に基づいている。しかし、そもそも２次が１次を上回るなら摂動論自体が破綻しており、自己矛盾をはらんでいると言わざるを得ない。摂動論に基づかない理論計算は、昨年初めて、close-coupling法とCTMC法によって行われた。

近年、衝突過程中における電子相関効果の重要性が実験、理論の両面において着目されている。例えば、ヘリウム原子の陽子、反陽子による電離断面積はMeV領域までずれを示し、電子相関効果の重要性を示している。もちろん１次Born近似ではこの効果は全く考慮できないが、電子相関はそもそも衝突相互作用には繰り込めない性質のものであるがために、満足な理論手法はまだ開発されていない。

一口に高エネルギー衝突といっても電子が衝突前にどの電子状態にあるかによって絶対的なエネルギーは大きく異なる。核子当り数百keV のエネルギーは水素原子の標的にとって高エネルギーであるが、数百MeVであってもウランの1s軌道にある電子にとっては高エネルギーと言えない。このような内殻電子の遷移を扱う場合には相対論的なエネルギーであっても、close-coupling法のような非摂動論的な手法が必要になる。また、相対論的な衝突では、非相対論的な場合には存在しないmonopole型の長距離相互作用が重要な役目を果たすことが近年の研究で見いだされている。

(C)－3

高エネルギー原子衝突実験

理化学研究所原子過程研究室　　金井保之

重イオン加速器からの高エネルギー重イオンを用いたイオン・原子衝突実験のうち、最近、原研タンデム、理研で行われた実験について報告する。

Ⅰ．　零度電子分光法を用いた研究

高エネルギー重イオンと零度電子分光法を用いることにより、プロジェクタイルイオンからの放出電子の高分解能測定が容易となった。この種の研究は、Stolterfohtらによりすすめられているが、原研・東大・京繊大・理研・ＨＭＩの共同グループでも原研タンデム等を用いて、ここ数年研究を行っている。図１に零度方向から測定された典型的な電子スペクトルを示す。原研タンデムからの６４ＭｅＶ　S^{12+}イオンとカーボンホイルの衝突における零度電子スペクトルである。1.1KeV付近のピーク（ＥＬＣ、ＥＣＣ）のほかに、このピークの上下に多くのピークが見える。これらは衝突により形成されたプロジェクタイルイオンの自動電離状態から放出された電子である（$1s^2 2pnl \rightarrow 1s^2 2s + \varepsilon l$）。図２にこのCoster-Kronig遷移に対応する部分のスペクトルをプロジェクタイルイオンの静止系に変換したものを示す。図１の1.2－1.5KeVの部分に対応している。このスペクトルからわかるように、高エネルギー重イオンと零度電子分光法を組み合わせることにより、プロジェクタイル系での1eV以下の分解能の測定が容易に行える。この特徴を生かしてＳイオン（原研タンデム）、Ｎイオン（理研リニアック）等の自動電離状態の研究等を行っている。

図　１．

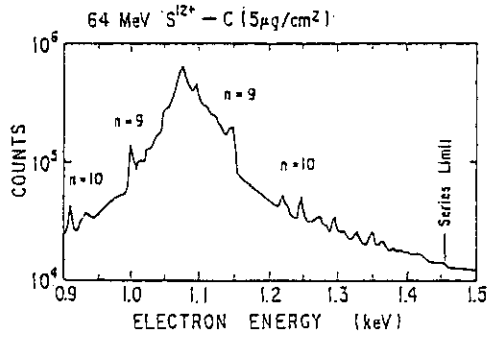

図　２．

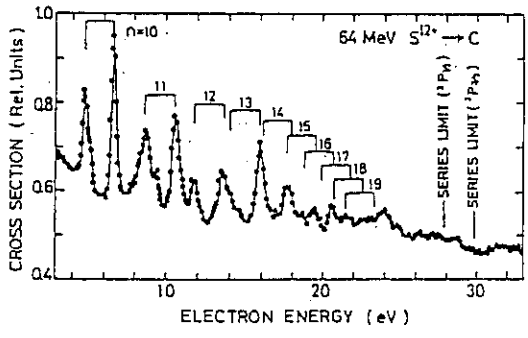

ＩＩ．　２６、８０ＭｅＶ／ｕ　Ａｒイオンの荷電変換

理研では１９８６年よりリングサイクトロンが稼働を開始し、これにより１００ＭｅＶ／ｕ程度までの重イオン衝突実験が可能となった。このビームを用いて、理研・東大・筑波大・京繊大等のグループが原子衝突実験を開始している。ここではその中から、Ａｒイオンの荷電変換についての実験を報告する。

理研リングサイクロトロンからの２６、８０ＭｅＶ／ｕＡｒイオン（入射荷数：１６＋、１７＋、１８＋）を種々の厚さの炭素薄膜に衝突させ、衝突後の荷電分布を測定する事により、（１）厚い標的に対する測定値から炭素薄膜通過後の平衡荷電分布を得、（２）薄い標的に対する測定値からＡｒイオンの電子捕獲・損失断面積を求めた。更に、Ar^{18+}イオンについては放射性電子捕獲断面積を求めた。表１にそれぞれのエネルギーでの平衡荷電分布を示す。２６ＭｅＶ／ｕの平衡荷電分布はShima等の経験式と一致するが、８０ＭｅＶ／ｕの平衡荷電分布は一致しない。これは、二つの衝突エネルギーでのAr^{18+}の主要な電子捕獲過程が異なる事によると考えられる。実際、測定から２６ＭｅＶ／ｕではAr^{18+}の一電子捕獲はほとんど非放射性電子捕獲であり、８０ＭｅＶ／ｕでは６０％程度が放射性電子捕獲である事がわかった。

表１　Ａｒイオンの炭素膜通過後の平衡荷電分布

エネルギー (ＭｅＶ／ｕ)	平衡平均荷電数	荷電分布 16＋	17＋	18＋
２５．３	１７．９８	1.2×10^{-4}	2.0×10^{-2}	9.80×10^{-1}
７７	１７．９９９４	5×10^{-7}	5.6×10^{-4}	9.994×10^{-1}

(D)－1

高温超電導物質の放射線照射効果

数又　幸生（原研）

高温超電導物質の放射線照射効果についてこれ迄の報告をもとにその概要を述べる。照射効果については臨界温度（T_c）及び臨界電流密度（J_c）に関する報告が圧倒的に多く、臨界磁場H_{c1}及びH_{c2}については、2～3の報告があるに過ぎない。本報告では、T_c及びJ_cについて述べる。

欠陥生成のための放射線としては殆ど全ての放射線が－X－，γ－線、電子線、中性子、及び各種のイオン－用いられている。

(1)臨界温度（T_c）の照射効果

- γ線照射については全く異なる結果が報告されている。つまり、照射によるT_cの上昇、下降そして変化なし（2×10^{9} rad 迄）。
- 電視線照射では、Y系について最大～－1 K／10^{18}／cm^2である。
- 原子炉中性子照射については、Y系で～－3 K／10^{18}n／cm^2程度。
- イオン照射については、イオン種及びエネルギーに依存しているが、GeV領域とMeV以下の領域では異なる結果が報告されている。つまり、GeV領域では核衝突の他に電子励起過程が欠陥生成に寄与しているのに対しMeV以下の領域では、核衝突のみが欠陥生成に寄与していると考えられている。

核衝突のみを考慮した場合照射によるT_c変化の規格化は容易でありその例が第1図に示されている。

(2)臨界電流密度（J_c）の照射効果

J_cは(i)電流法及び(ii)磁気的方法の2つの方法で測定されている。(i)は結晶全体に渡っての臨界電流密度を与えるのに対し(ii)の方法は粒界内部でのそれを与えていると考えられる。照射効果はT_c同様全ての放射線が用いられている。一般に電流法による測定では、印加磁場がない時、照射によってJ_cは減少している。これに対し磁気的方法の測定では、全ての照射についてJ_cは増加している。増加の割合は最大で照射前の4倍程度である。

（参考文献）

1. 数又　幸生　”高温超電導物質の放射線照射効果” JAERI-memo 02-438
2. 小沢　国夫　”A bibliography of Irradiation effect on High T_c Superconductors”
3. 数又　幸生、楢本　洋　”高温超電導　放射線照射　データ集（Ⅰ）～（Ⅳ）” JAERI-memo 01-210～01-213

第1図

照射によるT_c変化の規格化

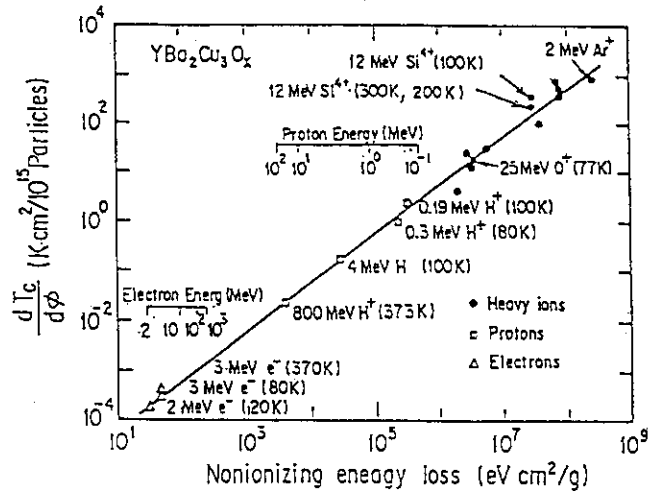

G. P. Summers et al. Appl. phys. Lett 55 (1989) 1469

○核衝突のみ（弾性衝突）

Ⓓ－2

FCC金属の高ｴﾈﾙｷﾞｰｲｵﾝ照射損傷

原研　物理部　固体物理第二研究室　　岩瀬彰宏

我々はここ数年の間、ｲｵﾝ照射したFCC金属の損傷生成やｱﾆｰﾘﾝｸﾞに関する研究を、原研ﾀﾝﾃﾞﾑ加速器及び2MVVdG加速器を用いて行ってきた[1-8]。その結果、金属においても、照射ｲｵﾝによる電子励起が照射損傷生成、照射ｱﾆｰﾘﾝｸﾞの過程において重要な役割を演ずることを初めて見いだした。本講演では、この電子励起効果に力点をおきながら、我々の研究のﾚﾋﾞｭｰを行う。

高ｴﾈﾙｷﾞｰ(＞100MeV)の重ｲｵﾝを極低温で照射したNiの照射後昇温実験において、ｽﾃｰｼﾞⅠにおける損傷回復量が異常に減少、或は消失してしまう現象がみいだされた[3,5,6]。また、この損傷回復量は、電子的阻止能と大きな相関を持っている。これに対して、Cuにおいて同様な実験を行った場合、ｽﾃｰｼﾞⅠにおける損傷回復量は、低ｴﾈﾙｷﾞｰｲｵﾝ照射の時と同じく、弾性的衝突を表すﾊﾟﾗﾒｰﾀで記述できる。さらに、予め単純な構造の欠陥を導入したNi、Cuに100MeV重ｲｵﾝを照射することによって行った、いわゆる照射ｱﾆｰﾘﾝｸﾞ実験を定量的に解析した結果、Niにおいては、ｽﾃｰｼﾞⅠの回復に寄与すべき欠陥(自由な格子間原子)に対する消滅断面積が、Cuの場合に比べて1桁以上も大きいという結果を得た[5,6,7]。これらの結果から、高ｴﾈﾙｷﾞｰ重ｲｵﾝ照射したNiの場合、ｲｵﾝによって励起した電子のｴﾈﾙｷﾞｰが格子系に伝達され、照射欠陥の一部を消滅させたものである、と結論した。そしてNiとCuの違いはその電子格子相互作用の大きさによって説明できる。これは他のFCC金属における実験結果によっても支持される[5]。Niと同様電子格子相互作用の大きなPtでは、高ｴﾈﾙｷﾞｰ重ｲｵﾝ照射によるｽﾃｰｼﾞⅠの異常な減少、消滅が起こり、Cu同様電子格子相互作用の小さいAgでは、電子励起効果は観測されない。

さらに、最近の損傷生成率の測定結果によれば、照射ｱﾆｰﾘﾝｸﾞにおいては電子励起効果の観測されなかったCu、Agにおいて、照射初期において極めて大きな損傷生成率が得られ[6]、しかもこの量が電子的阻止能と大きな相関を持っている[8]。これは、照射初期に電子励起によって欠陥が生成されていることを示唆するものであり、現在さらに実験中である。

[1]A. Iwase, S. Sasaki, T. Iwata and T. Nihira, J. Nucl. Mater. 133/134 (1985) 365.
[2]A. Iwase, S. Sasaki, T. Iwata and T. Nihira, J. Nucl. Mater. 141-143 (1986) 786.
[3]A. Iwase, S. Sasaki, T. Iwata and T. Nihira, Phys. Rev. Lett. 58 (1987) 2450.
[4]A. Iwase, S. Sasaki, T. Iwata and T. Nihira, J. Nucl. Mater. 155-157 (1988) 1188.
[5]A. Iwase, JAERI-M 89-071 (1989).
[6]T. Iwata and A. Iwase, Rad. Effects and Defects in Solids, 113 (1990) 135.
[7]A. Iwase, T. Iwata, S. Sasaki and T. Nihira, J. Phys. Soc. Jpn. 59 (1990) 1451.
[8]A. Iwase, T. Iwata, T. Nihira and S. Sasaki, to be published.

Ⓓ－3

宇宙用半導体デバイスの重イオン照射効果（シングルイベント現象）

宇宙開発事業団　筑波宇宙センター　五家建夫

宇宙用機器に使用される部品のうち特に半導体デバイスは宇宙の放射線に対してセンシチブであり、使用に当っては耐放射線性を充分配慮しなければならない。

耐放射線性として考慮すべきは、トータルドーズ効果とシングルイベント現象があるが、ここでは、近年特に重要性を増しているシングルイベント現象について、研究の現状を紹介する。

シングルイベント現象とは、高エネルギー粒子１個の入射により突然発生する、ＩＣのフリップフロップ回路のビット反転による誤動作（ＳＥＵ：シングルイベント・アップセットまたはソフトエラー)、ＣＭＯＳ構造のＩＣでの寄生サイリスタをトリガして起きる焼損故障（ＳＥＬ：シングルイベント・ラッチアップ）、パワーＭＯＳＦＥＴトランジスタでの寄生トランジスタをトリガして起きる焼損故障（ＳＥＢ：シングルイベント・バーンアウト）を総称する現象である。　ＳＥＵは、民生用ＩＣメモリがＬＳＩ化したときの問題点の１つであったα線ソフトエラー、すなわちＩＣのパッケージ材料に微量に含まれるウランやトリウムからのα線に起因するビット反転と同じ現象が、このα線よりはるかにエネルギーの高い宇宙放射線によって発生する現象である。

シングルイベント現象を起こす宇宙放射線としては、銀河宇宙線（ＧｅＶ～ＴｅＶ）や太陽フレアの重イオン（α線～鉄イオン）またはバンアレン帯内帯で特に数百㎞の高度まで下がっているブラジル上空（ＳＡＡ：南大西洋異常地域）の高エネルギー陽子（～５００ＭｅＶ）が考えられる。ただし、後者の陽子の場合、陽子が直接シングルイベントを起こすのではなく、陽子が半導体のシリコン原子核にヒットした結果の核反応で生じた重イオン（α線～シリコン）がシングルイベント現象を起こすと考えている。

本報告では、シングルイベント現象の発生メカニズム、宇宙放射線環境、筑波宇宙センターで行なっているシングルイベント実験の概要（カリホルニウムの核分裂片による実験装置、電子線マイクロビーム実験）、人工衛星で観測されたシングルイベントの実測例について報告する予定。

(D)－4

核融合炉セラミック増殖材の照射効果

日本原子力研究所　野田　健治

1．はじめに

核融合炉セラミック増殖材は核融合炉の稼働中に14MeVまでのエネルギーをもつ高エネルギー中性子、$^{6}Li(n,\alpha)^{3}H$反応に起因するトリチウムイオン（2.7MeV）及びHeイオン（2.1MeV）により著しい照射損傷を受ける。この照射損傷はスエリングや機械的性質の劣化を引き起こすばかりでなく、拡散現象への照射効果を通して増殖材中のトリチウム輸送や構造材料との化学的両立性にも影響を及ぼす。

本発表ではタンデム加速器及び原子炉照射を用いたセラミック増殖材（Li_2O及びLi_4SiO_4等）の照射損傷及び照射効果の研究を紹介する。

2．セラミック増殖材の照射損傷

Li_2Oの照射欠陥をESR法及び光吸収法により調べた。原子炉照射（熱中性子照射量：10^{20}-10^{22} n/m²）及び高エネルギー（100-120MeV）酸素イオン照射（イオン照射量：10^{20} ions/m²)を行ったLi_2O単結晶のESRスペクトルは20本以上のピークより成る超微細構造をもち、その超微細構造の結晶方位依存性よりこのESRスペクトルをF^{+}中心によるものと同定した。また、上記の照射を受けたLi_2Oの光吸収スペクトルにおいて、F^{+}中心による310nm（3.90eV）吸収バンドの他にF中心の集合欠陥と考えられる375nm（3.23eV）及び570nm（2.12eV）吸収バンドを観察した。さらに、照射量が高くなると（熱中性子照射量：10^{23}n/m²、100MeV酸素イオン照射量：$3X10^{20}$ ions/m²）、F^{+}中心のスペクトルに加え、コロイド状Li金属の析出を示すESRスペクトルを観察した。

これらの照射欠陥の等時焼鈍中における回復挙動については、F^{+}中心が420-570Kで回復し、一方、コロイド状Li金属は400-600Kで一旦増加後約700Kより減少し始め、870K以上で消滅した。

3．セラミック増殖材の照射効果

Li_2O及びLi_4SiO_4等のイオン電導度はLiイオン及びトリチウムの拡散を反映すると考えられている。これらのセラミック増殖材中のLiイオン及びトリチウム輸送に及ぼす照射効果を調べるため、タンデム加速器を用いたその場測定実験により照射中及び照射後のイオン電導度変化を測定した。

照射後におけるLi_2Oの電導度は440K以下の温度でイオン照射量とともに増加し、一方、453-573Kの温度範囲で減少した。等時焼鈍中における電導度の回復挙動から、この照射による電導度の減少はF^{+}中心に帰され、照射による増加は未同定の欠陥（Li空孔と予想される）に起因すると考えられた。これより、照射後のLiイオン及びトリチウムの拡散速度は440K以下の温度で照射とともに増加し、453-573Kの範囲で減少すると考えられる。

照射中のLi_2Oの電導度は照射前後に比べ大きく、照射イオン束とともに増加する。これは、Liイオン及びトリチウムの拡散の照射下促進が生じる可能性を示している。

この他、Li_4SiO_4の照射中及び照射後におけるイオン電導度変化の測定結果についても言及する予定である。

Ⓔ－1

タンデム加速器研究会　　平。３。１。２２－２３。　　原研・東海

ウラン化合物の物性

名大・工　　松井尚之

５ｆ電子を持つ物質としてのアクチナイド化合物に対する物性研究が、最近、基礎物性論の立場から、脚光を浴びている。　一つは、５ｆ電子の局在・非局在によると考えられる、アクチナイド化合物の非常に特異な磁気特性の出現（Anomalous Magnetism)と、もう一つは、４ｆ電子をもつランタナイド（おもに、Ce）の化合物に見いだされた「重い電子系」の存在が、アクチナイド化合物にも発見され、新しい物性現象（Heavy Fermion）として、実験的にも 理論的にも注目されるに至ったからである。　しかし、一般的には、アクチナイドの使用には多くの困難があり、特にわが国では、取扱規制の厳しさにより、この種の研究はウラン化合物に集中しているのが現状である。

本研究会では、我々がこれまで調べてきたウラン化合物について、

(1)　Anomalous Magnetism
　　強磁性体　（β-U_2N_3）;　　反強磁性体（UP）

(2)　Heavy Fermion
　　U-Au系;　　U-T(T:遷移金属)系化合物

を示す物質の低温物性、特に、磁気特性の測定結果を中心に紹介する。

Ⓔ－3

量子細線の電気伝導

筑波大・物質工、落合勇一

最近、電子ビーム露光リソグラフィやイオンビームエッチング等の半導体微細加工技術の発展に伴い、ＳｉやＧａＡｓ等の２次元電子系を基にしてミクロン以下の極微細線を製作することが可能となった。このようなメゾスコピック領域の半導体微小回路での低温電気伝導は新しい輸送現象が容易に観測できる系として注目され、この数年の間に固体中の電子波干渉によるアハロノフボーム（ＡＢ）効果やキャリアーが散乱を受けないバリスティック伝導等の発見が報告されて現在も研究が盛んに行われている。これは新輸送現象の探求という基礎物性的な側面と、新固体素子への応用という電子工学的な側面の両面にわたる研究の発展が大いに期待されている。しかしながら実際にバリスティック伝導が観測できる回路素子の大きさは伝導電子の平均自由行程以下の尺度となるので、当面応用上においても問題となるのは、平均自由行程に等しいかあるいは少し長い回路素子での電子波伝導であろう。またこのような素子においては、主として電子波の強い干渉が特徴的であり、その量子力学的性質が輸送現象に現われている。このように伝導が完全にバリスティックになっていないメゾスコピック領域（以下準バリスティックと記述する）での電子波伝導の効果をＧａＡｓ系超格子の量子細線を用いて調べた研究についてまず報告する。そしてこのような準バリスティック細線の低温におけるシュブニコフドハース(SdH)振動等の磁気抵抗測定の結果より、電子波の界面散乱や不純物散乱等による電子波伝導への影響を調べ、従来の古典的解釈と比較して、まだ理解の得られていない準バリスティク領域での電子波伝導機構の解明を行った。特に量子細線の試料尺度依存性等を調べることにより見いだされた電子波伝導の量子細線中でのサイズ効果の解析についても報告する。

文献

1) Y.Ochiai et al.,J.J.A.P.vol.29,1990,L793.

2) K.Ishibashi etal.,Proc.5th ICSM Berlin 1990.

(E)－4

金属人工格子の磁性

藤森　啓安（東北大　金研）

金属人工格子と呼ぶ人工設計の層状原子構造金属を合成して、機能性を持つ新しい金属材料を開発しようとする研究、また、金属物理学に新しい展開を図ろうとする研究が最近進展している。ところで、材料に有用な物質のさまざまな機能性は根本的には物質中の電子が演じており、故にその舞台である原子構造を制御・設計することは材料開発の基本である。　金属人工格子研究はこの考えに沿うもので、その意味では合金組成制御、組織制御、新化合物探索といった従来の材料開発手法の延長線上にあるといえる。しかし、金属人工格子の研究は、もっとロマンチックなものであり原子を自由に操って構造的にも、組成的にも、強いては物性・機能的にも全く新しい物質を造ろうという意図を持っており、、今までの考えの単なる延長ではない。　つまり、原子１個１個を人工的に操作して、何か今のところは分らない未知の理論、応用が新しいものとして見出せるような新物質、
Tailored Material を創成しようというところに金属人工格子研究の夢がある。　現在のところは、薄膜作製技術を使った原子の２次元的な積層技術に限られているが、それでもここ数年の間に特に磁性の分野で興味ある現象が見出されている。

講演では、最近我々の行なっているＦｅ／Ｇｄ 人工格子について、作製法、構造評価、磁化プロセス、磁気抵抗効果を紹介し、人工格子の特徴を検討する。その上で、他のグループで見出したＦｅ／Ｃｒ，Ｃｏ／Ｃｕ／ＮｉＦｅ 等の巨大な磁気抵抗効果を紹介する。その際、磁気抵抗の基本となっている人工格子における磁気相互作用の変調効果とその結果で現れる巨大周期反強磁性やフェリ磁性について、それらの特徴的なスピンフロップ磁化過程の問題も含めて、検討する。